ABSTRACT

Title of Document: PHARMACY-ON-A-CHIP: MICROFLUIDIC SYNTHESIS AND PREPARATION OF TUMOR-TARGETED LIPOSOMES

Renee Robin Hood, Ph.D., 2014

Directed By: Professor Don L. DeVoe,
Department of Mechanical Engineering

This dissertation describes a microfluidic technique for the synthesis and preparation of tumor-targeted liposomes for drug delivery applications plus the utilization of these liposomes for innovative pharmaceutical and preclinical research applications. Microfluidic hydrodynamic flow focusing enables the production of nearly monodisperse populations of nanoscale liposomes while providing exquisite control over size in comparison to traditional bulk-fluid liposome synthesis methods. Here, the microfluidic process was first implemented using lipids functionalized with high molecular weight polymers and other molecules to determine the ability to prepare long-circulating, tumor-targeted liposomes. Additionally, the process was realized in thermoplastic microchannels which require simpler, less expensive fabrication methods than the silicon-based devices in which this technique was originally demonstrated. Second, additional functionalities were integrated into the microfluidic platform, including buffer exchange and remote drug loading in-line with liposome

synthesis, to yield a continuous process for microfluidic preparation of liposomes containing high concentrations of amphipathic drugs which are commonly used for the treatment of cancer and other diseases. Next, the microfluidic technique, which is typically performed in two-dimensional rectangular microchannels, was implemented within a three-dimensional concentric capillary structure to assess the impact of edge effects during flow focusing on liposome synthesis in the two-dimensional system and to demonstrate a higher-throughput method for microfluidic liposome preparation. Along with exploring these additions to and variations upon the established microfluidic platform, microfluidic-enabled populations of liposomes were used for innovative pharmaceutical and preclinical research to demonstrate their utility in practical applications. First, nanoscale liposomes with discrete diameters were produced in order to investigate the effect of liposome size on cellular uptake mechanisms *in vitro* for a human epithelial colorectal adenocarcinoma (Caco-2) cell line. Next, liposomes with diameters below a proposed size cutoff for transdermal delivery (~40 nm) were produced to examine their ability to passively traverse layers of *ex vivo* porcine skin. The original research presented in this dissertation demonstrates the capacity to incorporate additional on-line liposome preparation functionalities into an established microfluidic technique, advances the platform to render it more amendable for widespread use, and highlights the advantages of microfluidic-prepared liposomes for practical applications through pharmaceutical and preclinical research.

PHARMACY-ON-A-CHIP: MICROFLUIDIC SYNTHESIS AND PREPARATION OF TUMOR-TARGETED LIPOSOMES

By

Renee Robin Hood

Dissertation submitted to the Faculty of the Graduate School of the
University of Maryland, College Park, in partial fulfillment
of the requirements for the degree of
Doctor of Philosophy
2014

Advisory Committee:
Professor Don L. DeVoe, Chair
Professor Keith E. Herold
Professor Adam H. Hsieh
Professor Silvia Muro
Professor Srinivasa R. Raghavan

Acknowledgements

I would first like to express my gratitude to my advisor, Prof. Don DeVoe, for providing such wonderful guidance and encouragement throughout my graduate studies. I have no doubt that his dedication and enthusiasm for research has had a profound impact on my experience as a graduate student. I would also like to acknowledge the remaining members of my committee, Profs. Keith Herold, Adam Hsieh, Silvia Muro and Srinivasa Raghavan, for dedicating their time to my defense.

I am very thankful for Dr. Wyatt Vreeland's advising and patience; I truly appreciate your warm, continuous support. Many thanks go to my co-authors and colleagues, particularly Dr. Donna Omiatek Dr. Eric Kendall, and Dr. Abhay Andar, for their meticulous paper edits, constructive criticism, and friendship throughout our time working together. I would like to recognize my fellow MML members, both current and former, for their continuous advice and friendship throughout the past 5 years. Also, I would like to express my gratitude toward the members of the FabLab and NispLab staff at the University of Maryland NanoCenter, Dr. Peter Swaan and his lab members at the University of Maryland Baltimore, and the Bioassay Methods Group at NIST for generously granting me access to their laboratory equipment.

Lastly, I would like to thank my family. I am especially thankful for my parents, Fred and Barbara Hood, for their continuous support throughout not only school but my every endeavor. I would like to recognize my twin sister, Kaylene, for being my lifelong source of friendship, entertainment, and healthy competition. And finally, I would like to thank Chris for his incredible patience and encouragement.

Table of Contents

List of Tables

List of Figures

List of Abbreviations

AF^4	Asymmetric flow field-flow fractionation
AO	Acridine Orange
BSA	Bovine serum albumin
Caco-2	Human colon adenocarcinoma cell line
CFD	Computational fluid dynamics
Cryo-TEM	Cryogenic temperature transmission electron microscopy
D_X	Diffusion coefficient of substance "X"
DAPI	4',6-diamino-2-phenylindole
DCP	Dihexadecyl phosphate
DiI-C_{18} (DiI)	1,1'-dioctadecyl-3,3,3',3'-tetramethylindocarbocyanine perchlorate
DMEM	Dulbecco's modified eagle's medium
DMPC	Dimyristoyl phosphatidylcholine
DOX	Doxorubicin hydrochloride
DPBS	Dulbecco's phosphate buffer saline
DPPC	Dipalmitoylphosphatidylcholine
DYN	Dynasore
EDTA	Ethylenediamine tetra acetic acid
EE	Encapsulation efficiency
EEA-1	Early endosome antigen -1
FIL	Filipin
FPL	Folate–PEG-modified liposomes
FR	Folate receptor
FRR	Flow rate ratio
FWHM	Full width at half maximum
HBSS	Hank's balanced salt solution
HCl	Hydrogen chloride
HEPES	4-(2-hydroxyethyl)-1-piperazineethanesulfonic acid
ID	Inner diameter
IPA	Isopropyl alcohol
LAMP-1	Lysosome-associated membrane protein - 1
MALLS	Multiangle laser light scattering
MDC	Monodansyl cadaverine
MHF	Microfluidic hydrodynamic focusing
MW	Molecular weight
OD	Outer diameter
PBS	Phosphate buffer saline
PDI	Polydispersity index
PDMS	Poly (dimethylsiloxane)
PEEK™	Poly(ether ether ketone)
PEG	Poly(ethylene glycol)
PEG_{2000}-PE	Dipalmitoylphosphatidylethanolamine-poly(ethylene glycol) 2000
PEG_{2000}-Fol-PE	Distearoylphosphatidylethanolamine-[folate(poly(ethylene glycol)) 2000]
PEG_{5000}-PE	Dipalmitoyl phosphatidylethanolamine-poly(ethylene glycol) 5000
PL	PEG-modified (PEGylated) liposomes
Q	Volumetric flow rate
QELS	Quasi-elastic light scattering
RC	Regenerated cellulose
Re	Reynold's number
SC	Stratum corneum
SD	Standard deviation
UV	Ultraviolet
WORT	Wortmannin
WST-1	Water-soluble tetrazolium salt

Chapter 1 : Introduction

1.1 Liposomes: Definition and Impact on Nanomedicine

Liposomes are self-assembled vesicles composed of lipid molecules which sequester small aqueous volumes within an enclosed lipid bilayer. Existing in diameters ranging from tens of nanometers to hundreds of microns, liposomes have been used in a variety of applications ranging from biomedical research to cosmetic formulations,[1] making a particularly high impact in the field of drug delivery.[2] In addition to their capacity to encapsulate aqueous solutions within their core, liposomes are able to isolate lipophilic compounds within their lipid bilayer as well as support tailored surface chemistries for targeted delivery of these encapsulated compounds (**Figure 1.1**). Furthermore, liposomes are typically made from biodegradable, nontoxic, nonimmunogenic lipid molecules and resemble cellular membranes both in composition and structure, thus liposomal drug delivery systems have excellent biocompatibility, low toxicity, and lack immune system activation.[1–3]

Liposome-encapsulated drugs demonstrate improved efficacy and decreased toxicity over non-encapsulated conventional drugs,[4] particularly for cancer applications due to their ability to accumulate within tumor microenvironments as a result of the

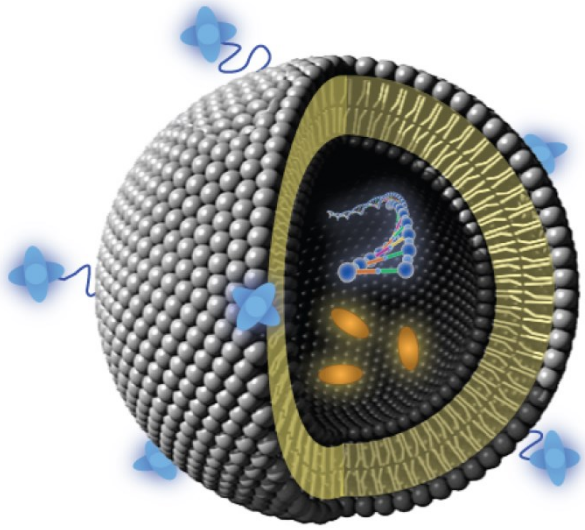

Figure 1.1: Liposome with encapsulated drug molecules and functionalized membrane for targeted delivery. *Figure generated by D.L. DeVoe.*

enhanced permeation and retention (EPR) effect which enables nanoscale liposomes to passively target cancerous tissue through leakage from the characteristically porous neovasculature and insufficient drainage present in tumors.[5] Liposomal anthracyclines (*e.g.,* doxorubicin (DOX)) have exhibited similar efficacy with substantially reduced toxicity in comparison to traditional administration of non-encapsulated drugs for both adjuvant and metastatic breast cancer treatments.[6] Liposome-encapsulated reagents have also shown to be very effective for the treatment and diagnosis of a variety of cancers including ovarian cancer[7] and other solid tumors,[8,9] as well as for use in vaccinology,[10] ophthalmology,[11] pulmonology,[12] and the treatment of other pathologies.[13–15]

1.2 PEG-and Folate- Modified Liposomes

Improved passive targeting for systemic administration of liposomes may be achieved through the use of "stealth" or long-circulating liposomes, which contain a flexible hydrophilic polymer such as poly(ethylene glycol) (PEG) on their exterior that occupies the space immediately adjacent to the liposome surface and excludes other molecules from binding to the vesicle.[3] The protective shield provided through PEG prevents the attachment of serum proteins (opsonins) and subsequent recognition by the mononuclear phagocyte system, which would trigger an immune response and lead to rapid elimination of the liposomes during circulation in the bloodstream.[14] The PEGylation of liposomes results in increased blood circulation time, allowing the drug carrier a longer timeframe to reach its target site before it is ultimately cleared from the bloodstream and has a toxic effect on healthy tissues such as the liver, kidney, and spline.[14] As an example, studies have shown free drug, liposomal drug, and PEG-conjugated liposomal drug half-life times of 52 min, 260 min, and 665 min (respectively).[16]

In addition to attaching a protective barrier of PEG to liposomes to guard from unspecific uptake by the immune system and lengthen blood circulation time, cell-specific targeting ligands

may also be tethered to the terminal end of the PEG molecules to instigate specific uptake by targeted tissues. This active targeting strategy delivers liposomal drugs to their intended site by allowing the liposomes to efficiently and selectively dock with pathologic cells that overexpress high-affinity receptors for these ligands.[17,18] While a range of macromolecules including antibodies, antibody fragments, lectins, and lipoproteins have been explored for targeted delivery,[19] small molecule targeting ligands (MW < 500 Da) are particularly well suited for conjugation with nanoparticles due to their affordability, accessibility, and small molecular weight in comparison to the overall size of nanoparticles.[20] Folate is a particularly attractive small molecule (441.4 Da) targeting ligand which is receiving increasing attention for selective drug delivery to cancer tissues.[21–24] Possessing many advantages over competitor targeting moieties such as antibodies, folate is non-immunogenic, not prone to denaturation, highly stable, has simple and defined conjugation chemistry, has excellent specificity to tumors, and is readily accessible in large quantities.[25] Folate is also compatible with organic solvents, which are necessary during the preparation of liposomes and other types of nanoparticles.[25] Folate receptors (FR) are greatly overexpressed in a wide range of cancer and inflammatory disease tissues, and folate binds to these receptors with an exceptionally high affinity.[21–25] Finally, folate may be readily conjugated with liposomes using PEG linkers without affecting its activity.[18] The low molecular weight, low cost, ease of conjugation, stability in diverse solvents and pHs, lack of immunogenicity, and high affinity for its receptor on target cells make folate a valuable choice as a targeting moiety for liposomal drug delivery systems.[21–25]

1.3 Limitations of Contemporary Liposome Synthesis Techniques

Despite the ongoing developments for targeted liposomal drugs, liposome synthesis remains based on cumbersome bulk scale processes including thin-film hydration,[26] reverse-phase evaporation,[27,28] detergent depletion,[29] and alcohol injection.[30–33] These standard preparation

methods rely on the self-assembly of lipid molecules into vesicles within environments which contain turbulent and uncontrolled fluid flows, resulting in large, polydisperse populations of liposomes which require multiple laborious post-processing steps (*e.g.,* serial membrane extrusion[30] or sonication[32,34]) to control the size and reduce the polydispersity of the final sample. Liposome size and size distribution are critical factors for ensuring well-regulated drug dosage, proficient cellular uptake, and extended *in vivo* circulation time.[35,36] Liposomes which are smaller in diameter have exhibited slower blood clearance rates, accordingly resulting in enhanced bioavailability and thus an improved opportunity to traverse tumor capillaries.[35,36] In addition to improved circulation times, smaller liposomes show enhanced accumulation within tumor tissues and enhanced *in vivo* drug release.[37] It has also been reported that both liposome uptake rate and final internalized concentration increase as particle diameter is reduced, further illustrating the impact of liposome size on delivery to cancer cells.[38] Consequently, large, polydisperse liposome populations encompass lower safety profiles due to the need for higher concentrations of drug to be administered to achieve desired therapeutic indices.[38]

As formerly mentioned, PEG- and ligand-conjugated liposomes have been developed to assist in alleviating the recognition of opsonins to increase blood circulation time and to enhance specific uptake by the tissues of interest. These decorated liposomes are typically generated through the appendage of these additional moieties to pre-formed vesicles, which entails additional processing steps for the post-insertion of functionalized lipids or conjugation of the ligands, further complicating the preparation of the liposomal drug[39] and inevitably increasing the cost for development and manufacturing.[40] The need to decrease liposome size in addition to developing a less laborious method for targeting ligand conjugation remain key challenges in the future advancement of liposomes as drug carriers. Therefore, liposomal drug delivery systems would benefit greatly from the ability to generate less polydisperse preparations of targeted

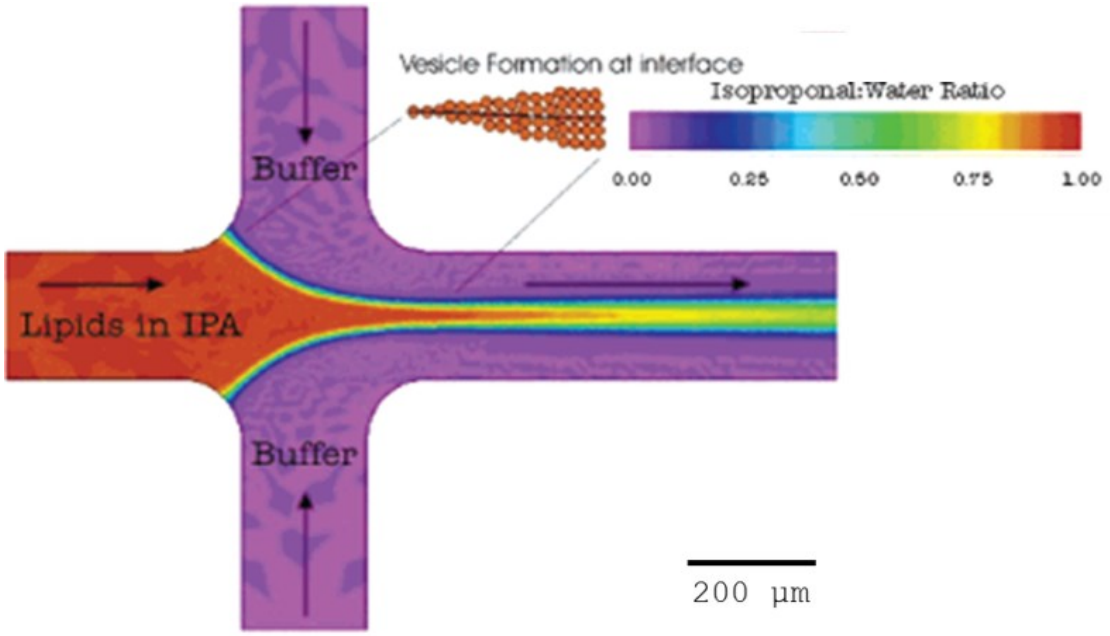

Figure 1.2: Schematic of the liposome formation process via hydrodynamic focusing in a microfluidic channel. Concentrations ratios of isopropanol (IPA) to aqueous buffer are depicted through color scale. Adapted from Jahn, *et al.,* 2004.[41]

liposomal drugs with tunable sizes below the limits defined by contemporary bulk scale production methods, while supporting flexible protocols that may be optimized for specific liposome sizes, concentrations of encapsulated compounds, and functionalization of liposome membranes with targeting ligands.

1.4 Continuous Flow Microfluidic Liposome Synthesis

A microfluidic platform which supports one-step, continuous flow formation of nearly monodisperse liposomes of tunable sizes within a single device has previously been demonstrated.[41–44] Microfluidics offers the exquisite manipulation of fluid flow conditions, allowing for the unique control over the self-assembly of lipids into liposomes. Specifically, this occurs through simultaneous control of interfacial interactions between fluid and chemical species, particle diffusion, and mixing of dissimilar fluid phases, a level of manipulation which is

not available in larger size scale batch preparation systems.[44] Using a simple microfluidic flow focusing technique which incorporates the alcohol-injection synthesis method[30–33] into a microfluidic chip, nearly monodisperse populations of liposomes with tunable sizes have been generated without the need for any post-processing steps to achieve unilamellarity or to reduce the size or size distribution.[41–44] This method involves a center fluid stream of alcohol and solvated lipid which is sheathed by two oblique streams of aqueous buffer via microfluidic hydrodynamic focusing in a Y-channel microfluidic device (**Figure 1.2**). Due to the characteristically laminar flow (*i.e.* Reynolds number <2300; microfluidics generally has Re <1) plus the miscibility of alcohol in water, precise formation of nearly monodisperse populations of liposomes is achieved as a result of the controlled diffusive mixing at the nanoscale which occurs at the interface of the two fluid species, allowing the lipids to systematically diffuse into the aqueous buffer in which they are insoluble, forming unilamellar lipid vesicles of exceptionally

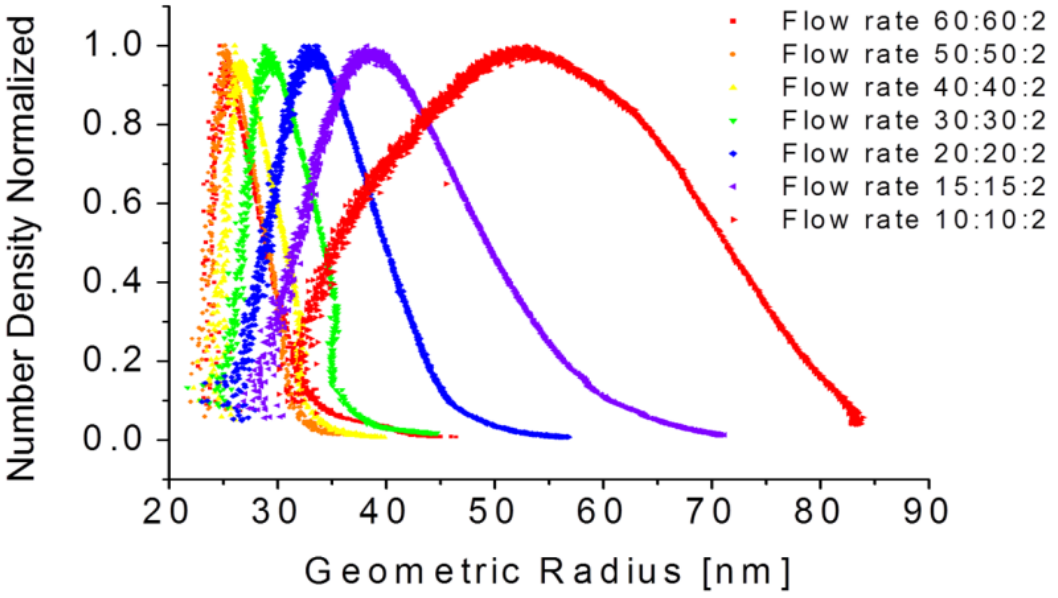

Figure 1.3: Liposome size and size distribution at different flow rate ratios (FRRs). As the FRR increases by a factor of 6, resulting liposome size decreases in diameter from approximately 120 to 50 nm and the size distribution decreases from ±50 nm to ±10 nm (~3σ). Adapted from Jahn, *et al.,* 2007.[42]

consistent size. By adjusting the ratio of buffer to alcohol volumetric flow rates and thus altering the flow focusing conditions, the size of the resulting liposome populations may be controlled (**Figure 1.3**).[41–44] In comparison to bulk scale synthesis methods, this technique provides a one-step, continuous flow process for the production of small, unilamellar liposomes without the need for additional homogenization steps.

1.5 Microfluidic Filtration and Sample Purification

The generation of liposomes[41–44] as well as other types of nanoparticles[45,46] in microfluidic devices has shown great promise due to the ability to produce on-demand, nearly monodisperse, highly controllable populations with less preparation steps compared to traditional bulk scale processes. However, microfluidic nanoparticle synthesis methods often result in samples containing unused solvents and compounds which are undesirable in the final solution, thus necessitating an additional off-chip purification step.

Microfluidic separations are a widely exploited feature in microchannels in order to precisely control and direct small volumes of fluid.[47] The sorting of nanoparticles formed by continuous flow microfluidics could be achieved through a variety of established separation methods. Free flow separations, which are characterized by continuous injection, real-time monitoring, and constant collection, are compatible with continuous flow microfluidic applications.[48] Numerous continuous flow separation methods have been demonstrated in microfluidic devices, and although most have focused on micrometer-sized particles,[48] a few techniques have proven feasible for the on-line separation of nanoparticles. First, microchannels could be fabricated in polyimide which would allow *in situ* integration of ion track-etched nanoporous structures for filtration.[49,50] This method encompasses several advantages, such as high pressure operation and the ability to achieve 10 nm pore sizes; however, the microchannel aspect ratio would be limited due to the maximum thickness achievable by available polyimide resists and processing

techniques.[51] For microfluidic production of nanoscale liposomes, higher aspect ratios (6:1 or greater) are preferable[44] and therefor e microchannels fabricated in polyimide would not be ideal.

Another potentially viable method for microfluidic purification of nanoparticles is electrokinetic separation of the liposomes from the buffer. Electrokinetic-controlled microfluidic networks have proven useful for precise isolation of nanoscale biological samples.[52] To facilitate this process, charged components could be incorporated into the bilayer lipid membrane in order to impose an overall charge on the liposomes. When anionic or cationic surfactants are incorporated into the liposomal bilayer at constant concentrations, the charged species are theoretically equally distributed throughout the membranes of all liposomes and thus the charge-to-size ratio remains constant, enabling size-based electrokinetic separation due to the variance in net individual liposome charge.[53] To be implemented, this method would need to be converted into a continuous flow separation technique, which has been demonstrated for free flow electrophoretic separation of amino acids in both aqueous and binary media.[54] However, this version of electrokinetic separation necessitates an electric field above 1.5 kV/cm in order to accomplish the transverse purification, which could potentially cause lysis of fragile particles such as liposomes.[53] In addition, the fundamental task for this application is to separate the liposomes from all other components of the buffer, thus any compounds with a charge (*e.g.,* charged dyes, therapeutics, anionic membrane components, etc.) may also migrate under an electric field, consequently presenting numerous challenges for thorough purification.

Accordingly, a rapid, transverse microfluidic filtration method which is appropriate for continuous flow separation of delicate, nanometer-scale particles must be implemented in order to achieve a highly purified sample of undamaged liposomes. A less common but well-fitting method of continuous flow filtration and rapid buffer, which circumvents issues associated with previously mentioned methods, is the incorporation of a nanoporous membrane within the

microfluidic device. Adequate porosities, flexibility, mechanical robustness, and compatibility with plastic microfluidic networks make commercially available polymeric membranes an ideal choice for rapid microfluidic buffer exchange.[55] In addition, the large surface area-to-volume ratio presented by porous membranes is particularly essential for accomplishing expedited buffer substitution during microdialysis.[55] Regenerated cellulose membranes comprise many advantages over other polymeric membranes for buffer exchange and nanoparticle sample filtration due to their high porosity, excellent chemical compatibility, and wide range of pore size availabilities in the sub-micrometer range.

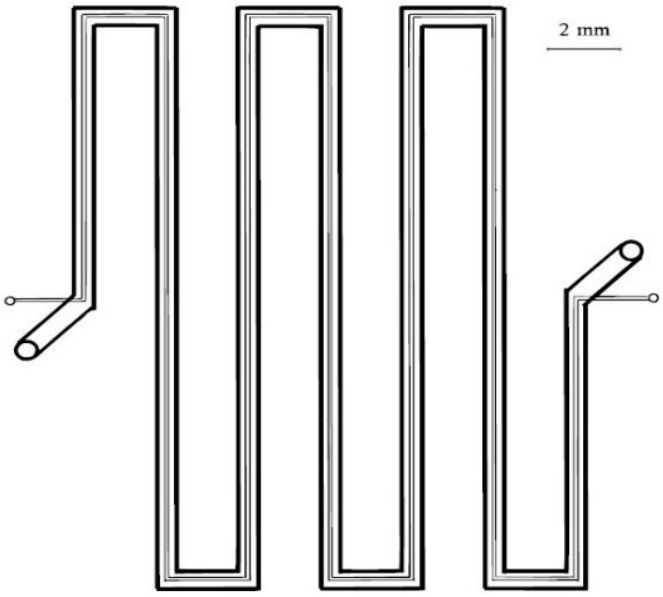

Figure 1.4: Schematic of overlapping sample and buffer channels separated by a regenerated cellulose membrane (MWCO 8000) after alignment of the microchannel chips for microfluidic buffer exchange. Adapted from Xu, *et al.,* 1998.[56]

A microfluidic technique facilitating sample clean-up for electrospray ionization-mass spectrometry of nanoscale biological samples has been demonstrated using a commercially available regenerated cellulose membrane embedded in a thermoplastic device (**Figure 1.4**).[56,57] Efficient buffer exchange is achieved as a result of the chemical potential between the two compartments in combination with the transmembrane pressure gradient established by the dimensional variance between the sample channel and the buffer channel, plus the continuous buffer counterflow which causes the cleanest sample solution to be in constant contact with the cleanest dialysis buffer.[56] This method utilizes both methods of dialysis, or displacement of

solutes from a partition in which they are in high concentration to one in which they are diluted driven by the electrochemical gradient in the system, and ultrafiltration, or transport of a solute across a semipermeable membrane from one fluid compartment to another in response to a transmembrane pressure gradient.[56,57] The result is a rapid, efficient method for microfluidic buffer exchange. This purification technique is compatible with microfluidic-directed liposome synthesis and would provide highly purified samples with minimal impact on the resulting populations of liposomes.

1.6 Methods for Solute Encapsulation into Liposomes

The unique ability to sequester small volumes of aqueous solutions within their core and confine lipophilic compounds within their bilayer is a key advantage of liposomal drug delivery systems. Various approaches for encapsulation of reagents into the liposomal core fall into two categories: passive and active loading. Passive encapsulation strategies rely on loading of compounds during liposome formation and are highly dependent on chemical properties. Although simpler, passive loading methods typically yield a loading efficiency of 5-20%[15] while active loading techniques achieve 93-97% efficiency.[58] Although methods such as lyophilization, evaporation, or freeze-thaw cycles may be employed to improve passive loading proficiencies,[15] passively encapsulated solutes can readily penetrate the membrane and thus are unstable, plus they necessitate post-formation filtration due to the large amount of remaining unloaded drug in the extra-liposomal buffer.[15] Moreover, passive loading methods often result in polydisperse liposome sizes, difficulties with regularization, and low reproducibility.[15]

Active encapsulation, or remote loading, methods involve systematic entrapment of therapeutics into pre-formed liposomes, typically utilizing a driving force such as a transmembrane pH- or ion-gradient.[59] Remote loading techniques all comprise a similar concept: first, the interior pH of the liposome is acidified while the exterior buffer is adjusted to

physiological pH conditions. Uncharged amphipathic weak bases (*e.g.,* anthracyclines such as the commonly used DOX) are then incubated with the liposomes where they diffuse into the vesicles, becoming protonated intravesiculary and thus inhibiting membrane repermeation.[58] This reaction ensues, resulting in an accumulation of anthracycline inside the liposome which leads to precipitation through drug self-association or precipitation with interior liposomal salts present in the buffer, achieving intravesicular drug levels that exceed the solubility of the drug.[60] This method achieves extremely stable therapeutic liposomes with high drug-to-lipid ratios, an important feature for *in vivo* applcations.[61]

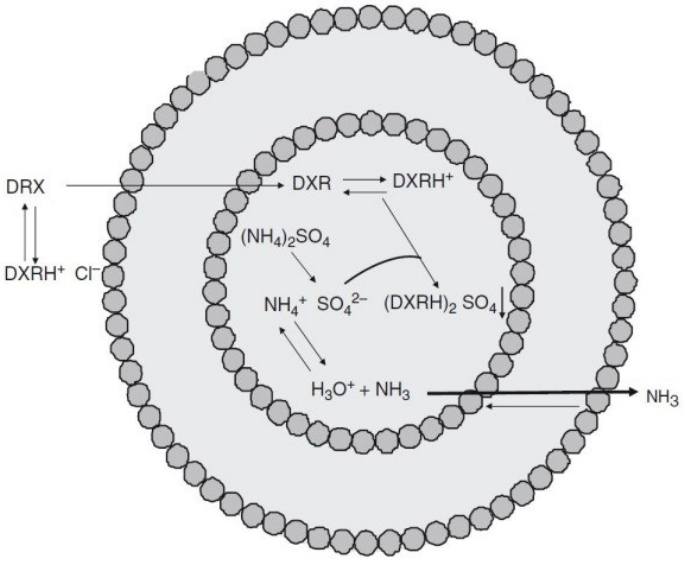

Figure 1.5: Overview of the remote loading process. Here, an amphipathic weak base (doxorubicin, 'DXR') is actively driven into a pre-formed liposome through a transmembrane ammonium sulfate gradient. Adapted from Lewrick, *et al.,* 2010.[58]

Remote loading specifically through a transmembrane ammonium sulfate gradient is a widely-used, rapid, simple, stable, and efficient method of encapsulation for amphiphilic molecules such as anthracyclines into liposomes.[60] For example, DOX is commercially available as Doxorubicin Hydrochloride (DOX-HCl), an amphipathic weak base which is both water and alcohol soluble. When introduced to liposomes with an acidic interior compared to their neutral environment, active entrapment occurs as a result of the base exchange with the ammonium ions

inside the liposome (**Figure 1.5**).[60] The first nanoparticle therapeutics approved for clinical use (Doxil®, a PEG-coated form of liposomal DOX), liposomal anthracyclines were developed to mitigate the cardiac and gastrointestinal toxicity triggered by conventional anthracyclines injected intravenously for the treatment of various epithelial cancers and other ailments while sustaining antitumor efficacy by altering tissue distribution and pharmacokinetics.[62]

Moreover, the drug-to-lipid ratio is a very important detail to consider in liposomal drug delivery systems. Various lipid compositions and entrapment methods yield different entrapment efficiencies, fluctuating more with passive encapsulation than with remote loading techniques,[61] generating the probability of dosage uncertainty. There is evidence that the *in vivo* toxicity of liposomal DOX decreases with increasing drug-to-lipid ratios.[61] Finally, a high drug-to-lipid ratio is likely to reduce the cost of formulations.[63]

Smaller liposomes are advantageous to their larger counterparts due to their greater uptake rates and internalized liposome concentrations in cancer cells,[38] ability to exhibit longer circulation times (and thus enhanced bioavailability[35,36] and higher levels of accumulation within tumor tissues), and improved *in vivo* drug release.[37] One caveat to this phenomenon is that smaller liposomes have a reduced interior volume and consequently less available space to retain encapsulated material. Hence, remote loading techniques prove even more vital for drug entrapment as the radius of the liposomes produced decreases in order to maximize the payload of drug delivered to the target site. Consequently, remote loading strategies provide enhanced stability, improved efficacy, reduced toxicity, and decreased manufacturing costs in comparison to passive loading strategies, and are extremely beneficial to reach high drug-to-lipid ratios and thus encapsulation efficiencies of DOX into liposomes.

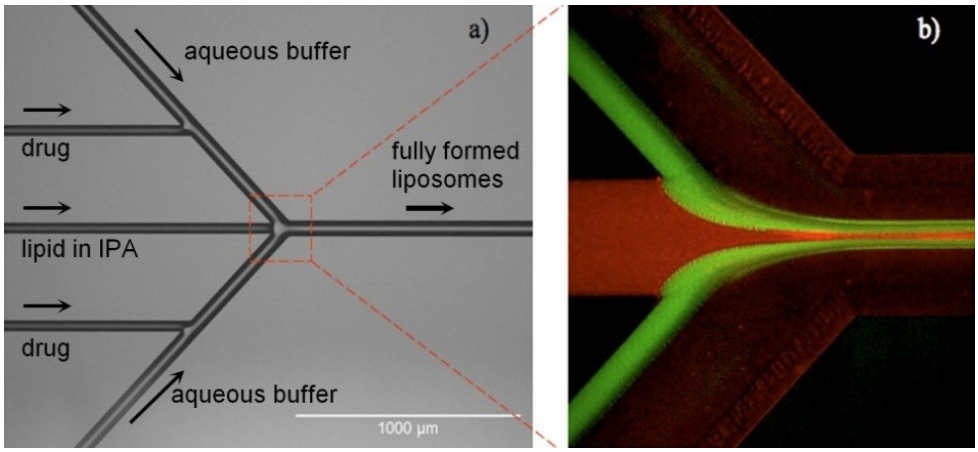

Figure 1.6: (a) 5-inlet chip design, and (b) fluorescent micrograph of a hydrodynamically focused lipid/alcohol stream employing a passive encapsulation technique. Adapted from Jahn, *et al.*, 2008.[43]

The established microfluidic network for liposome synthesis has previously been demonstrated to incorporate a method of passive encapsulation of hydrophilic molecules with the benefit of lower consumption of the solute to be encapsulated as a result of the narrowed fluid stream width of the solute-containing fluid kept close to the interface with the lipid/solvent stream where spontaneous liposome self-assembly occurs (**Figure 1.6**).[43] Although advantageous for molecules which cannot be encapsulated through remote loading, one goal of this dissertation is to further evolve the established microfluidic technique to include on-line remote loading of amphipathic compounds in order to produce microfluidic-enabled populations of stable liposomal drugs at high concentrations.

1.7 Medical Applications of Liposomes

Liposomes are highly versatile nanoparticles which benefit applications across many fields of interest. Liposomes have provided important advancements for medicine, immunology, diagnostics, cosmetics, ecology, cleansing, and the food industry.[64] Specifically for the medical field, liposomes have an immense clinical utility and have been developed as pharmaceutical carries for various practical applications,[65] showing enhanced efficacies when delivered through

intravenous,[3,66,67] intramuscular,[68] oral,[69,70] pulmonary,[71–73] and topical[74] application. Liposomes have been used as pharmaceutical carriers to deliver a variety of reagents including drugs,[75] proteins and proteins,[76] nucleic acids (*e.g.,* DNA[77] and siRNA[78]), vaccines,[79] and viruses.[80] Liposomes are also suitable to carry contrast reagents for various types of diagnostic imaging, including magnetic resonance imaging (MRI), computed tomography imaging (CTI), positron emission tomography (PET), and sonography.[81] Furthermore, enhanced manipulation of liposomes has been achieved through the development of pH-sensitive liposomes,[82,83] temperature- sensitive liposomes,[84] magnetic liposomes,[85] and ultra-flexible transferosomes.[74] The multitude of advancements for liposomes as pharmaceutical and diagnostic reagent carriers continues to increase; therefore, an enhanced preparation method which provides purified liposomal drugs or imaging reagents at high concentrations through a one-step, continuous flow process would greatly improve the effectiveness of liposomes for practical applications and greatly benefit the medical field.

1.8 Motivation and Global Hypotheses

Microfluidic-directed liposome synthesis provides an alternative approach for vesicle production with various benefits over bulk-scale production methods, including lower levels of polydispersity, high control over resulting vesicle size, . The motivation behind this research is to evolve the existing microfluidic technique to make it more amendable for widespread use and to highlight the benefits of the technique through actual preclinical applications. The addition of downstream functionalities to the microfluidic liposome synthesis method such as active drug encapsulation would enable point-of-care liposomal drug production by generating customized formulations in a one-step process. The advantages of microfluidic systems will be exploited to form new processes for the synthesis of liposomal drugs. For example, it is hypothesized that the reduced diffusion lengths in microfluidics will support rapid, efficient drug loading, and that

radially symmetrical flow focusing will further decrease the polydispersity of the resulting liposomes. In addition, the high level of size control together with the significantly low levels of polydispersity enabled by the microfluidic liposome synthesis method could assist in the exploration of new pharmaceutical and preclinical research applications, including size-dependency of cellular uptake mechanisms and passive transdermal uptake of liposomal carriers. This dissertation explores the pilot microfluidic method for liposome synthesis through the implementation of these concepts.

1.9 Dissertation Overview

The ability of a microfluidic technique to form liposomes encompassing a range of fine-tuned diameters, tailored surface chemistries, and encapsulated therapeutics is demonstrated within the subsequent chapters. In addition, the usefulness of these liposomes with optimized properties provided through the meticulous control over their characteristics enabled by microfluidic preparation is highlighted through their use in innovative research applications. This dissertation focuses on pharmaceutical research investigating drug carrier optimization using *in vitro* studies and preclinical research to examine transdermal delivery of liposomes though *ex vivo* application of liposomes to porcine skin. These are just two practical uses among a vast collection of purposes in which the microfluidic method for liposome synthesis has potential to further advance the already burgeoning topic of liposomes in the medical field.

The goal of the research presented through this dissertation is to evolve the established microfluidic hydrodynamic focusing technique for liposome synthesis from its preliminary state to a more amendable platform for widespread use and to demonstrate the benefits of liposomes synthesized through the technique through actual preclinical research applications. The dissertation is organized around the following interrelated topics, with the presentation of each research thrust adapted from our published results as noted:

Chapter 1: Demonstrate the microfluidic technique for liposome synthesis using functionalized lipids (specifically, PEG and PEG-folate) for continuous flow production of long-circulating, tumor-targeted liposomes. In addition, establish the method within thermoplastic microfluidic devices which utilize simple, scalable, low-cost fabrication techniques. Adapted from Hood, *et al.*, 2013.[86]

Chapter 2: Incorporate on-line sample cleanup and remote drug loading to the liposome synthesis technique to enable production of liposome populations requiring no additional dialysis or separation methods together with rapid liposomal encapsulation of cancer-targeting compounds, opening the door to "pharmacy-on-a-chip" drug formulations suitable for on-demand applications. Adapted from Hood, *et al.*, 2014.[87]

Chapter 3: Perform the microfluidic liposome synthesis technique within a concentric capillary device to both investigate the effect of radially symmetric, three-dimensional flow focusing on liposome production as well as address the issue of scale up by producing liposomes at greater volumetric flow rates. Adapted from Hood, *et al.*, 2014.[88]

Chapter 4: Investigate the effect of liposome size on cellular uptake mechanisms with high resolution by examining the interaction of microfluidic-prepared liposomes with human epithelial colorectal adenocarcinoma cells (Caco-2) *in vitro*, taking advantage of the technique's unique ability to produce populations of distinctly-sized, nearly monodisperse functionalized liposomes. Adapted from Andar, *et al.*, 2014.[89]

Chapter 5: Demonstrate passive transdermal uptake of liposomes through *ex vivo* sections of porcine skin by utilizing the microfluidic liposome synthesis technique to generate liposomes below the proposed size cutoff for transdermal delivery of nanoparticles. Adapted from Hood, *et al.*, 2014.[90]

Chapter 2 : Microfluidic Synthesis of PEG- and Folate-Conjugated Liposomes for One-Step Formation of Targeted Stealth Nanocarriers

2.1 Summary

A microfluidic hydrodynamic flow focusing technique enabling the formation of small and nearly monodisperse liposomes is investigated for continuous flow synthesis of poly(ethylene glycol) (PEG)-modified and PEG-folate-functionalized liposomes for targeted drug delivery. Controlled laminar flow in thermoplastic microfluidic devices facilitated liposome self-assembly from initial lipid compositions including lipid/cholesterol mixtures containing PEG-lipid and folate-PEG-lipid conjugates. The relationships between flow conditions, lipid composition, and liposome size were evaluated, and the impacts of these parameters on PEG and folate incorporation were determined through a combination of UV-vis absorbance measurements and characterization of liposome zeta potential. Both PEG and folate were successfully incorporated into microfluidic-synthesized liposomes over the full range of liposome sizes studied. The efficiency of PEG-lipid incorporation was found to be inversely correlated with liposome diameter. Folate-lipid was also effectively integrated into liposomes at various flow conditions. Liposomes incorporating relatively large PEG-modified and folate-PEG-modified lipids were successfully synthesized using the microfluidic flow focusing platform, providing a simple, low cost, rapid method for preparing functionalized liposomes. Relationships between preparation conditions and PEG or folate-PEG functionalization have been elucidated, providing insight into the process and defining paths for optimization of the microfluidic method toward the formation of functionalized liposomes for pharmaceutical applications.

2.2 Introduction

Liposomes possess a range of highly attractive characteristics which make them excellent drug delivery vehicles. However, despite ongoing advances in the development of targeted liposomal drugs, their preparation remains a cumbersome bulk scale process based on classical bulk synthesis methods which require laborious post-processing steps to control the size and reduce the polydispersity of the resulting liposome population.[91] Using a simple microfluidic flow focusing technique which integrates the alcohol-injection method into a microfluidic device, nearly monodisperse populations of unilamellar liposomes with controllable sizes have been realized without the need for any post-processing steps to reduce size variance (**Figure 2.1**).[41–44] The excellent control over fluid flow conditions provided by microfluidics offers a

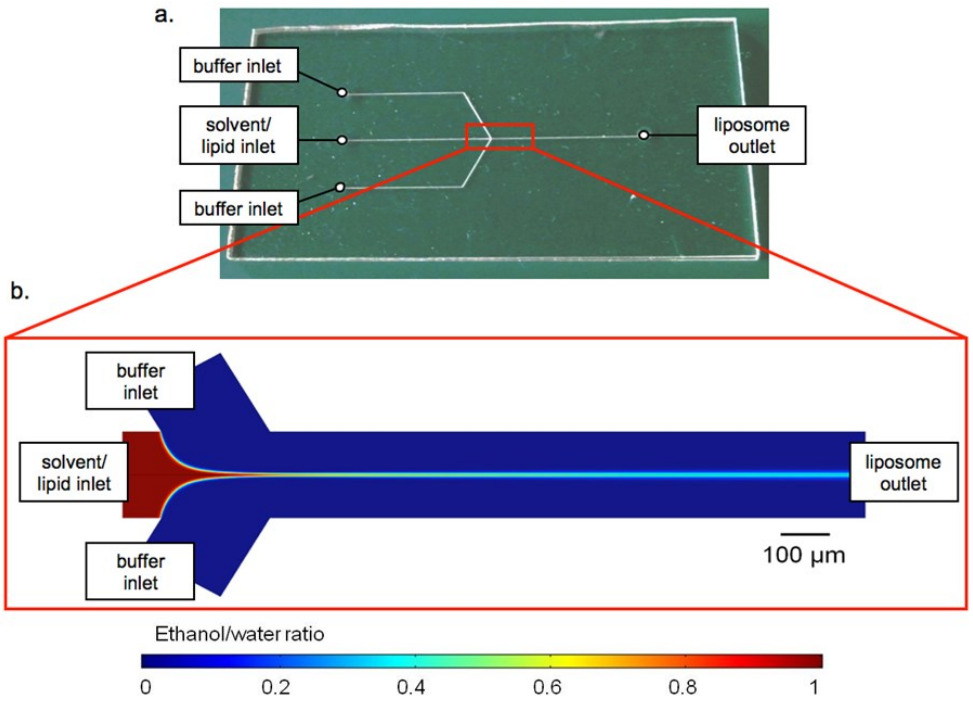

Figure 2.1: (a) Photograph of the thermoplastic liposome synthesis chip, and (b) numerical simulation of hydrodynamic flow focusing in the microfluidic device, illustrating the diminishing mole fraction of ethanol along the center of channel as the alcohol (red) and aqueous buffer (blue) streams interact at a flow rate ratio of 70 within a 190 µm wide microchannel.

unique path to liposome self-assembly through manipulation of interfacial interactions, particle diffusion, and convective-diffusive mixing of fluid phases.[44] However, the attachment of ligands such as PEG or targeting moieties to pre-formed liposomes can require additional processing steps for the post-insertion of functionalized lipids, further complicating established methods of liposomal drug preparation[39] and inevitably increasing the cost for development and manufacturing.[40]

Previous work on liposome production using the microfluidic flow focusing technique has concentrated on exploring the impact of changes in the ratio of volumetric flow rates between the buffer and alcohol streams on mean liposome size using a single native lipid species.[41,42,44] This chapter explores microfluidic flow focusing as an effective method for the continuous flow preparation of nanoscale liposomes functionalized with PEG, enabling rapid and automated formation of stealth liposomes, and further extending the technique to the formation of liposomes functionalized with folate-PEG conjugates. The resulting functionalized liposomes containing a combination of native lipids, PEG-lipids, and folate-PEG-lipids are characterized using a variety of analytical methods to explore the impact of microfluidic flow parameters on liposome size and surface properties. Asymmetric flow field-flow fractionation (AF^4) paired with multi-angle laser light scattering (MALLS) and quasi-electric light scattering (QELS) is used to evaluate size distributions of liposome populations formed under varying flow conditions and lipid compositions. To investigate the incorporation of the various lipid conjugates into the liposomes, UV-visible absorption spectroscopy, zeta potential measurements via phase analysis light scattering, and cryogenic temperature transmission electron microscopy are employed. Based on measurement results, the microfluidic platform is shown to provide a rapid, one-step method for preparing nearly monodisperse populations of folate receptor-targeted stealth liposomes of tunable size, with significant potential for drug delivery applications.

In addition to evaluating the microfluidic technology as a suitable method for on-line formation of functionalized liposomes, this chapter presents several ancillary advancements over previous studies. Unlike established efforts based on the use of silicon and glass microfluidic platforms, the application of thermoplastic microfluidics has been explored as an alternative technology platform suitable for low-cost scale-up of the liposome synthesis technique. Furthermore, while prior studies have employed relatively toxic solvents such as isopropyl alcohol as a lipid carrier during microfluidic flow focusing,[41,42,44] this work utilizes ethanol as a less toxic solvent system to enhance biocompatibility for future *in vivo* applications.

2.3 Materials and Methods

2.3.1 Device Fabrication

Microfluidic devices were fabricated in cyclic olefin copolymer (COC), a low-cost thermoplastic with excellent compatibility with a wide range of organic solvents, using a 2-step hot embossing process in which microfluidic channel features were first milled onto a polished Alloy 260 brass sheet (McMaster-Carr, Dayton, NJ) using a precision computer numerical control (CNC) milling machine (MDX-650A; Roland, Lake Forest, CA). The brass template was cleaned with a mild detergent, placed in a sonicator for 15 min, and examined under a microscope for imperfections. The brass template was then stacked in a commercial hot press (Carver, Wabash, IN) with a 48 mm thick polycarbonate plate (McMaster-Carr, Dayton, NJ) and held at a pressure of 0.8 MPa and temperature of 170 °C for 5 min. The polycarbonate template with inverted channel features was then placed in the hot press with a 2 mm thick sheet of COC (Zeonor 1060 R, Zeon Chemicals L.P., Louisville, KY) and held at 0.4 MPa and 128 °C for 10 min to transfer the pattern features from the PC intermediate template to the final COC chip.

Using a LV-100 UDM microscope (Nikon, Melville, NY) for optical profilometry, microchannel dimensions were found to be approximately 270 μm deep by 190 μm wide.

A cover plate with fluidic access ports was fabricated from a second 2 mm COC sheet using a CNC milling machine, and both COC pieces were degassed at 70 °C under vacuum overnight. The chips were mated using solvent bonding with vapor-phase cyclohexane by placing the cover plate face down on top of a sealed glass beaker containing anhydrous cyclohexane (Sigma-Aldrich, St. Louis, MO) at 30 °C, with the chip surface 5 cm away from exposed solvent, for 8.5 min. The chips were aligned and bonded in a hydraulic press (Carver, Wabash, IN) at 1.9 MPa for 1 min at room temperature. The bonded COC was held at room temperature for at least 24 h before use to maximize bonding strength. Press-fit needles were inserted at each fluidic access port and attached to nanoport fluidic connectors (Upchurch Scientific, Oak Harbor, WA) and silica capillary tubing (Polymicro Technologies Inc., Phoenix, AZ). The device was attached to glass gastight syringes (Hamilton Co., Reno, NV) containing buffer and lipid solution. Two programmable syringe pumps (Harvard Apparatus, Holliston, MA) were used for fluidic delivery and control.

2.3.2 Lipid Mixture and Hydration Buffer Preparation

For PEG-modified (PEGylated) liposomes (PL), 1,2-dimyristoyl-sn-glycero-3-phosphocholine (DMPC), cholesterol, and 1,2-dimyristoyl-*sn*-glycero-3-phosphoethanolamine-N-[methoxy(polyethylene glycol)-5000] (PEG_{5000}-PE) (all from Avanti Polar Lipids Inc., Alabaster, AL), and dihexadecyl phosphate (DCP) (Sigma-Aldrich, St. Louis, MO) were mixed in chloroform (Mallinckrodt Baker Inc., Phillipsburg, NJ) in the following proportions: DMPC/cholesterol/DCP/PEG_{5000}-PE in molar ratio (50-x):40:10:x, where x = 0, 5, 10, creating liposomes with 0 mol %, 5 mol %, and 10 mol % of PEG_{5000}-lipids. For folate-targeted PEGylated liposomes (FPL), DMPC, cholesterol, 1,2-dimyristoyl-sn-glycero-3-

phosphoethanolamine-N-[methoxy(polyethylene glycol)-2000] (PEG_{2000}-PE), and 1,2-distearoyl-*sn*-glycero-3-phosphoethanolamine-N-[folate(polyethylene glycol)-2000] (PEG_{2000}-Folate-PE) (all from Avanti Polar Lipids Inc.), and DCP (Sigma-Aldrich) were mixed in chloroform (Mallinckrodt Baker) in the following proportions: DMPC/cholesterol/DCP/PEG_{2000}-PE/PEG_{2000}-Fol-PEin molar ratio 40-x:40:10:10:x, where x = 0 or 2, as well as DMPC/cholesterol/DCP (50:40:10), creating PEGylated and folate-receptor targeted liposomes with 2 mol % PEG_{2000}-Fol-PEand both PEGylated and non-PEGylated liposomes as controls. The anionic surfactant DCP was included in all lipid preparations to prevent aggregation of liposomes in populations which did not contain PEG, as well as to assist in zeta potential measurements performed on all PLs. For PLs and FPLs, the lipid mixtures were prepared in scintillation vials then placed in a vacuum desiccator for at least 24 h to allow complete solvent removal. The dried lipid mixtures were then redissolved in anhydrous ethanol (99.5% Sigma-Aldrich) for a total lipid concentration of 20 mM. A 20 mM solution of 4-(2-hydroxyethyl)-1-piperazineethanesulfonic acid (HEPES) at pH 7.5 (Sigma-Aldrich) was used as an aqueous buffer in the microfluidic device. All solutions (solvent and buffer) were passed through 0.22 μm filters (Millipore Corp., New Bedford, MA) before being introduced to the microfluidic device.

2.3.3 Microfluidic Liposome Synthesis

Liposomes were prepared by injecting the lipid-solvent mixture between two buffer inputs into a microfluidic device, as done previously.[42] HEPES buffer was injected into two oblique side channels intersecting with the center channel. The flow rate ratio (FRR), which is defined as the ratio of the volumetric flow rate of aqueous buffer to solvent, was set to 40, 70, and 100 for each PEG-lipid concentration to prepare PLs. The linear flow velocity of the combined fluid stream within the liposome formation channel was kept constant for all FRR values at 0.125 m/s, corresponding to a total volumetric flow rate of 384 μL/min. The hydrodynamic focusing region

was observed with a TE-2000 S epifluorescence inverted microscope (Nikon, Melville, NY) throughout the liposome formation process to monitor for consistent flow conditions.

2.3.4 Asymmetric Flow Field-Flow Fractionation (AF^4) with Multi-Angle Laser Light Scattering (MALLS) and Quasi-Elastic Light Scattering (QELS) and UV-Vis Absorption Spectroscopy

High-resolution size-based separations of the liposome populations were carried out with AF^4. This fractionation method is useful for characterizing nanoparticles through high resolution separation. Because the nanoparticles are sorted by size and eluted at different time intervals based on size, the subsequent light scattering measurements provide highly detailed descriptions of each sample size which exists in the sample and reveals the presence of any aggregates or micelles in the liposomal solution. The AF^4 system is well-maintained at the National Institute of Standards and Technology and is calibrated at least every few months using bovine serum albumin (BSA) and the system's ability to separate the trimers, dimers, and monomers within the BSA solution.

HEPES buffer was used as a carrier buffer for the AF^4 separations. This was combined with MALLS, QELS, and UV-Vis absorption for liposome detection and characterization (DAWN EOS and QELS, Wyatt Technology, Santa Barbara, CA). A vendor-supplied spacer (250 μm thickness) was used to define the flow channel thickness with a 10 kDa molecular weight cut-off regenerated cellulose membrane for the cross-flow partition (Millipore, Bedford, MA). The flow was controlled with Eclipse 2 software (Wyatt Technology, Santa Barbara, CA). A sample volume of 30 μL (all samples) was injected at a flow rate of 0.1 μL/min while focusing at 1.5 mL/min for 5 min. The injection step was succeeded by a second focusing step of 1.5 mL/min for 5 min. The crossflow was ramped linearly from 0.5 mL/min to 0 mL/min over a 30 min period while eluting the separated particles at 1 mL/min. The radii of the separated particles were

measured using the MALLS and QELS detectors with data processing using ASTRA software (Wyatt Technology). Static light scattering intensity (λ=690 nm) was measured at 15 angles simultaneously. The sample was analyzed at 1 s intervals by MALLS and 5 s intervals by QELS. The autocorrelation function of the QELS was fitted to a single-mode exponential decay model to resolve the hydrodynamic radii of the liposomes. A coated sphere model (*i.e.* a spherical structure with two radial regions of differing refractive index) of the MALLS data was consistent with this particle architecture and was used for size analysis of the geometric radius of the fractionated liposome samples. The ASTRA software generates information on the differential size distribution of each sample, which was used to analyze each population of liposomes. The differential distribution of each fractionated liposome sample produced a unimodal, sharp Gaussian distribution, indicating nearly monodisperse population with a continuous size distribution. The modal diameter was taken to be the average diameter of each liposome population, in addition to the full width at half maximum (FWHM) to account for any polydispersity in the sample. In addition, UV-vis absorption spectroscopy was also used in-line to detect the presence of PEG on PLs (λ=520 nm) and folate on FPLs (λ=280 nm) in the fractionated samples.

2.3.5 Zeta Potential from Phase Analysis Light Scattering

The PL zeta potential was determined using phase analysis laser light scattering (ZetaPALS, Brookhaven Instruments Corp, Holtsville, NY) using undiluted PL samples (1.5 mL). All liposome mixtures used for zeta potential characterization contained 10 mol % DCP as an anionic surfactant, and were prepared in a low conductivity buffer (20 mM HEPES, conductivity ~60 μS). The incorporation of anionic DCP aided in electrophoretic measurements by providing the liposomes with a consistent surface charge density for each liposome sample. Electrophoretic motilities were measured and converted into zeta potentials using the Smoluchowski equation.[92]

Zeta potential measurements extrapolated from electrophoretic mobility measurements were averaged over 5 replicate runs of 10 cycles each. All measurements were carried out at 23 °C.

2.3.6 Cryo-TEM Analysis

Aliquots from PL samples containing 0% and 10% PEG-lipid (FRR 40) were imaged using cryo-TEM. Sample preparation for cryo-TEM investigation was carried out using a Cryoplunge 3 unit (Gatan, Inc., Pleasanton, CA). A 3 μL volume of sample from 0%-PEG and 10%-PEG liposomes was pipetted onto a support grid held by tweezers directly above the cryoplunge workstation. The grid was aligned with the blot pads and was subsequently blotted for 4 s, giving a thin film between 100 nm-200 nm. The grid was then plummeted into liquid ethane in the workstation held at a temperature below -170 °C with liquid nitrogen. This was repeated for both liposome samples and the grid was transferred to a cryo-holder for examination via transmission electron microscopy on a JEM 2100 LaB_6 TEM (JEOL, Japan).

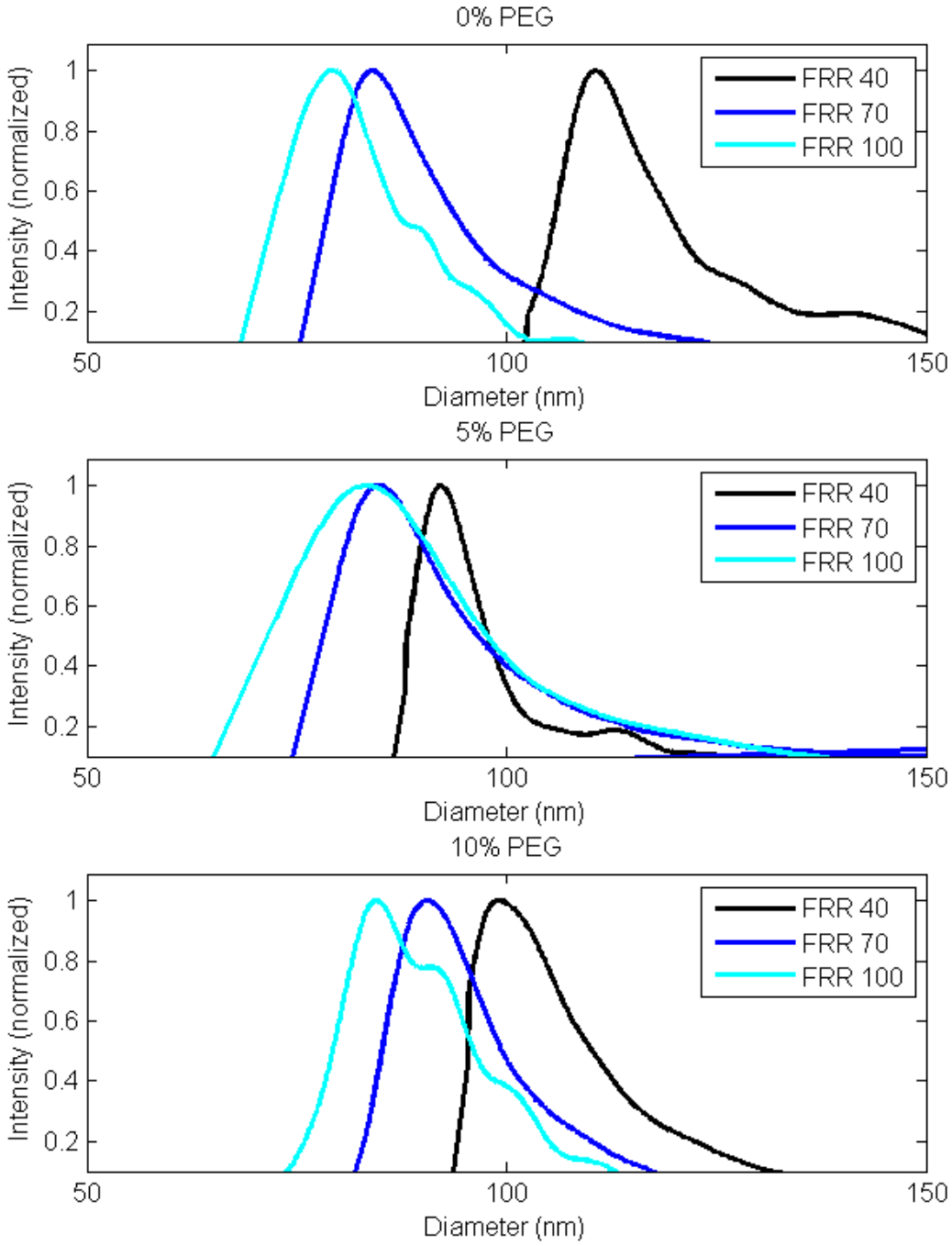

Figure 2.2: Size distributions for liposomes composed of 0%, 5%, and 10% PEG-PE at each FRR. With increased flow focusing (higher FRR values), the diameters of the liposomes decrease in size. This trend is seen across all populations of liposomes, as well as the decrease in average size of liposome across the different lipid compositions at each FRR.

2.4 Results

2.4.1 Impact of PEG on Liposome Size and Distribution

MALLS and QELS in-line with AF^4 provided size information about the populations of liposomes produced by the microfluidic device. A single peak was present in each set of light scattering data obtained for all PL samples, indicating the presence of one primary species in the liposome samples with no aggregate formation (data not shown). The average geometric radii of the particles were determined by comparison against a coated sphere model (provided in the ASTRA software) and converted to diameters (**Figure 2.2**). The modal diameter was taken as the average for each population (**Figure 2.3**).The size distributions of the liposomes followed the

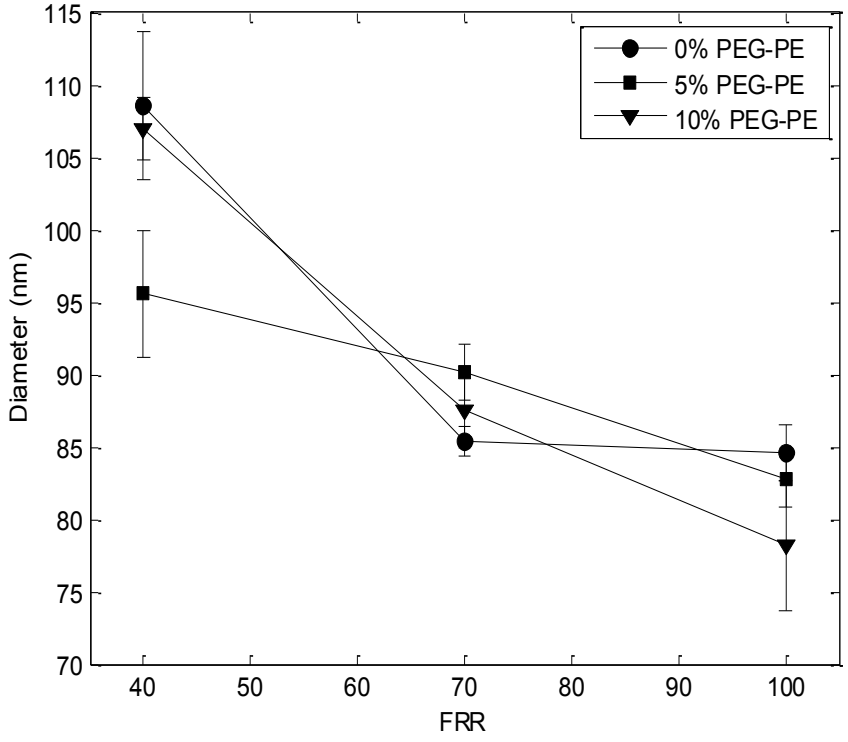

Figure 2.3: Average geometric diameters of liposomes synthesized from lipid solutions with 0%, 5%, and 10% PEG-PE. Error bars are derived from the differential distribution of each liposome population, taken as the full width at half maximum divided by the modal diameter as seen in Figure 2.2.

overall trends observed in former studies, which demonstrated that liposome size is influenced by the flow focusing conditions with size declining as the magnitude of flow focusing increases (*i.e.* higher FRRs).[41,42,44] The increased mismatch of fluid velocities between the alcohol and aqueous buffer flow streams as well as the narrower width of the alcohol flow stream, and therefore decreased diffusion lengths, observed at higher FRRs are thought to play a role in decreasing the size of the liposomes produced.[93] Unlike these previous studies of liposome synthesis by microfluidic hydrodynamic focusing, which employed hybrid silicon/glass chips, the present work was performed using low-cost thermoplastic chips. It is notable that although the microchannel geometries, aspect ratios, roughness, precision, and surface properties all varied significantly from the previous silicon/glass chips, the devices were successful in producing size-tunable liposome populations with similarly low polydispersity as previous work, albeit with somewhat different relationships between flow rate ratio and mean liposome diameter.

2.4.2 Characterization of PEG Incorporation into PLs

The integration of PEG-lipids into PLs was first characterized through zeta potential measurements (**Figure 2.4**). Zeta potential measurements are useful for determining the level of surface coverage by a flexible polymer (*i.e.* PEG), with a decrease in the absolute value of zeta potential corresponding to an increase in PEG grafting on the liposome surface.[94] This decrease corresponds to one of two phenomena: 1) the slipping plane, or the plane where the fluid directly adjacent to the particle becomes mobile,[95] being moved farther away from the liposome's outer surface and thus decreasing the absolute zeta potential, or 2) the physical drag caused by the incidence of long PEG chains on the liposome's exterior membrane leaflet, hence reducing the liposome's mobility and, consequently, zeta potential.[96]

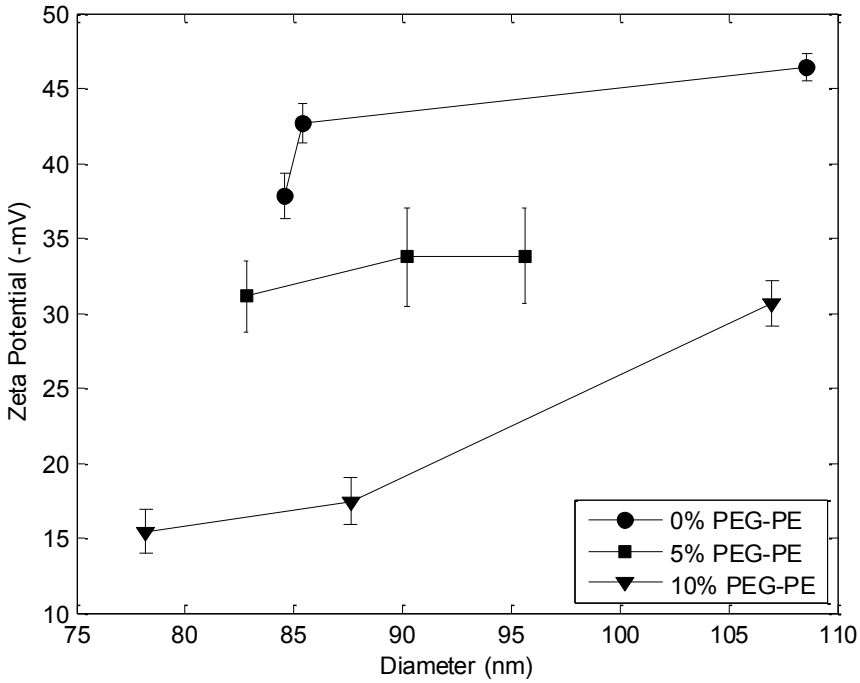

Figure 2.4: Zeta potentials of 0%, 5%, and 10% PEG-PE liposomes. The absolute value of zeta potential decreased with increasing PEG-PE content at each given size, indicating the shielding effect of DCP, an anionic surfactant included in the liposomes, by the PEG molecules on the exterior of the liposomes.

All PL samples exhibited a negative zeta potential due to DCP present in the liposomes, which decreased in absolute value as the PEG-lipid content of the liposomes increased. The absolute value of zeta potential remained relatively constant across the range of sizes produced, with the exception of the largest size formed at the lowest FRR for 10% PEG-PE.

Zeta potential represents the electrokinetic potential of the liposome at a distance from the outer membrane surface and expresses the degree of repulsion of adjacent particles from one another; it is a function of both particle surface charge and the nature of the surrounding environment including surface-bound ligands and thus is a useful tool for investigating the surface characteristics of PEGylated liposomes.

All liposome populations in this study contain equivalent concentrations of anionic DCP (10 mol %) and therefore have approximately equal negative net surface charge per unit area of membrane. However, the long, hydrophilic chains of PEG_{5000} serve as a shield to the liposome exterior, obstructing the negative surface charge provided by anionic DCP. Thus an increase of PEG molecules within the double layer will reduce the absolute value of the zeta potential due to the shielding effect of PEG on the negatively-charged liposome surface. Although a small amount of ethanol is present within each sample, the low mole fraction of ethanol in water at the various FRRs used does not result in significant changes in viscosity or dielectric constant,[97] and thus does not appreciably alter liposome mobility.

Zeta potential measurements performed using microfluidic-synthesized liposomes convey successful integration of PEG-modified lipids into the liposomes. As revealed in **Figure 2.4**, zeta potential is inversely correlated with PEG-PE concentration over the full range of liposome sizes studied here, confirming an increase in shielding of lipid charge resulting from higher surface density of PEG in the liposomes at higher PEG-PE concentrations. Overall, the decrease in the magnitude of zeta potential with increase in PEG-PE content provides strong confirmation that the PEG-lipid conjugates are successfully incorporated into the bilayer during the microfluidic flow focusing process.

Incorporation of PEG lipids into PLs was further evaluated using absorption spectroscopy measurements performed in-line with AF^4. **Figure 2.5** depicts absorbance measurements over the same ranges of FRR and PEG_{5000}-PE concentration employed in the previous set of experiments. The presented data reflects the integrated absorbance at λ=520 nm measured over a 3 min AF^4 elution time centered at the liposome elution peak to account for variations in liposome size distributions at each FRR. Note that the AF^4 fractionation ensures that any free PEG_{5000}-PE or PEG_{5000}-PE micelles within the microfluidic outflow do not contribute to the

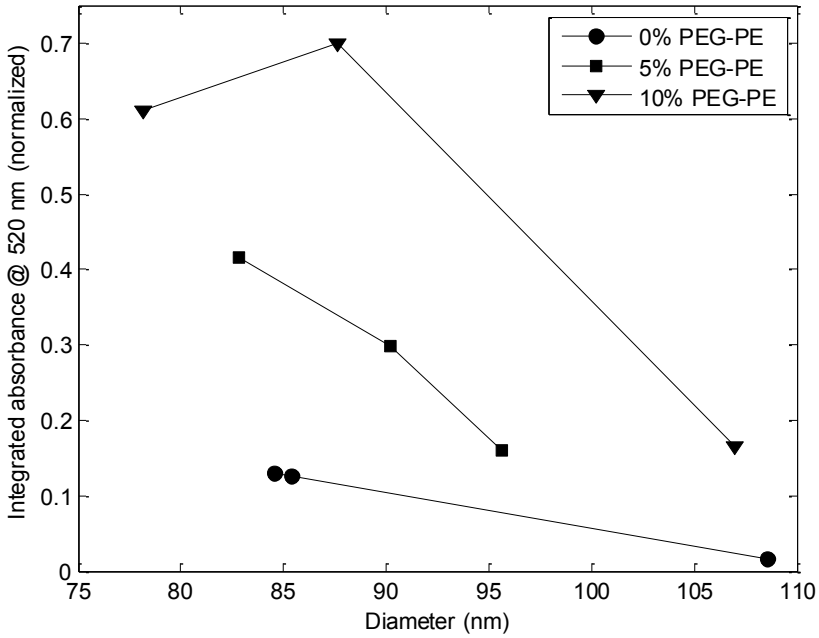

Figure 2.5: Absorption measurements at λ=520 nm performed in line with AF^4 for 0%, 5%, and 10% PEG-PE liposomes. Each datum reflects the integrated absorbance intensity over a 3 min elution period centered on the liposome elution peak. Liposomes with 5% and 10% PEG-PE show significantly enhanced absorbance due to the presence of PEG on the liposomes.

measurements in this test, which solely reflect the absorbance of the liposomes themselves. The integrated absorbance values presented in **Figure 2.5** are further normalized to the maximum level measured in this set of experiments.

Finally, PLs were analyzed with cryo-TEM imaging with 0 and 10 mol% PEG_{5000}-PE to verify liposome size and lamellarity. The cryo-TEM images of the 10% PEG liposomes did not reveal any form of micelles or aggregates, which supports the previous arguments that all PEG-lipids were incorporated into the liposomal membranes (**Figure 2.6**).

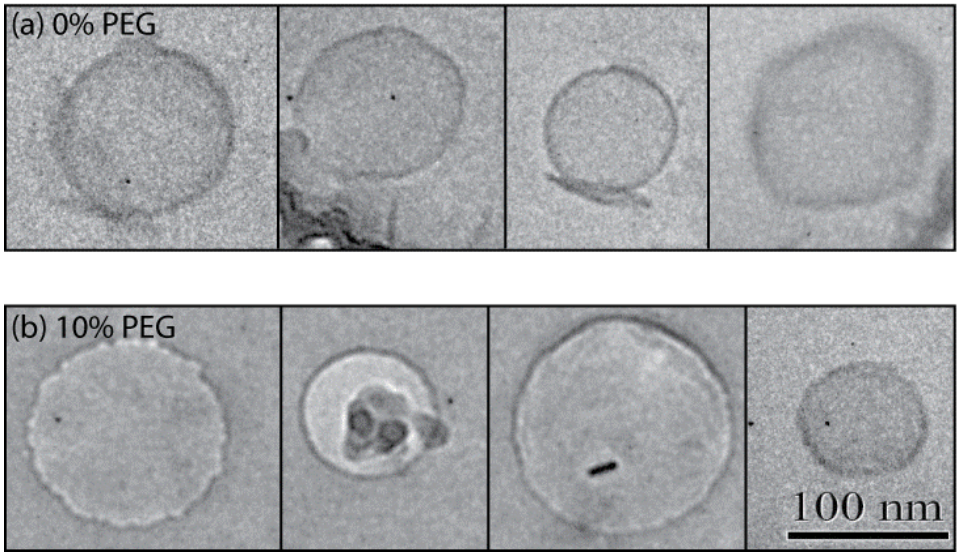

Figure 2.6: Cryo-TEM images of liposomes formed using a lipid solution containing (a) 0% and (b) 10% PEG-lipid. Imaging results confirm the formation of unilamellar vesicles absent micelles or aggregates in both cases. Small ice crystals or artifacts that commonly form during vitrification, sample transfer, or elevation of specimen temperature due to the electron beam during cryo-TEM imaging seen in several images[105] do not reflect the presence of lipid aggregates.

2.4.3 Characterization of Folate Incorporation into FPLs

To evaluate the incorporation of folate-PEG lipids into FPLs, quantitative analysis of the concentration of folate in the liposomes was enabled by absorbance measurements taken at λ=280 nm after being fractionated via AF^4. Using a molar extinction coefficient of (ε = 25,280 M^{-1} cm^{-1}),[98] the concentration of folate was determined by UV-Vis absorption measurements performed in-line with AF^4. A comparison of the measured folate content as a percentage of the hypothetical folate concentration calculated from the lipid mixture introduced for the given flow conditions is presented in **Figure 2.7**. Absorbance values obtained for control liposomes were used as a baseline for all measurements to account for the absorbance caused by native lipid species. All of the resulting liposome populations, formed using a lipid mixture containing 2 mol

% PEG_{2000}-Folate-PE, showed a single peak of maximum absorbance coincident with the peak signal from light scattering, confirming that folate is only present in the liposome sample and is not eluted at a later time point as an aggregate. Folate content for FPLs was in general agreement with the calculated values. Additionally, a small signal was seen for PLs, indicating the presence of an additional species (PEG) on these vesicles (data not shown).

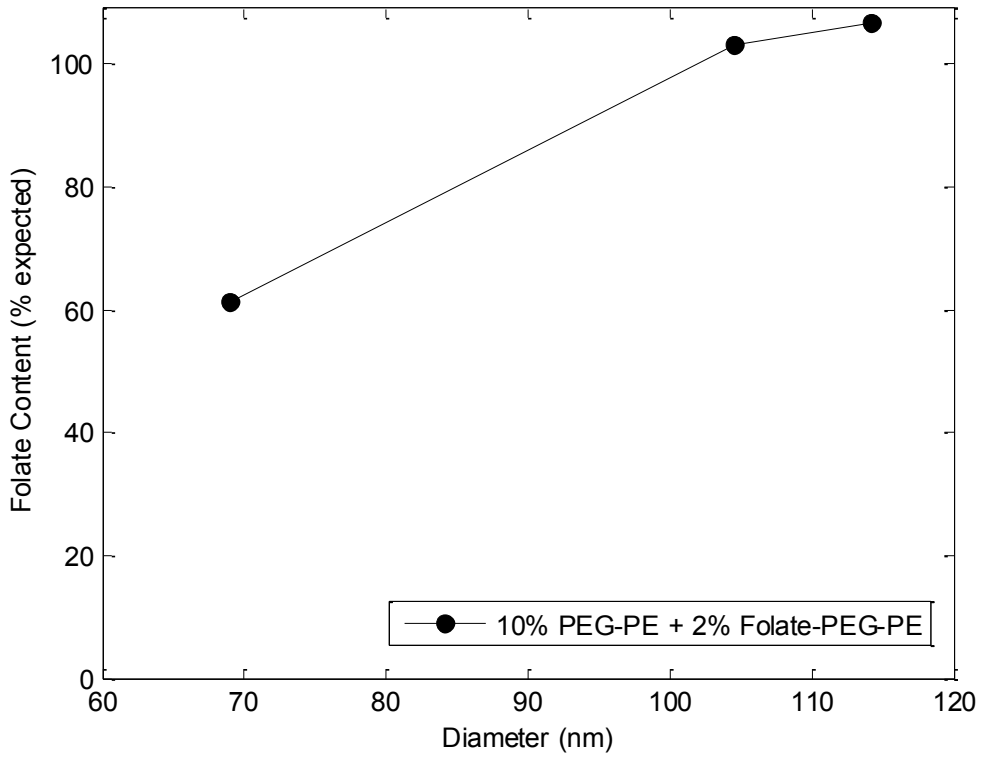

Figure 2.7: UV-vis absorption data in line with AF^4 from folate (10% PEG-PE + 2% folate-PEG-PE) liposome samples, normalized to control (0% PEG-PE + 0% folate-PEG-PE) liposomes. Experimental values of liposome folate content are overall in agreement with theoretical values.

2.5 Discussion

Ongoing developments in the field of nanotechnology are enabling advances in drug delivery systems based on precisely engineered and functionalized nanoparticles. In particular, liposomes are a widely exploited class of nanoparticles due to their advantageous qualities and have played a noteworthy role in recent pharmacological advancements.[65] Despite rapid growth in nanoparticle-enabled therapeutics, there remain significant limitations which must be addressed in order for nanoparticles to reach their full potential as pharmacological agents. Key challenges facing existing nanoparticle systems include restricted particle size control and reproducibility, high cost of production, challenging and costly methods for realizing tailored formulations, and indeterminate stability of the resulting therapeutic nanoparticles.[99,100]

Nanoparticle behavior *in vivo* can vary drastically as a function of size, with significantly dissimilar pharmacokinetics and biodistribution resulting from small size variations.[101] The synthesis of liposomes possessing well-defined sizes is particularly challenging, with conventional preparation methods commonly relying on poorly-controlled self-assembly of amphipathic constituents in turbulent flows, resulting in broad size distributions that require multiple post-processing steps to reduce polydispersity. This constraint increases both the time and cost of production, using processes that are further limited by the precision of the available materials used for the post-processing modification steps (*e.g.,* size irregularity of nanometer-scale pores in polycarbonate membranes used for extrusion). The microfluidic method employed here enables controlled formation of liposomes by utilizing the intrinsic property of lipids to systematically self-assemble under laminar flow profiles which facilitate controlled diffusive mixing between miscible fluids and lipid species that exhibit differential solubility within the diffusing fluid streams. Microfluidic-directed formation of liposomes is a rapid process that produces liposomes with exceptionally low polydispersity, with narrow size distributions

significantly smaller than liposome populations obtained through conventional bulk scale methods. At the same time, it is a single-step in-line process that eliminates the need for additional steps and equipment to be used for size homogenization. A central advance in the present work lies in application and characterization of the microfluidic technique toward the formation of functionalized liposomes, including the appendage of PEG and folate as a targeting ligand to the liposomal exterior, in a simple one-step process. Moreover, because the microfluidic technique eliminates the need for time consuming post-processing size homogenization and ligand insertion, liposomes may be rapidly prepared with custom formulations. This concept offers future potential for point-of-care applications, reducing the need for liposome preparations to maintain a prolonged shelf life. For example, liposomes with encapsulated enzymes and proteins have a limited shelf life, in some cases on the order of only hours or days, when simple electrostatic stabilization is employed.[1] As a more aggressive future application of the technology, the microfluidic technique may also offer a path to on-demand synthesis of personalized drug formulations based on custom dosing, drug mixtures, or targeting ligands. The microfluidic technique is also shown to produce functionalized liposomes with tunable size and extremely narrow size distribution. It is expected that this feature will improve control over dosage while allowing more accurate prediction of the therapeutics' fate *in vivo*. In addition, the ability to synthesize narrow distributions of functionalized liposomes will enable unique pharmaceutical research opportunities, such as the investigation of pharmacokinetic and pharmacodynamic relationships across a range of liposome sizes which are nearly impossible to accurately assess using traditional methods.

Here the ability to produce liposomes of tunable size with narrow size distributions is demonstrated, similar to previous studies,[41,42,44] but within a low-cost thermoplastic microfluidic platform. Preceding studies relied on microchannels created using costly materials (silicon or

glass wafers and nanoports) as well as expensive, unnecessarily complicated fabrication techniques involving photolithographic patterning and high aspect ratio etching methods such as deep reactive ion etching. The present study abolishes the need for expensive materials and processes by exhibiting the ability to produce nearly monodisperse liposomes in a continuous flow process similar to previous studies within microchannels created in thermoplastic microfluidic chips via a two-step hot embossing technique, utilizing simple, inexpensive fabrication methods with much lower processing times. The transition from silicon to thermoplastic devices enables the microfluidic-directed liposome formation technique to be easily adopted in settings without cleanroom capabilities and significantly reduces the cost of device production. In addition, the use of inexpensive replication methods for microfluidic chip fabrication presents a realistic and cost-effective path toward parallelizing the synthesis process, using multiple flow focusing chips acting in tandem for the rapid production of large volumes of liposomes.

Unlike previous work using isopropanol as a solvent for microfluidic-assisted liposome formation, here ethanol has been employed as a lipid carrier. The use of ethanol is significant for *in vivo* applications as its toxicity is significantly lower than that of other organic solvents, with a lethal blood level between 350–500 mg/dL, compared with 130–200 mg/dL for both methanol and isopropanol.[102] While solvents other than ethanol may also be suitable for use with the microfluidic technique, each must be evaluated on an individual basis. For example, because chloroform is immiscible in water, the microfluidic method is not compatible with chloroform as a lipid carrier. Other carriers that are both miscible in water and compatible with the COC substrates used in these studies, such as butanol, are likely to be feasible. However, the lateral distribution of solvent during flow focusing, and thus the point at which lipids self-assemble into leaflets and ultimately closed vesicles, is dependent on the nonlinear relationship between

viscosity and solvent concentration across the diffusive water/solvent interface,[44] and thus the size distributions of the resulting liposomes are expected to vary with solvent selection.

While prior work has focused on relationships between flow conditions and liposome size using native lipids, here the focus is to evaluate the impact on liposome size and size distribution by the addition of PEG5000-lipid to the initial lipid mixture used in the microfluidic flow focusing process. The microfluidic device produced narrowly-distributed populations of liposomes with an overall decrease in liposome size with an increase in FRR, regardless of the presence of PEG-PE in the lipid mixture (**Figure 2.2**). Liposomes formed in the absence of PEG were found to exhibit an inverse relationship between FRR and liposome diameter, as shown in **Figure 2.3**. The error bars in this figure reflect the FWHM distribution of each liposome population. This figure also reveals a very similar behavior for PLs formed at both concentrations of PEG5000 explored in this study. The liposome populations produced by the microfluidic flow focusing method do not significantly change with PEG5000-lipid concentration, but remain largely controlled by the flow conditions used in the focusing process. This is not necessarily an expected outcome considering the roles of hydrodynamics and diffusion in the liposome formation process.[44] The average on-chip residence time in these studies was only 250 ms, and liposome formation likely occurs within an even shorter time during the initial mixing zone at the confluence of the lipid and aqueous streams. Given that PEG5000 is approximately eight times the molecular weight of the native lipids used in the initial mixture, differences in diffusive transport for the PEG-modified lipids as well as steric hindrance during the self-assembly process could be expected to affect the liposome formation process. The data presented in **Figure 2.2** and **Figure 2.3** reveals that the microfluidic process produces liposomes with consistent size under the given range of flow conditions despite the

inclusion of PEG-modified lipids. Similarly, no significant variation in liposome size distribution is observed.

As revealed in **Figure 2.4**, zeta potential was found to be directly correlated with liposome radius, with the strength of this correlation depending on PEG-PE concentration. This latter observation may result from reduced steric interactions between PEG chains for higher curvature vesicles,[103] encouraging preferential incorporation of PEG-PE into smaller liposomes and concomitant increase in charge shielding. Additionally, the shielding effect PEG on the liposome is greater at 10 mol % PEG-PE than at 5 mol % PEG-PE. The greater degree of observed charge shielding at each liposome size for the 10 mol % PEG-PE liposomes may be due to the anticipated formation of a brush configuration at this high PEG concentration, Although further characterization is needed to verify this hypothesis, surface-grafted PEG molecules are known to prefer a tightly packed brush configuration resulting in extension of the linear PEG chains at high surface concentrations, while a more loosely arranged mushroom or transition regime occurs at lower concentrations.[104] Overall, the inverse correlation between zeta potential and PEG-PE content reveals that the PEG-conjugated lipids are effectively incorporated into the liposomes using the microfluidic flow focusing process. The incorporation of PEG-lipids was further confirmed by UV-vis absorbance analysis (**Figure 2.5**), with the resulting data consistent with the hypothesis that incorporation of PEG-PE lipids is favored during interactions with higher curvature membranes, and thus are more readily incorporated into smaller liposomes.

Cryo-TEM imaging was performed to ensure that the presence of large PEG molecules did not affect vesicle unilamellarity. The imaging results shown in **Figure 2.6** reveal a spherical morphology and overall agreement in size compared to the size information obtained from light scattering. PEGylated liposomes and control liposomes appear similar size and shape. While PEG cannot be directly imaged via electron microscopy without the addition of contrast

surfactants due to insufficient electron density,[105] the data confirms that unilamellar liposomes are formed in both cases, with an average membrane thickness of 5.4 ± 0.6 nm corresponding to the expected bilayer membrane thickness of DMPC in water.[106] Lipid bilayer thickness was determined using the scale bar provided by the TEM instrument, with each reported value reflecting the average from 4 measurements performed on 4 individual liposomes.

Figure 2.7 shows the concentration of folate on FPLs from values obtained via the UV-vis absorption spectroscopy. The integrated values for folate are largely in agreement with the expected folate content, indicating successful inclusion of PEG_{2000}-Fol-PEinto the FPLs at approximately the same molar ratio of folate-conjugated lipids in the initial lipid mixture. The larger FPLs with diameters above 100 nm, corresponding to FRRs of 40 and 70, exhibited folate concentrations slightly above the initial mixture concentration. While the measured folate concentration in the smaller FPLs was only 60% of the initial molar ratio, this may be due to the reduced liposome concentration associated with the high FRR value of 100 used to form these FPLs, resulting in absorbance signals near the detection limit of the UV-vis spectrometer. Thus, while all of the liposomes exhibited clear evidence of folate incorporation, the high level of uncertainty in the absorbance data for the smallest liposomes does not support a conclusion that the final concentration of folate is related to liposome size.

Application of the microfluidic technique to liposomal drug preparation will require scale-up of the technology for the production of large liposome volumes at concentrations suitable for *in vivo* use. Ultimately, a dense array of individual flow focusing elements fabricated on a single 10 cm square thermoplastic chip could be implemented, with on-chip flow splitters used to control the delivery of solvent, buffers, and functional reagents to the parallel flow focusing channels. Of the parameters known to have a direct impact on liposome size, including channel geometry, temperature, and buffer ionic strength, liposome size is most sensitive to changes in FRR.

Photolithographic control of the imprinting mold used for channel fabrication can ensure uniform hydrodynamic resistance across the microchannel array, and thus uniform flow rates and FRR values for precise and reliable control over liposome size during process scale-up.

2.6 Conclusion

This chapter demonstrates the successful extension of microfluidic-directed liposome formation technology to include the continuous, controlled synthesis of nearly monodisperse populations of PEG-modified and folate receptor-targeted liposomes. Liposomes comprised of DMPC and cholesterol with varying compositions of PEG_{5000}-lipids, PEG_{2000}-lipids, and folate-PEG_{2000} lipids have been successfully formed using a thermoplastic microfluidic chip enabling adjustable hydrodynamic focusing of a stream of lipids dissolved in an organic solvent by miscible streams of an aqueous buffer. Despite the large difference in molecular weight between the native lipids explored in previous studies and the PEG-lipid and folate-PEG-lipid conjugates used in this chapter, no significant difference in liposome size or size distribution was observed between these two cases. This technique opens doors for a variety of liposome applications, such as the ability to provide PEG-modified liposomes and folate-targeted liposomes with tunable characteristics and lipid compositions for targeted drug delivery. Further, the ability to achieve rapid, one-step synthesis of functionalized, unilamellar liposomes has great potential for further development toward the realization of on-chip liposome "microfactories" wherein liposome formation, liposome functionalization, and drug encapsulation is performed with real-time control over the resulting nanocapsule properties.

Chapter 3 : Microfluidic Remote Loading for Rapid Single-Step Liposomal Drug Preparation

3.1 Summary

Microfluidic-directed formation of liposomes is combined with in-line sample purification and remote drug loading for single step, continuous flow synthesis of small, nearly monodisperse vesicles containing high concentrations of stably loaded drug compounds. Using microfluidic buffer exchange within an on-chip microdialysis zone, the system enables the rapid formation of large transmembrane pH and ion gradients, followed by the immediate introduction of amphipathic drug for remote loading into the vesicles. The result is a microfluidic process enabling in-line formation of liposomes containing remotely loaded compounds at drug:lipid molar ratios of up to 1.3 with a total on-chip residence time of approximately 3 min, representing a significant improvement over conventional bulk scale methods which require hours to days for combined liposome synthesis and remote drug loading. The microfluidic platform may be further optimized to support real-time generation of purified liposomal drug formulations with high concentrations of drugs and minimal reagent waste for effective liposomal drug preparation at or near the point of care.

3.2 Introduction

An important feature for the enhanced clinical utility of liposomal drugs has been the development of effective methods for loading high concentrations of therapeutic compounds into lipid vesicles. Strategies for encapsulation of drugs into liposomes may be categorized as either passive or active. Passive encapsulation is inefficient,[15] provides limited attainable drug-to-lipid ratios (D/Ls) due to drug solubility,[107] and often results in instable formulations in which drugs

are able to migrate out of the vesicles over time.[108] In contrast, active encapsulation (remote loading) results in stable formulations of liposomes with a high D/L. Because *in vivo* toxicity is inversely related to D/L,[61] increased drug concentration is a highly desirable attribute for nanoparticle-enabled therapeutics.

A microfluidic system that enables rapid and efficient remote loading of amphipathic drugs into nanoscale liposomes is reported in this chapter, combining liposome synthesis and remote drug loading in a seamless integrated process. Unlike established bulk methods for remote drug

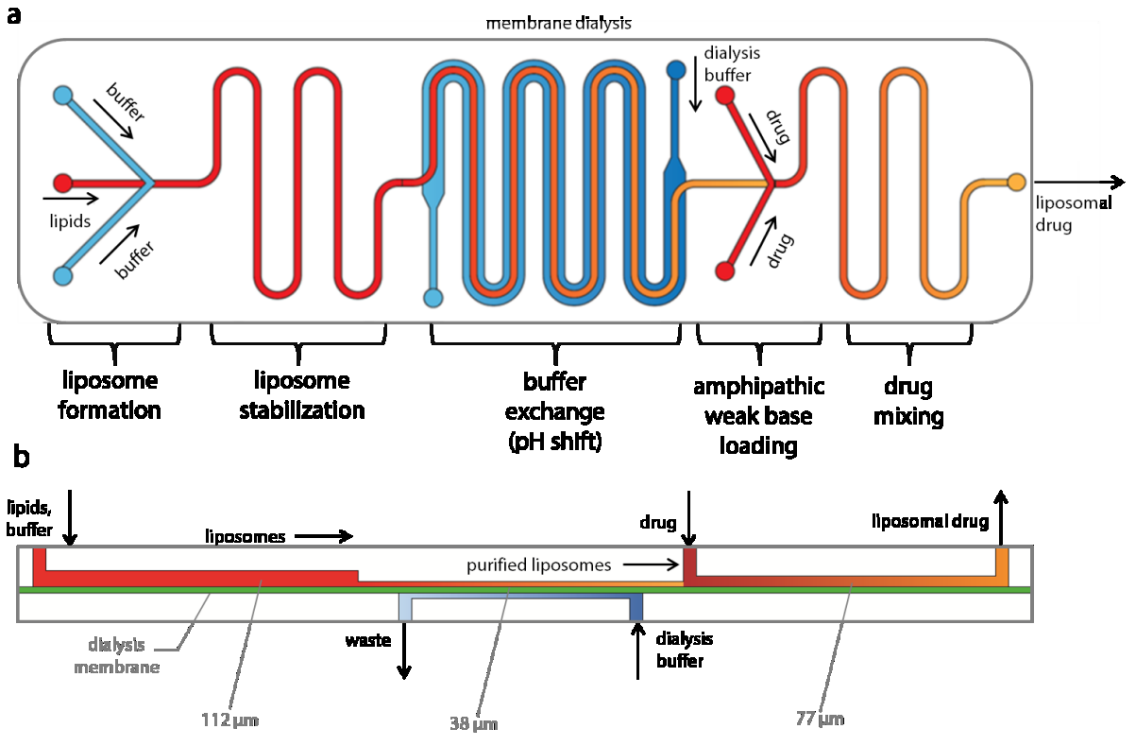

Figure 3.1: (a) Schematic of the fully-integrated microfluidic device for remote loading of liposomal therapeutic nanomedicines in-line with liposome synthesis and buffer exchange via microdialysis for rapid generation of nearly monodisperse, functionalized liposomes with tunable diameters containing high concentrations of stably loaded compounds. (b) Cross-sectional view of the microfluidic system, revealing the differing channel heights for different microfluidic processes, enabled by the dry film resist fabrication process.

loading, in which each process step is performed in a series of discrete manual operations using large fluid volumes, the microfluidic system incorporates liposome formation, buffer exchange, and liposome/drug mixing and incubation in a continuous flow process. The platform (**Figure 3.1**) takes advantage of an established microfluidic hydrodynamic flow focusing method for the formation of functionalized, nearly monodisperse liposomes.[41–44,86] The liposome synthesis technology is extended in this chapter with the addition of a counterflow microdialysis element, enabling steep transmembrane ion gradients to be formed immediately prior to remote drug loading. The system further implements a drug loading and incubation zone that includes micromixer structures to enhance interactions between liposomes and amphipathic compounds during the remote loading process. The resulting device decreases the processing time for liposome preparation and remote drug loading from a multi-day process to less than 3 minutes, with resulting D/L values up to 5 times greater than typical liposomal therapeutics prepared by conventional bulk scale processes.[109]

3.3 Materials and Methods

3.3.1 Device Fabrication

Microchannels were fabricated in polydimethylsiloxane (PDMS) substrates by soft lithography techniques using dry film photoresist molds[110] produced in a multilayer lamination process. Dry film photoresist (Riston MM115i, DuPont, Research Triangle Park, NC) was laminated onto a clean glass slide at 110 °C using a feed rate of 0.02 m/s and placed on a hot plate at 110 °C for 20 min to promote adhesion. The substrate was patterned by contact photolithography using an ultraviolet (UV) flood exposure instrument (PRX-1000; Tamarack Scientific Co., Corona, CA) at a dose of 72 mJ/cm^2 for a single layer of photoresist. Multiple photoresist layers were processed sequentially using this approach, with a 1.2x increase in UV

dose per layer. Each layer of the dry film photoresist is approximately 37 μm, as measured using by stylus profilometry. Following UV exposure, the multilayer substrate was developed using a 1 wt% sodium carbonate solution. The resulting molds feature 3 regions with 3 different channel heights (**Figure 3.1**). Specifically, the flow focusing and liposome stabilization region was 30 μm wide and 112 μm deep, the buffer exchange region was 1.2 mm wide and 37 μm deep, and the drug loading and mixing region was 30 μm wide and 77 μm deep. Buffer counterflow channels were 1.2 mm wide and 37 μm deep.

The dry film photoresist molds were next used to create microchannels in PDMS. Two separate molds were used to form an upper substrate containing flow focusing, buffer exchange, and drug loading channels, and a lower substrate containing a buffer counterflow channel to assist in microdialysis. The molds were placed in plastic petri dishes and a 10:1 (w:w) mixture of pre-polymer PDMS elastomer and curing agent (Sylgard 184, Dow Corning Corp. Midland, MI) was poured on top. Vacuum was applied to remove air bubbles, and the petri dish was placed in a convection oven at 80 ºC for 4 h to ensure complete curing of the PDMS. The PDMS substrates were removed from the molds and sectioned using a fresh scalpel. Holes for inlet and outlet interfacing were made using a microbore biopsy punch (Harris Uni-Core, Ted Pella, Inc., Redding, CA). All PDMS surfaces were cleaned with isopropanol and DI water.

To form the microdialysis elements, 12-14 kDa molecular weight (MW) cutoff regenerated cellulose (RC) membranes Spectra/Por 4, Spectrum Laboratories Inc., Rancho Dominguez, CA) were placed between the upper and lower PDMS substrates. The membranes were selected to ensure that the nominal pore size (<4 nm)[111] is below the minimum liposome size but large enough to allow all individual chemical species and buffer salts to transport efficiently through the membrane. The RC membranes were cut into patterns similar to the microchannel geometries using an automated craft cutter (Cameo Digital Craft Cutting Tool, Silhouette America, Inc.,

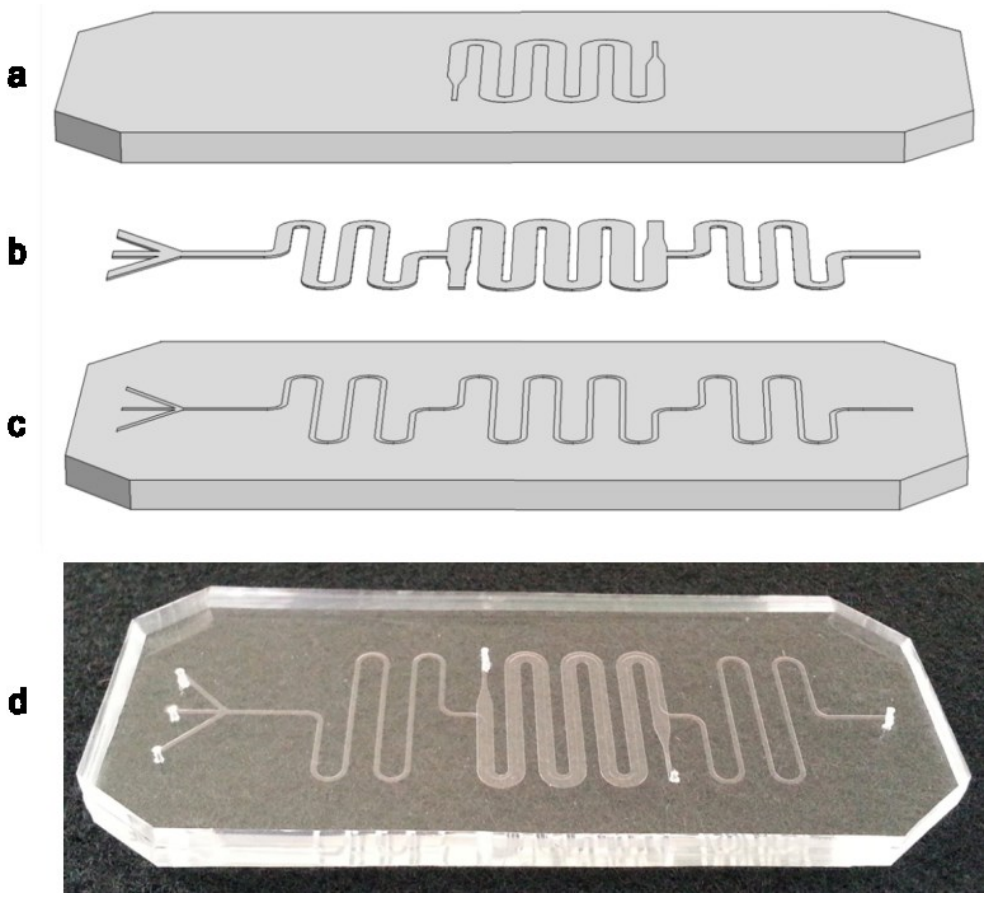

Figure 3.2: Schematic (exploded view) (a-c) of the PDMS/cellulose hybrid microfluidic device with a) a channel for buffer counterflow b) patterned nanoporous regenerated cellulose dialysis membrane, and c) sample channel for liposome synthesis, buffer exchange, and remote drug loading; and d) a photograph of a fabricated device.

Orem, UT), allowing space between adjacent channels for direct PDMS-PDMS contact in these regions. The patterned membranes were flattened using a hydraulic hot press (Carver, Wabash, IN) at 0.7 MPa for 10 min at 110 ºC prior to chip integration. To enhance sealing between the PDMS substrates, a 10:1 (w:w) mixture of pre-polymer PDMS elastomer and curing agent was poured over a glass slide and spin coated at 3500 rpm for 60 s. The bottom piece of PDMS containing the counterflow channels was stamped onto the thin layer of PDMS, which served as a sealing agent for the microchannels. The patterned RC membrane was aligned with the microchannels on the top piece of PDMS containing the flow focusing, dialysis, and drug

loading regions. The two substrates were aligned and pressed together by hand, then placed in a convection oven at 80 ºC overnight to cure the intermediate PDMS bonding layer. **Figure 3.2** represents a schematic of an exploded view of the device components as well as a photograph of the actual device.

3.3.2 Lipid Mixture and Hydration Buffer Preparation

Lipid mixture preparation and hydration buffer were prepared as previously described (Chapter 2.3.2, p. 21). Briefly, DMPC, cholesterol, and PEG2000-PE were combined in chloroform at a molar ratio of 55:35:10. The lipid mixture was desiccated under vacuum then re-dissolved in anhydrous ethanol for a total lipid concentration of either 40 mM or 20 mM, as noted.

Ammonium sulfate (250 mM, adjusted to pH 4.6) and isosmotic HEPES (10 mM with 140 mM sodium chloride, adjusted to pH 7.6) were prepared for microdialysis and remote loading experiments. In some cases, trisodium 8-hydroxypyrene-1,3,6-trisulfonate (pyranine) (Invitrogen) was added to the buffers for pH measurements (1 μM). Acridine Orange hydrochloride (AO) at an initial concentration of 10 mg/mL (Sigma-Aldrich) was further diluted in deionized water as noted and used for remote loading experiments. Doxorubicin hydrochloride (DOX) (Sigma-Aldrich) was diluted to 1.4 mg/mL for in-line synthesis and remote loading experiments. All solvents and buffers were passed through 0.22 μm filters before being introduced to the microfluidic device.

3.3.3 Buffer Exchange and Remote Drug Loading

Microfluidic devices comprising only the 27 cm long buffer exchange zone (sample channel and buffer counterflow channel) were first used to characterize performance of the microdialysis element for rapid ion exchange and remote drug loading. To evaluate buffer exchange,

ammonium sulfate (pH 4.6) was injected into the sample inlet and isosmotic HEPES (pH 7.6 or pH 9.6) was injected into the buffer counterflow inlet with the resulting sample collected for analysis. Sample and counterflow flow velocities were kept equal to one another, and varied from 0.3 cm/s to 0.6 cm/s (approximately 7 μL/min to 14 μL/min, respectively). Pyranine was used as a pH-sensitive molecular probe to determine the pH of the sample and counterflow buffer eluents. Fluorescence intensity maxima of pyranine at 400 nm and 450 nm is strongly dependent on hydrogen ion concentration, and thus measuring the ratio of the 510 nm fluorescence signal at these excitation wavelengths allows solution pH to be determined.[112] Off-chip samples as well as standard curves for calibration over the range from pH 3 to pH 12 were measured using a SpectraMax plate reader (Molecular Devices, Sunnyvale, CA).

To assess the remote drug loading process following buffer exchange, liposomes were first prepared in a separate microfluidic chip by hydrodynamic flow focusing.[41–44] Briefly, hybrid PDMS-glass devices with 50 μm wide and 300 μm deep microchannels were fabricated, and lipid-ethanol mixture (40 mM) was injected into the microfluidic device between two sheath flows of ammonium sulfate buffer (250 mM, pH 4.6). The flow rate ratio, defined as the ratio of the volumetric flow rate of the aqueous buffer to the flow rate of lipids in ethanol,[41–44] was set to 20. Total linear flow velocity was set to 12.5 cm/s, or an equivalent volumetric flow rate of 112 μL/min. To reduce vesicle size, the microfluidic device was operated on a hot plate at 50 °C throughout synthesis.[93] The resulting liposome size distributions were characterized via dynamic light scattering (Nano ZSP, Malvern Instruments Ltd., UK).

The liposomes in ammonium sulfate buffer were injected into the inlet of the microdialysis chip with isosmotic HEPES (pH 7.6) as the buffer counterflow. AO, an amphipathic dye used as a drug analog for remote loading experiments, was introduced through a secondary channel immediately after buffer exchange at a ratio of 1:3 relative to the sample channel volumetric

flow rate. Liposome sample velocity was varied from 0.17 cm/s to 0.44 cm/s with AO concentration constant at 0.25 mg/mL to investigate the effect of flow velocity and residence time on loading concentration and efficiency. AO concentration was varied from 0.125 mg/mL to 2.5 mg/mL (corresponding to D/L values of 0.22 to 4.35, respectively) with the flow velocity held constant at 0.26 cm/s to explore the effect of AO concentration on loading efficiency and maximum D/L levels in the resulting drug-laden liposomes.

To analyze AO concentrations, liposome samples were collected following AO loading and placed into 7 kDa MW cutoff dialysis units (Slide-A-Lyzer MINI; Pierce, Rockford, IL) with isosmotic HEPES as the exchange buffer. The samples were dialyzed for 4 h with 3 buffer exchanges to ensure complete purification of free AO. Absorbance measurements of the purified samples as well as a serial dilution of AO in buffer at λmax=495 nm were taken using a plate reader (SpectraMax; Molecular Devices, Sunnyvale, CA) to determine encapsulated AO concentration.

3.3.4 Numerical Simulation of Ion Exchange via Microdialysis

Exchange of ammonium sulfate ions during microdialysis was investigated via numerical simulations with a two-dimensional model using COMSOL Multiphysics 4.1 (COMSOL, Inc., Burlington, MA). The Transport of Diluted Species (chds) physics interface was applied for the simulation to depict the concentration profiles of the ammonium sulfate salt within the microchannels. Microchannel dimensions from the actual devices fabricated and RC membranes used for the study were used to build the model, as well as the known value of the diffusion coefficient of ammonium sulfate in water at room temperature ($D_{Ammoinum\ Sulfate}$= 8.0 x 10^{-6} cm^2/s).[113]

3.3.5 In-Line Liposome Synthesis and Drug Loading

An integrated device containing a liposome formation region, microdialysis buffer exchange region, and drug loading region was used to evaluate the overall process. For liposome formation, lipid-ethanol solution (20 mM) was injected into the flow focusing element between two sheath flows of aqueous ammonium sulfate buffer (250 mM, pH 4.6). The total volumetric flow rate was 6 μL/min (corresponding to 0.26 cm/s in the dialysis region) with a flow rate ratio of 10. The microdialysis counterflow buffer flow rate was matched to the primary flow rate to minimize the average pressure gradient across the RC membrane. The drug:liposome sample flow rate ratio was 1:3 for all experiments. For drug loading, both AO (0.5 mg/mL and 1.0 mg/mL, corresponding to initial D/L values of 0.22 and 0.44, respectively) and DOX (1.4 mg/mL, corresponding to an initial D/L of 0.44) were investigated. Multiple samples were collected (n=3) for each test.

To ensure that free drug remaining in the collection buffer following remote loading did not affect concentration measurements, collected liposome samples were further dialyzed off-chip with isosmotic HEPES as the exchange buffer. Two aliquots of each sample, one off-chip and one two-fold dilution, were dialyzed for 4 h with 3 buffer exchanges for complete purification of free DOX or AO. Absorbance measurements of the purified samples as well as a serial dilution of DOX or AO in buffer were compared with standard curves to determine final encapsulated drug concentration. Size distributions of collected samples were further characterized by dynamic light scattering (Nano ZSP, Malvern Instruments, Inc.).

3.4 Results and Discussion

3.4.1 Counterflow Microdialysis for Buffer Exchange

Counterflow microdialysis provides an efficient method for on-chip buffer exchange, enabling rapid transport and removal of free ions from the sample buffer while preventing loss of nanoparticles during the exchange of small ions across the microdialysis membrane. To evaluate performance of this approach for establishing transmembrane ion gradients prior to remote drug loading in a rapid flow-through format, a PDMS-RC device consisting solely of the counterflow microdialysis zone was fabricated. Characterization of the device for ion exchange was first evaluated by introducing buffers at different pH values through the sample and counterflow ports. Rapid pH change of the sample flow was observed, as revealed through pyranine

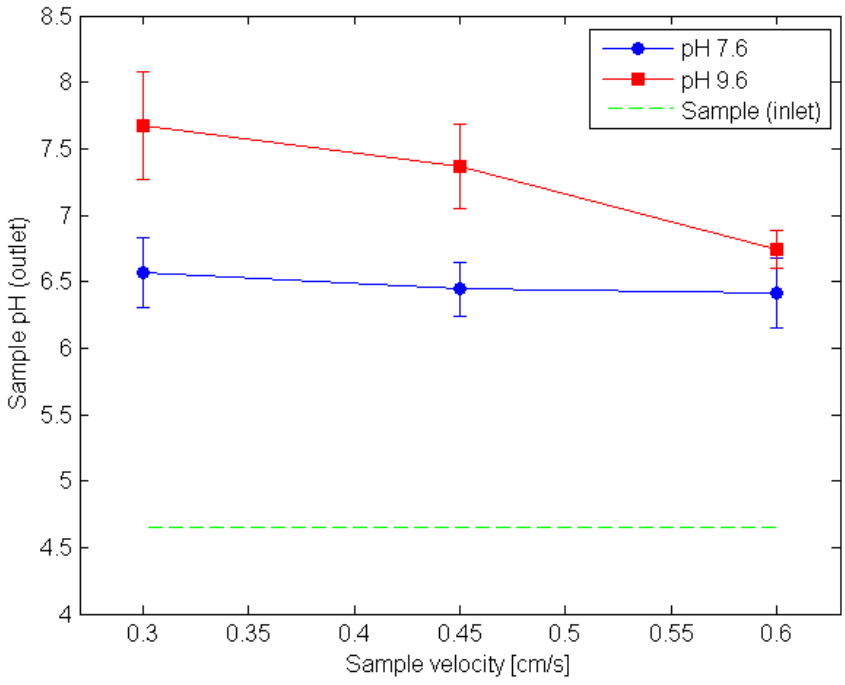

Figure 3.3: Demonstration of on-chip microfluidic buffer exchange via membrane dialysis at various counterflow pH and flow velocities. Residence times vary from 40 s to 80 s, resulting in a ΔpH 1.7 to 3.0. Total flow rates vary approximately 7 µL/min to 14 µL/min (0.6 cm/s to 0.3 cm/s, respectively).

fluorescence measurements, with the level of pH shift roughly proportional to residence time as determined by the applied flow rate (**Figure 3.3**). As expected, microdialysis performance was also found to be dependent on counterflow buffer pH, with a greater difference in pH between the sample and counterflow buffers resulting in a larger pH shift at the sample buffer outlet. For the experimental conditions tested, a maximum shift of 3 pH units was achieved using pH 9.6 counterflow buffer and a residence time within the dialysis channel of 83 s. This is substantially faster than bulk scale microdialysis which can take hours for complete buffer exchange to occur.

A prediction for the transport of ammonium sulfate ions during microdialysis can be made by considering simple diffusion within the system. Using the value $D_{Ammonium\ Sulfate}$ = 8.0 x 10^{-6} cm^2/s for the diffusion coefficient of ammonium sulfate in water at room temperature,[113] the diffusion time for a characteristic length scale given by the microchannel height (37 µm) is 1.71

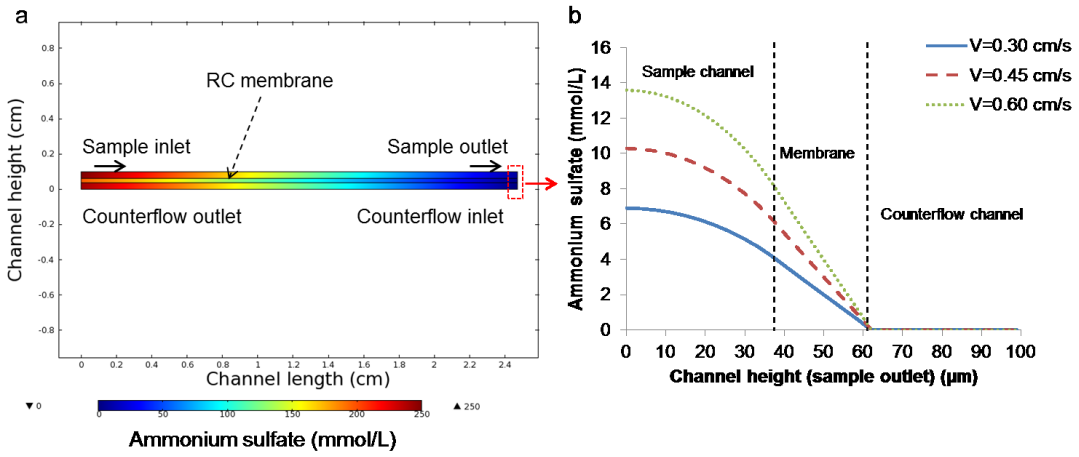

Figure 3.4: Numerical simulation of ammonium sulfate (initial concentration 250 mM) transport in the microfluidic device to verify adequate ion removal: a) depiction of the ammonium sulfate concentration throughout the microdialysis segment of the device (channel length scaled by a factor of 10 for more rapid computation), and b) concentration profile of ammonium sulfate along the sample channel, RC membrane, and counterflow channel at the exit of the dialysis region for flow velocities varying from 0.3 cm/s to 0.6 cm/s.

s, significantly smaller than the residence times explored in these studies which ranged from 42 s to 83 s, To verify this prediction, ammonium ion transport was evaluated through a two-dimensional numerical simulation of the device. As shown in **Figure 3.4**, the model suggests that the extra-liposomal ammonium ion content is reduced by more than 100 times from the initial concentration sequestered within the vesicles, a necessary condition for effective remote loading.[60,114]

A potential concern with the continuous flow microdialysis element is whether liposome size is affected by the process. Prior to buffer exchange, the microfluidic-synthesized liposomes were found to be 80.8 nm in diameter with a very low polydispersity index (PDI) of 0.049. Size distributions measured before and after on-chip microdialysis revealed only a slight increase in mean vesicle size to 91.5 nm, confirming that the on-chip counterflow microdialysis element did not significantly affect the liposome size. Buffer counterflow eluent was also collected and examined via light scattering. No detectable signal was observed, revealing that intact liposomes do not escape the membrane and enter the counterflow during microdialysis.

3.4.2 On-Chip Remote Drug Loading

Anthracyclines represent an important class of drugs for liposomal encapsulation. Received by nearly every patient undergoing systemic cancer chemotherapy, anthracyclines are among the most utilized and effective antitumor drugs developed to date.[115] Liposomal forms of anthracyclines can provide increased efficacy with significantly reduced toxicity,[116] enhancing the overall clinical value of the drugs.[117] Liposomal encapsulation of the anthracycline doxorubicin has proven particularly successful for treatment of a range of cancers, with remote loading of DOX into preformed liposomes being a key to this success.[114] Here, DOX is used as a model drug encapsulant to investigate the potential for continuous flow remote drug loading using the microfluidic process.

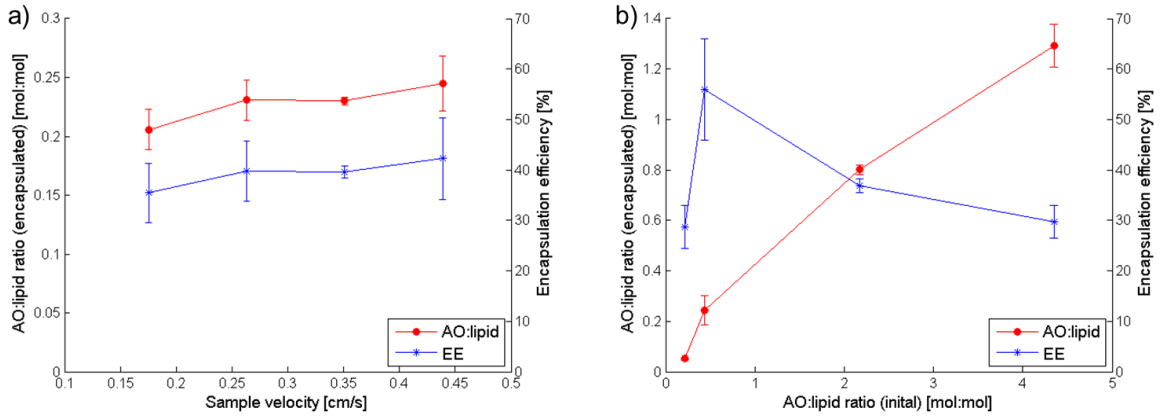

Figure 3.5: Relationships of (a) sample velocity and (b) initial AO concentration on final encapsulated concentration and loading efficiency. Microfluidic-generated liposomes, 80.8 nm ± 17.9 nm in diameter, were formed in a separate chip for this experiment.

Initial testing was performed using preformed liposomes injected into the counterflow microdialysis chip to form the desired transmembrane ion gradient, followed by on-chip introduction of AO as a suitable analog to DOX. AO is an amphipathic weak base with similar properties to DOX, and is known to behave similarly to DOX during remote loading with ammonium sulfate gradients.[60,118–120] **Figure 3.5a** presents the measured final D/L and encapsulation efficiency (EE) for AO-loaded liposomes prepared using an initial D/L of 0.44 when varying the sample velocity from 0.18 cm/s to 0.45 cm/s, for a total residence time within the mixing channel ranging from 4.25 min to 1.7 min, respectively. While a slight increase in both final D/L and EE was observed with increasing flow rate, overall remote loading using the microfluidic approach exhibited little dependence on flow velocity. In contrast, the initial concentration of drug compound introduced following ion exchange had a substantial effect on the final D/L (**Figure 3.5b**). By increasing the initial D/L level, final D/L values up to 1.3 were achieved. This effect is likely due to the significantly decreased diffusion lengths with increasing AO concentration and thus a greater quantity of AO may be loaded when the initial

concentration is higher. Reported D/L values for liposomal anthracyclines produced via conventional bulk scale remote loading are typically below 0.25,[109] significantly less than the levels achieved using the microfluidic process. This phenomenon is likely due to the rapid buffer exchange followed by AO introduction, the high initial D/L ratio, or a combination of the two. Encapsulation efficiency of the resulting liposomes was observed to increase with initial D/L, and then began to diminish for initial D/L values exceeding 2.17. This result is in accordance with previous studies based on bulk scale loading based on longer loading periods (hours to days), which suggest EE peaks at an initial D/L of 0.95 and decreases at higher ratios.[120] This behavior is due to insufficient intravesicular loading capacity above some limiting D/L level, resulting in a lower EE as drug concentration is further increased. The higher optimal D/L observed for the microfluidic platform is believed to result from the highly efficient formation of a transmembrane ion gradient due to rapid microfluidic buffer exchange, together with immediate interactions between the vesicles and the amphipathic molecules to be loaded. The steep transmembrane ion gradient achieved through rapid buffer exchange may enable higher D/L ratios to be achieved through microfluidic remote loading versus bulk scale processes.

To achieve remote loading through a transmembrane ion gradient, buffer exchange must occur prior to incubation with the drug to remove the loading salts from the exterior environment while simultaneously adjusting the carrier buffer to physiological pH. Because the transmembrane ion/pH gradient is transient, loading efficiency can be improved by decreasing the time between establishing the gradient and drug incubation.[121] Thus, if the amount of total ammonium sulfate ions are present in identical microfluidic versus bulk scale buffer exchanges, a higher ratio of the ions is likely to be present within the core of the liposomes versus the amount which have permeated through the membrane into the extra-liposomal space for the microfluidic method due to the rapid buffer exchange followed by immediate introduction of

drug/agent. Although typical D/L values of commercially available liposomal anthracyclines range from 0.125 to 0.250,[109] it has been shown that the behavior of amphipathic molecules during remote loading is highly dependent on environmental conditions,[120] with D/L as high as 1.7 obtained under ideal loading conditions (*i.e.* higher residual pH gradients and optimized D/L ratios and ionic concentrations).[122] However, liposomes generated through bulk manufacturing processes rarely approach this range, presumably due to limitations with maintaining steep transmembrane gradients during the relatively long drug diffusion time scales inherent to bulk scale processing, non-uniform distributions of the drug within the bulk fluid, or increased diffusion lengths after the initial loading period where adjacent drug is rapidly loaded into the liposomes. Microfluidic remote loading enables rapid buffer exchange for steeper pH and ion gradients together with microscale, homogeneous mixing for decreased diffusion lengths during drug loading, thus providing a more efficient method for drug loading in order to achieve higher final D/L ratios in the resulting populations of liposomes.

3.4.3 In-Line Liposome Synthesis and Remote Drug Loading

After demonstrating buffer exchange, pH adjustment, and remote loading of AO into preformed vesicles using the microfluidic approach, liposome synthesis in-line with microdialysis and remote loading of both AO and DOX was performed using an integrated device combining all of the process steps in a single flow-through chip. The resulting liposomes were first characterized for diameter (volume-weighted) when AO, DOX or buffer was alternately injected as the drug loading phase (**Figure 3.6**). Under the flow conditions used in these experiments, the resulting liposomes exhibited an average diameter of 225.5 nm ± 44.8 nm for the case of buffer without amphipathic encapsulant, while a reduction in liposome size to 190.9 nm ± 43.0 nm for DOX-loaded liposomes and 191.5 nm ± 33.4 nm for AO-loaded liposomes was observed. The reduction in liposome size of approximately 15% after remote

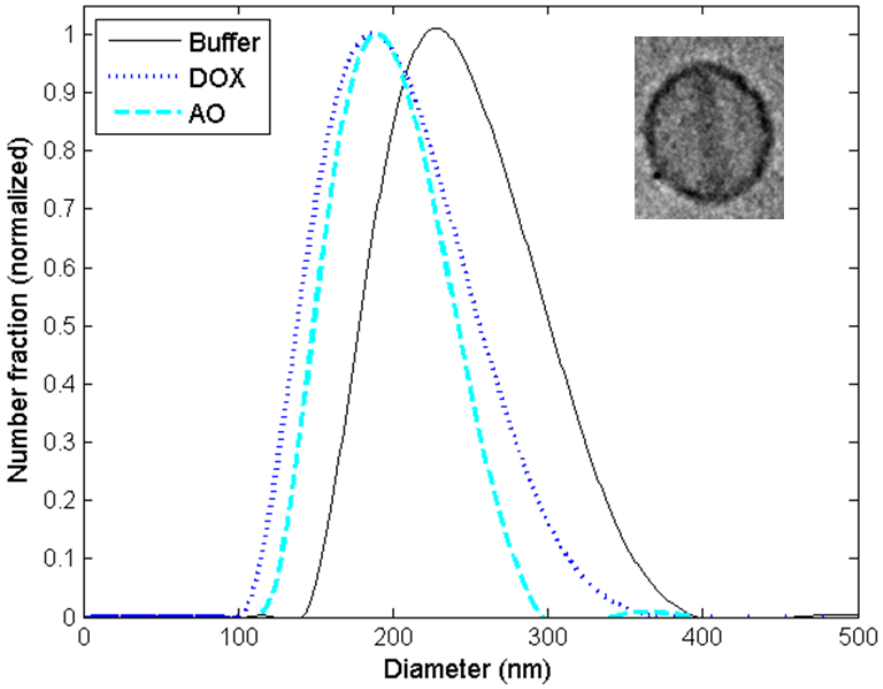

Figure 3.6: Volume-weighted size distributions from remote loading of DOX and AO into liposomes in-line with synthesis and microdialysis for buffer exchange in comparison to unloaded liposomes (buffer) generated by the same microfluidic device.

loading may reflect a change in morphology to a characteristic "coffee bean" resulting from drug aggregation within the vesicles,[59] leading to altered signals during dynamic light scattering. Confirmation of drug crystallization was verified through cryogenic transmission electron microscopy (cryoTEM) imaging (**Figure 3.6**).

A summary of measured final D/L values following AO and DOX loading within the integrated microfluidic device is presented in **Table 3.1**. Prior results for the case of AO loading using preformed liposomes generated in a separate chip are also shown for comparison. An initial D/L of 0.44 was selected for DOX, as this ratio was found to maximize loading efficiency in initial experiments using AO (**Figure 3.4**). The DOX loaded liposomes generated by the microfluidic device had a final D/L of 0.32 ± 0.03, which exceeds the typical D/L of 0.25 or less

Table 3.1: Summary of D/L and EE measurements for AO loaded liposomes (preformed liposomes produced in a separate chip) and DOX and AO loaded liposomes (formed in-line with synthesis in a single integrated chip). Similar results were achieved for DOX and AO loading within the integrated device. Slightly higher final D/L and EE values were observed when remote loading was performed in-line with liposome synthesis.

Loading case	Liposome diameter (nm)	Drug / agent	D/L (initial)	D/L (final)	EE (%)
Preformed	80.8 ± 17.9	AO	0.22	0.05 ± 0.01	23.5 ± 4.2
			0.44	0.24 ± 0.06	55.9 ± 10.0
In-line	191.5 ± 33.4	AO	0.22	0.06 ± 0.01	26.9 ± 2.2
			0.44	0.32 ± 0.11	69.8 ± 18.0
	190.9 ± 43.0	DOX	0.44	0.32 ± 0.03	71.8 ± 4.2

achieved by bulk remote loading employing overnight incubation.[59] The total on-chip residence time of within the microfluidic device was less than 3 min. In addition, initial D/L values of 0.22 and 0.44 were used for testing AO loading, resulting in final D/L values of 0.06 ± 0.01 and 0.32 ± 0.11, respectively.

Encapsulation efficiency using the integrated system was also evaluated. Referring to **Table 3.1**, the DOX-loaded liposomes yielded an EE of approximately 72%, lower than typical values for conventional remote loading which can exceed 99%.[121] Lower encapsulation efficiency compared to bulk scale remote loading is not surprising, since the incubation time is up to 300 times lower within the microfluidic system. Regardless, this is an aspect of the microfluidic approach which must be improved to minimize drug waste, for example by implementing a method for capturing and recycling drug in an additional on-chip stage following remote loading. In addition to reducing manufacturing costs by reducing waste of valuable drug compounds, optimizing loading conditions could also eliminate the need for off-chip purification, enabling real-time production of stably encapsulated, highly concentrated liposomal drugs at or near the point of care.

Direct comparison of in-line system performance with the previous results from remote loading using preformed liposomes is hampered by the different sizes of each liposome population. When performing in-line remote loading, fluidic coupling between the upstream liposome formation zone and downstream microdialysis and drug loading zones demands careful design of the channel dimensions, together with appropriate selection of inlet flow rates. Liposome size and polydispersity are both impacted by the buffer:lipid flow rate ratio, overall volumetric flow rate, and microchannel dimensions selected for effective liposome self-assembly during hydrodynamic flow focusing.[41–44,86] However, these same parameters also affect microdialysis and remote drug loading performance. While channel dimensions for each functional element in the system can be designed independently, allowing a degree of decoupling between these constraints, the current microfabrication process used for device manufacture presents some limitations. For example, to avoid sagging of the microdialysis membrane, a maximum channel width of 1.2 mm was used for the buffer exchange zone. Similarly, total volumetric flow rates were minimized to prevent delamination of the hybrid microfluidic device due to excessive internal fluid pressure. As a result of these constraints, liposomes formed using the on-line system were approximately twice the diameter of their preformed counterparts. Although residual pH gradients decrease with decreasing vesicle size due to decreased intravesicular volumes, it has been shown that this effect can be circumvented by including a buffering capacity greater than 300 mM.[122] Additionally, given the significantly larger volume of the in-line liposomes, it is notable that both the final D/L and EE values for in-line encapsulation were comparable to the case of preformed liposome loading, with slight increases in both values for the larger liposomes. This further emphasizes the observation that the initial D/L is the dominant parameter that defines encapsulation performance during remote loading within the continuous flow microfluidic system.

3.5 Conclusion

By combining liposome synthesis via microfluidic flow focusing, membrane microdialysis for buffer exchange and in-line introduction of amphipathic weak bases for remote loading within a single microfluidic device, this study converts a conventional multi-step bulk scale process requiring hours to days of labor into a microscale process which requires a total on-chip residence time of approximately 3 minutes. By taking advantage of the reduced diffusive length scales characteristic of microscale flows, the microfluidic method implements remote loading as a seamless continuous flow process, with the potential to simplify and increase the robustness of this critical step in nanoliposomal drug production. The further ability to perform integrated liposome formation using hydrodynamic flow focusing prior to formation of a transmembrane ion gradient for remote drug loading allows the entire sequence of steps required for liposomal drug production to be performed as a single in-line and continuous flow process. The microfluidic method demonstrated here enables exceptionally high drug loading levels, with D/L values above unity easily achieved. Future optimization of device design and flow conditions are expected to further improve encapsulation efficiency, enabling just-in-time production of purified liposomal drug formulations with minimal drug waste.

Chapter 4 : Synthesis of Nearly Monodisperse Nanoscale Liposomes Using 3D Microfluidic Hydrodynamic Focusing in a Concentric Capillary Array

4.1 Summary

A novel microscale device has been developed to enable the one-step continuous flow assembly of nearly monodisperse nanoscale liposomes using three-dimensional microfluidic hydrodynamic focusing (3D-MHF) in a radially symmetric capillary array. The 3D-MHF flow technique displays patent advantages over conventional methods for nanoscale liposome synthesis (*i.e.* bulk scale alcohol injection and film hydration and extrusion) through the on-demand manufacture of consistently uniform liposomes at unparalleled rates (factor of 10^4 liposomes/min increase in production rate relative to state-of-the-art liposome production strategies). Liposomes produced by the 3D-MHF device are of tunable size and have a factor of two improvement in polydispersity over previous MHF methods which can be attributed to entirely radially symmetric diffusion of alcohol-solubilized lipid into an aqueous flow stream. Moreover, the 3D-MHF platform is simple to construct from low-cost, commercial parts, which obviates the need for advanced microfabrication strategies necessitated by previous MHF nanoparticle synthesis platforms.

4.2 Introduction

Several approaches for liposome synthesis have been investigated to improve upon conventional manufacture shortcomings; however, few have effectively demonstrated delivery of an on-demand clinically reliable product of sufficient throughput.[7] Incremental advancements in liposome manufacture have been demonstrated to address synthetic throughput challenges *via*

microfluidic hydrodynamic focusing (MHF), a technique that enables the one-step continuous flow production of nearly monodisperse, nanoscale, unilamellar vesicles using two-dimensional (2D) flow focusing in rectangular microchannels.[41–44] It has been demonstrated that MHF can produce liposome populations that are consistently more uniform than the preparations of liposomes resulting from conventional manufacture strategies. Additionally, size control of vesicle preparations formed using MHF can be precisely tuned and easily automated using pre-programmed computer controlled flow inputs.[13]

Applying the benefits of liposome synthesis provided by MHF towards the widespread commercial manufacture of liposomes are known to be limited by several practical aspects of the technique including: (i) inherent drag forces that affect symmetric flow focusing in rectangular microchannels, (ii) low throughput due to characteristically low microfluidic flow rates, and (iii) expensive, time-consuming microfabrication techniques necessary to develop the liposome manufacture devices. Here, an attempt is made to ameliorate these practical short comings of MHF for liposome production by extending application of the technique to a facile, cost-effective annular coaxial flow system. The microfluidic coaxial flow system described is composed of an array of commercially available capillaries that enables three-dimensional fluid focusing for liposome synthesis. In comparison, previously demonstrated 2D-MHF strategies in planar devices only focus the solvated lipid stream in the lateral dimension. Further, the horizontal surfaces of the planar microfluidic devices are wetted with the organic lipidic stream (with a no-slip boundary condition), causing lipidic fluid further away from the channel center to convect more slowly through the fluidic channel. Although various strategies for three-dimensional hydrodynamic focusing have been demonstrated,[123–125] these processes involve piece-wise, rectangular focusing and the sample flow is not focused until a point farther downstream from the initial interaction of multiple fluid species. Liposome formation may occur

immediately after the initial ethanol-water interface is formed;[44] thus immediate hydrodynamic focusing in addition to complete radial symmetry through a coaxial flow system is a necessity. In the coaxial flow system, there are no surfaces in the mixing region wetted by the lipidic organic phase and thus no lipid fluid elements are subjected to the no-slip boundary condition. Therefore, the 3D-MHF strategy for liposome preparation maintains technical advantages over previously investigated 2D-MHF strategies as the annular flow geometry enables complete radially symmetric mixing of the fluidic inputs allowing for a more uniformly consistent product. As a result, nearly monodisperse liposomes can be manufactured at unparalleled rates with precise size control.

4.3 Materials and Methods

4.3.1 Device Fabrication

Concentric capillary devices were assembled from a stock seven-barrel glass capillary (World Precision Instruments, Sarasota, FL) (**Figure 4.1**). The multibarrel capillary contains seven identical borosilicate glass capillaries which individually have an inner diameter (ID) of 0.58 mm and outer diameter (OD) of 1.0 mm and are arranged in a circular pattern with an equivalent outer diameter of 3 mm. The multibarrel capillary array is 152 mm in length, but can be sectioned into smaller pieces for a smaller device assembly. Poly(ether ether ketone) (PEEK^{TM}) tubing (510 μm OD, 65 μm ID) unless otherwise specified) (Upchurch Scientific, Inc., Oak Harbor, WA) served as the solubilized lipid feed line and was threaded through the center of the multicapillary array. The lipid feed line was connected through minitight fittings (Upchurch Scientific, Inc.) to a glass Gastight® syringe (Hamilton, Reno, NV) that delivered the lipid solution. The solubilized lipid infusion was controlled by a programmable syringe pump (Harvard Apparatus Inc., Holliston, MA). Tygon tubing (3.96 mm ID) (Cole-Parmer Instrument

Co., Veron Hills, IL) was used as the support line for the extra-annular aqueous sheathing flow. A continuous supply of aqueous sheath flow was supplied by a quaternary pump (Agilent Technologies, Santa Clara, CA) at programmable volumetric flow rates. The junction between the lipid feed line and multicapillary device was sealed on the downstream end using UV-curable epoxy (NOA81) (Norland Products Inc., New Brunswick, NJ).

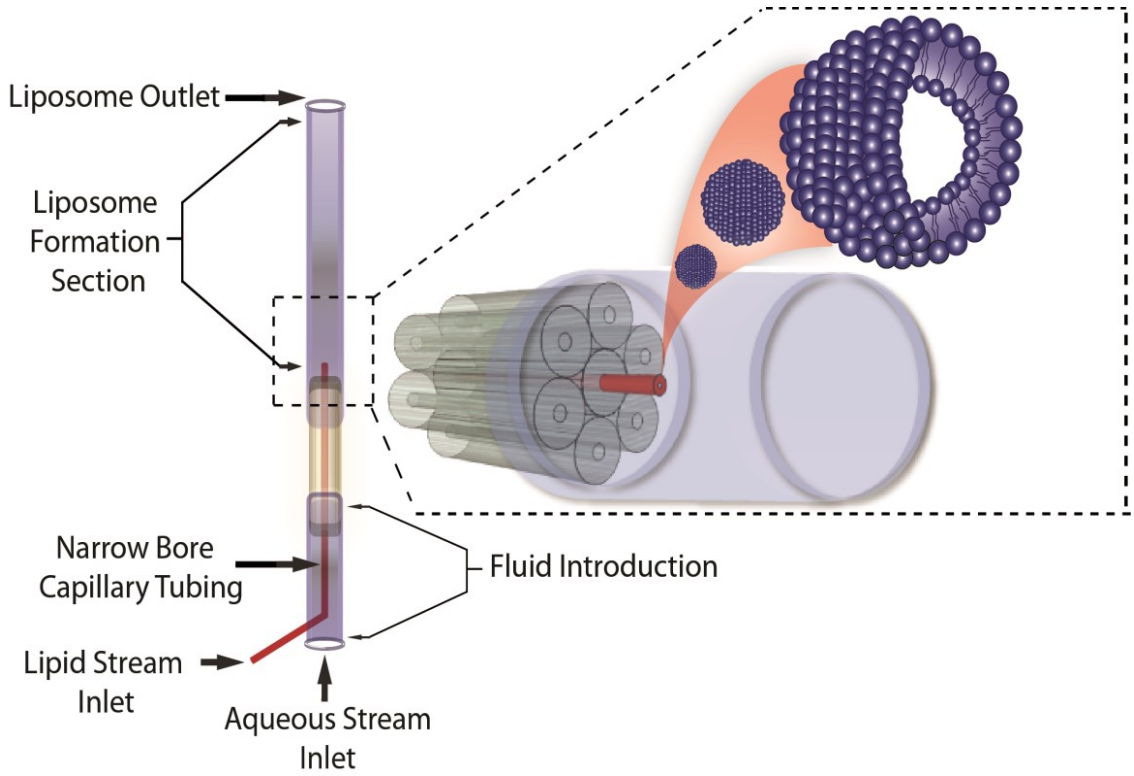

Figure 4.1: Schematic of the 3D-MHF annular flow liposome formation device. Narrow bore capillary tubing is secured by a glass multicapillary array which serves to precisely center the intra-annular flow stream in the concentric exterior coaxial flow stream. For liposome synthesis, an alcohol-solubilized lipid solution is continuously injected into the intra-annular capillary tubing and hydrodynamically focused in three-dimensions by an exterior sheath flow of aqueous buffer. Not to scale. *Schematic produced by D.M. Omiatek.*

4.3.2 Lipid Mixture and Hydration Buffer Preparation

Lipid mixture preparation and hydration buffer were prepared as previously described (Chapter 2.3.2, p. 21). Briefly, dipalmitoylphosphatidylcholine (DPPC), cholesterol, PEG_{2000}-PE were dissolved in chloroform in a molar ratio of 61:30:9, respectively. The lipid mixture was desiccated under vacuum then re-dissolved in anhydrous ethanol with 1 wt % of a lipophilic membrane dye, 1,1'-dioctadecyl-3,3,3',3'-tetramethylindocarbocyanine perchlorate (DiI-C_{18}) (Life Technologies, Carlsbad, CA), Carlsbad, CA)) for a total lipid concentration of 10 mM. A 1x Phosphate Buffered Saline (PBS) (Sigma Aldrich) solution at pH 7.4 was used as the hydration buffer. All fluids were passed through 0.22 μm filters before being introduced to the microfluidic device.

4.3.3 Microfluidic Liposome Synthesis

- Synthesis of liposomes using the 3D-MHF annular device

Liposomes were prepared via 3D-MHF by injecting the ethanol-lipid solution central intra-annular line and 1x PBS into the extra-annular line composed of PVC tubing to generate an aqueous outer sheath flow. For typical operation, a 65 μm ID intra-annular lipid-ethanol feed line was used and placed at a 5 mm protrusion length from the face of the multicapillary buffer supply. The buffer volumetric flow rate was set to 5 mL/min and the flow rate ratio (FRR), or the ratio of the volumetric flow rate of buffer to the volumetric flow rate of solvent, was set to 5000.

- Synthesis of liposomes using the 2D-MHF planar device

Liposomes were synthesized using the microfluidic flow focusing method as described previously.[41–44] Briefly, a lipid-ethanol mixture (10 mM lipid) was injected between two aqueous buffer inlets (1x PBS) into a PDMS glass microfluidic device with channel dimensions of 300 μm by 50 μm. The flow rate ratio (FRR), which represents the ratio of volumetric flow rate of the buffer to the volumetric flow rate of the lipid mixture, was set to 10. Linear flow velocity of

the total flow for all FRRs was kept constant (0.11 m/s) for a volumetric flow rate of 100 µL/min.

4.3.4 Asymmetric Flow Field-Flow Fractionation (AF^4) with Multi-Angle Laser Light Scattering (MALLS) and Quasi-Elastic Light Scattering (QELS)

Liposomes manufactured using MHF techniques were analyzed using Asymmetric Flow Field-Flow Fractionation (AF^4) paired to dual Multi-Angle Laser Light Scatter (MALLS) and Quasi-Elastic Light Scattering (QELS) detection (Wyatt Technology, Santa Barbara, CA). The procedure described in Chapter 2.3.4 (p. 23) was followed for liposome characterization.

4.3.5 Computational Fluid Dynamics (CFD) Simulation of Ethanol-Water Concentration Profile

A computational fluid dynamics simulation was developed to illustrate the difference in the ethanol-water concentration profiles between the two distinctive microfluidic device geometries: annular (3D) versus planar (2D). The concentration profile of a center stream of ethanol focused by an exterior sheath of water was represented in a three-dimensional model created using COMSOL Multiphysics 4.2 software (COMSOL Inc., Burlington, MA). The non-linear relationship for ethanol-water of the mutual diffusion coefficient (D) to ethanol mole fraction (X_E) was estimated using **Equation 4.1**, which was derived from experimental values:[126]

$$D\left[m^2 s^{-1} \cdot 10^{-9}\right] = 11.22 X_E{}^5 - 24.11 X_E{}^4 + 12.27 X_E{}^3 + 6.45 X_E{}^2 - 5.88 X_E + 1.42 \qquad \textbf{(4.1)}$$

Hydrodynamic flow focusing of a radial system and a rectangular system were analyzed using the simulation to illustrate the difference in diminishing ethanol mole fraction within the two microchannel architectures. For the comparison, the FRR in the simulation was set to 100 and total volumetric flow rate was 5.0 mL/min for the annular device and 90 µL/min for the planar device (corresponding to a linear flow velocity of 0.2 m/s for both devices). The

simulations do not account for the nonlinearity in viscosity of the mixtures, with the assumption that this does not have a critical effect on the resulting concentration profile for the purposes of comparison.

4.4 Results and Discussion

The 3D-MHF system consisting of a concentric capillary array is depicted in **Figure 4.1**. Liposomes of tunable size are formed through continuous injection of an alcohol-soluble lipid solution into a central feed line that is radially sheathed by external aqueous buffer. As soluble lipids from the alcohol stream controllably diffuse into the aqueous stream, lipids self-assemble into liposomes. The magnitude of flow focusing and the mixing geometry at the interface between these two fluids play an integral role in the size and size distribution of the resultant liposome products.

4.4.1 Interfacial Mixing Geometry Affects Liposome Particle Size Characteristics

Liposome preparation via MHF has been previously demonstrated in planar microfluidic systems, where microchannel depth-to-width aspect ratio significantly impacts the size characteristics of the resultant liposomal products.[44] It is known that hydrodynamic (or parabolic) flow in a rectangular channel experiences a non-uniform velocity profile across the vertical plane due to no-slip boundary conditions of flow streams sandwiched between the walls of the device. This is shown by the numerical CFD simulation in **Figure 4.2A**. In a controlled-flow particle assembly system like that required for reproducible liposome formation, these so-called "edge effects" induce asymmetric mixing at the interface between the aqueous sheathing fluid and the solubilized lipid at the point of particle formation, which can contribute to an increase in particle size polydispersity.[14] These effects can be partially alleviated if the microchannel depth-to-width aspect ratio becomes increasingly high (*i.e.* exceeds five);[127,128]

however, the practicalities of engineering rectangular microfluidic devices of increasing aspect ratio become increasingly more difficult and expensive.[127]

The 3D-MHF device described here allows for an important modification in the mixing condition at the miscible fluid interface where particle formation occurs within the planar device (**Figure 4.2B**). Here, the lipid input is entirely encapsulated in the annular sheathing fluid, resulting in radially symmetric mixing and subsequent formation of liposome populations with previously unforeseen size uniformity (see Section 4.4.3, page 72). Comparative simulations of

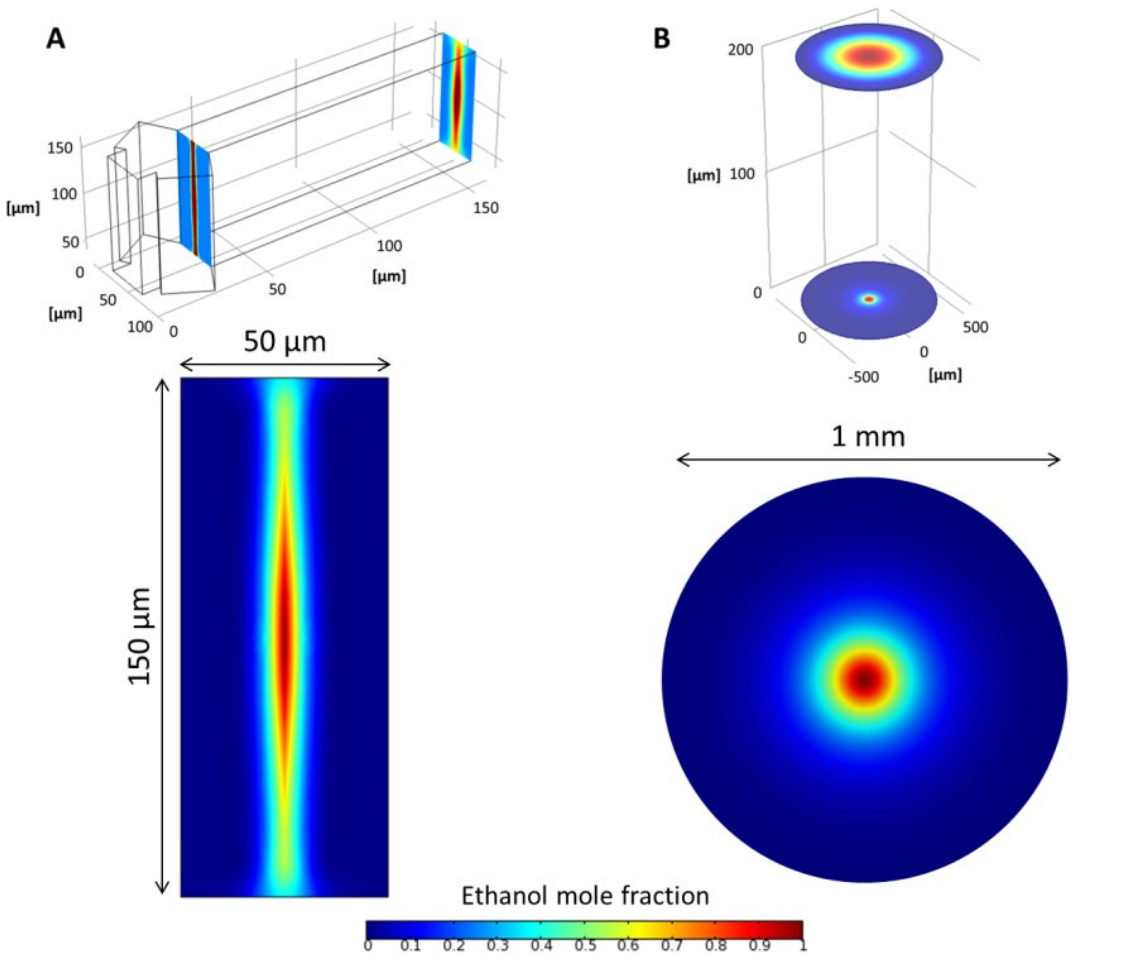

Figure 4.2: CFD simulation of ethanol concentration in (A) 2D-MHF vs. (B) 3D-MHF device. FRR set to 100 with linear flow velocity 0.2 cm/s (corresponding to a volumetric 5.0 mL/min, planar Q_{tot}=90 µL/min). Cross-sectional concentration profiles represent sections 150 µm downstream of the initial buffer-ethanol interface for both devices.

interfacial ethanol concentration from the 2D- and 3D-MHF device geometries at a distance 150 μm downstream from the fluid mixing interface are also displayed in **Figure 4.2**. Clear differences in the depletion of alcohol at the channel wall are observed between the two techniques. Numerical simulation of the planar device shows that a fraction of alcohol (~0.4 mole fraction to 0.6 mole fraction) approaches the device wall beyond the mixing interface. However, there is no observation of this in the 3D device, where alcohol concentration is completely depleted in the region approaching the device boundaries. As a result, the annular device enables the rapid, radially symmetric diffusion of alcohol components into the buffer, yielding less polydisperse populations of lipid nanoparticles.

Representative liposome preparations made by MHF using the planar device (red trace) versus the annular device (blue trace) are shown in **Figure 4.3**. Flow conditions were chosen such that the average liposome radius generated by each device was similar for direct comparison (51 nm for 2D-MHF versus 53 nm for 3D-MHF). The annular flow device shows an improvement in optimal liposome size uniformity relative to the planar microfluidic device (**Figure 4.3**). This observation can be quantified from the particle size polydispersity index (PDI), defined as the ratio of the square of the standard deviation of particle size to the square of the mean diameter, a normalized measure of the size distribution.[129] Interestingly, the average PDI of the resultant liposome populations decreases by half (0.083 to 0.044) when comparing the planar microfluidic to the annular microfluidic method. Under some flow conditions, the annular flow platform was shown to produce liposomes with PDIs as low as 0.007 (not shown). From a process manufacturing perspective, the 3D-MHF annular flow system maintains advantages over its planar flow counterpart, where it has been demonstrated to reliably produce uniform nanoscale vesicles up to a rate of 10^9 liposomes/min (final lipid concentration of approximately 4 μmol/L) of versus the optimized operational parameters of the planar device which yield

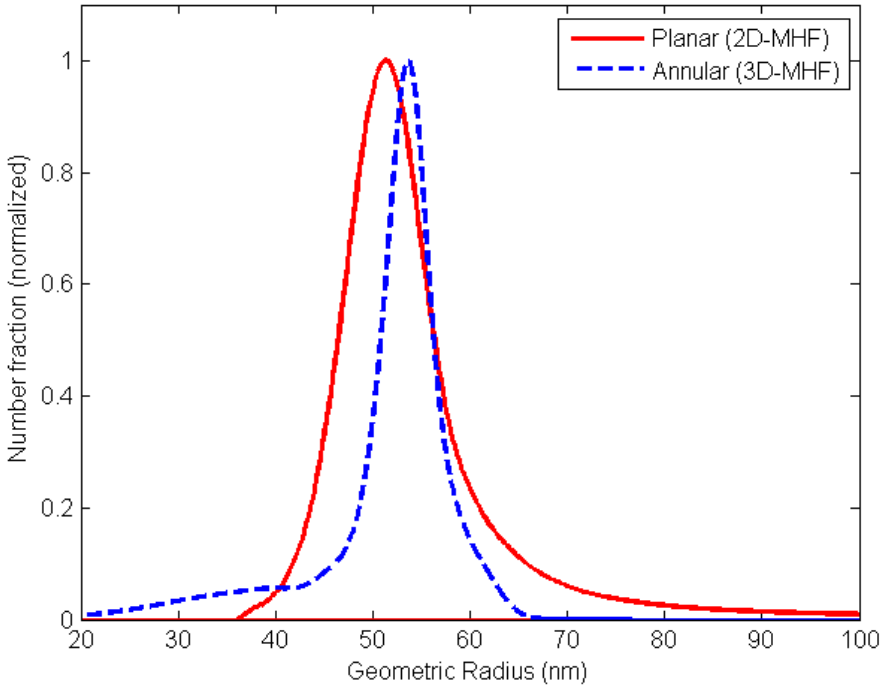

Figure 4.3: Comparison between 2D- and 3D-MHF liposome manufacture platforms. 2D-MHF experiments were carried out in rectangular microchannels with a 6:1 aspect ratio at FRR 10 and a total volumetric flow of 200 µL/min. 3D-MHF experiments were carried out in a device with a 65 µm intra-annular ID lipid feed line at FRR 5000 and a total volumetric flow of 5 mL/min. Average liposome radius for the 2D-MHF device was 51 nm (PDI =0.083) and 53 nm (PDI = 0.044) for the 3D-MHF device.

liposomes at a lower rate 10^5 liposomes/min (final lipid concentration of approximately 400 µmol/L).

4.4.2 3D-MHF Device Design Parameters Affect Liposome Size and Polydispersity

The effect of intra-annular capillary orifice size on the resultant liposome size characteristics was investigated under fixed flow conditions. The dimension of the capillary orifice is related to the effect of microchannel size and aspect ratio in the planar MHF. It was observed that a reduction in intra-annular capillary ID from 255 µm to 125 µm to 65 µm correlated with resultant average particle radii of 72 nm, 63 nm, and 53 nm, respectively (**Figure 4.4**). Here, a fixed

applied volumetric flow through a smaller orifice will generate a greater linear velocity of the soluble lipid stream and subsequent focusing condition which, in turn, reduces the total diffusion distance of lipids from their solvated state in alcohol into the aqueous buffer where they accumulate to form vesicles due to the decreasing physical width of the lipid-ethanol flow stream. Although a decrease in average vesicle radii was observed with a reduction in intra-annular capillary ID, there was no discernible effect on the resulting size distribution. The PDIs were comparable each of the intra-annular capillaries investigated at 0.02, 0.04, and 0.03 for the 65 µm, 125 µm, and 255 µm ID capillaries, respectively.

The effect of the protrusion distance of the intra-annular lipid feed capillary beyond the exit

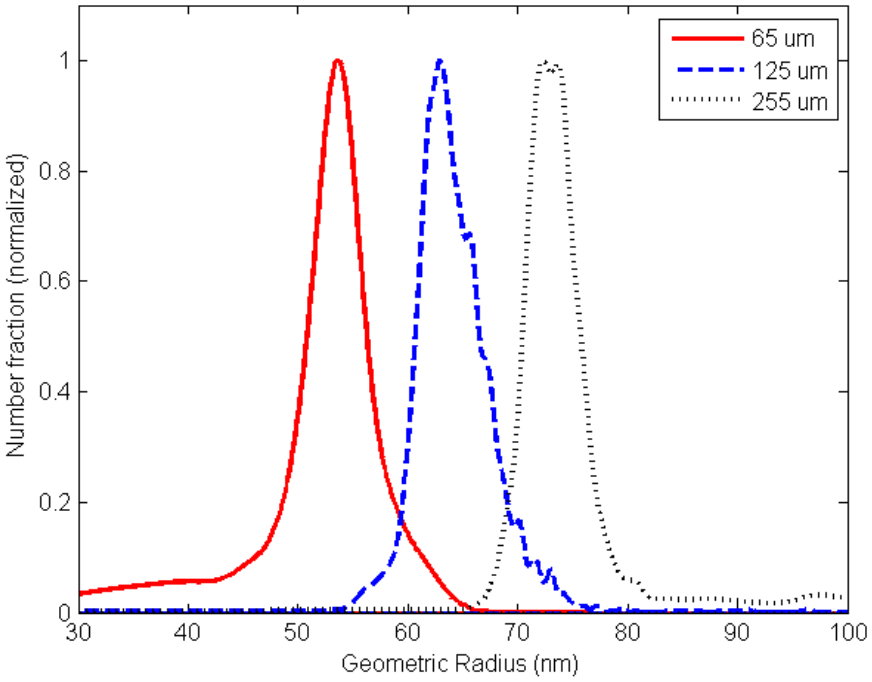

Figure 4.4: Effect of intra-annular orifice of lipid feed line on resultant liposome size characteristics using the 3D-MHF device. Volumetric flow rate and flow rate ratio of fluidic inputs are fixed at FRR 5000 with a total flow rate of 5 mL/min. A reduction in lipid feed line orifice results in a decreased-size average liposome size, likely due to the increased focusing condition. Average liposome radius was 53 nm (0.044 PDI) for 65 µm ID, 63 nm (0.040 PDI) for 125 µm ID, and 72 nm (0.030 PDI) for 255 µm ID.

of the extra-annular sheathing fluid was also investigated at fixed flow conditions. In this experiment, the intra-annular capillary was positioned 0 mm from the multicapillary outlet (flush to the multicapillary face) and then at a length 5 mm beyond the outlet. Resultant liposome particle size was found to be partially linked to the extension of the intra-annular lipid feed line into the aqueous sheath. At a 0 mm capillary protrusion length, the average liposome size was 96 nm with a PDI of 0.030 compared to the 5 mm protrusion length where the average liposome size was 53 nm with a PDI of 0.007. The difference in particle size and distribution for the two device constructs demonstrates that there is a critical distance from the inlet, Z_e, after which the flow is fully developed yielding conditions for systematic particle assembly.[130] This distance can be calculated using **Equation 4.2** for $1 < \mathrm{Re} < 100$:[130]

$$Z_e = (0.619 + 0.0567\,\mathrm{Re})D_H \qquad \textbf{(4.2)}$$

where *Re* represents the Reynolds number, which for pipe flow is represented by **Equation 4.3**:[131]

$$\mathrm{Re} = \frac{QD_H}{\nu A} \qquad \textbf{(4.3)}$$

Here, Q is the volumetric flow rate, A is the cross-sectional area of the annulus, ν is the kinematic viscosity (taken to be that of water at room temperature) , and D_H is the hydraulic diameter of the pipe, which is defined as $D_{(outer)}$ - $D_{(inner)}$ (3.46 mm).[131] The required length that the intra-annular capillary must reside distal to the multicapillary outlet of the 3D-MHF device was calculated to be 6.7 mm at a typical operational volumetric flow rate of 5 mL/min. The 5 mm protrusion length used in these experiments approaches this distance, which within placement error, enables for a platform where the sheath flow is nearly fully developed before particle formation, leading to uniformly small resultant vesicle suspensions.

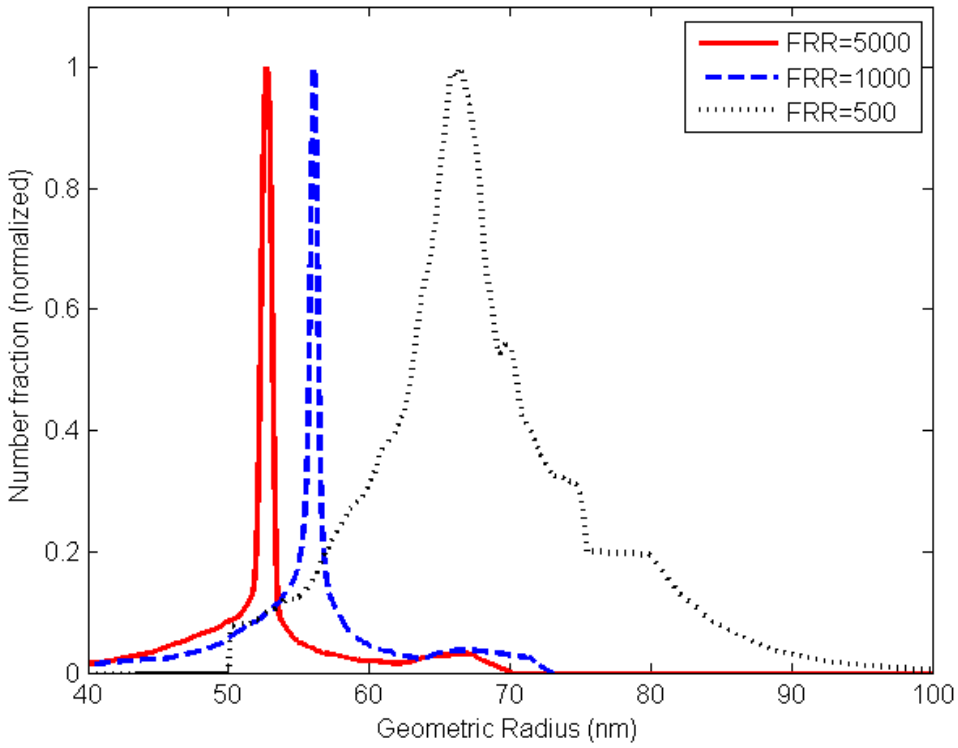

Figure 4.5: Effect of flow focusing on liposome size using 3D-MHF. Total volumetric flow rate was fixed at 5 mL/min. Device had a 65 µm intra-annular capillary ID. Average liposome radius was 53 nm (0.007 PDI) at FRR 5000, 56 nm (0.005 PDI) at FRR 1000, and 66 nm (0.047 PDI) at FRR 500.

4.4.3 3D-MHF Device Operational Flow Parameters Affect Liposome Size and Polydispersity

The magnitude of the ratio of sheathing buffer to soluble lipid flow rate (FRR) and total flow rate of MHF systems have been previously determined to play a significant role in liposome synthesis. Studies using planar (2D) microfluidic platforms have shown a relationship between liposome size and polydispersity linked to the degree of focusing experienced by the central lipid feed line. 2D-MHF demonstrated that a greater magnitude of focusing, or higher FRR, leads to smaller, less polydisperse liposomal populations.[41–44]

To investigate the effect of flow focusing on liposome synthesis in the 3D-MHF system, the flow rate ratio (FRR) of buffer to alcohol-soluble lipid was varied from 500, 1000, and 5000 and the resulting liposome populations were analyzed by light scattering, as described in Section 4.3.4 (page 65). As the FRR of sheathing buffer to alcohol-solubilized lipid increased from 500 to 1000 to 5000, the resulting average size of liposomes decreased from a radius of 66 nm to 56 nm to 53 nm, respectively (**Figure 4.5**). The trend observed here correlates with that from previous planar device syntheses and is likewise attributed to the increasing degree of focusing experienced by the center stream of solubilized lipid.

To investigate the effect of total flow rate on liposome production, 3D-MHF devices were operated with the volumetric flow rate of the sheathing buffer at 1 mL/min, 2 mL/min, and 5 mL/min (*Re* = 4.7, 9.4, and 23.6, respectively). In these studies, a device with 65 μm ID PEEK tubing extending 5 mm from the multicapillary interface was used and FRR was fixed at 5000. The average particle size of the resulting liposomes decreased as the input flow rate increased. Indeed, as the total flow rate of the system increased from 1 mL/min to 2 mL/min to 5 mL/min, the resulting liposome average radii are reduced from 88 nm to 80 nm to 70 nm data not shown). Although all flow parameters investigated are laminar and significantly below the transition threshold into the turbulent flow regime (an inherent characteristic of most microfluidic systems), a modest increase in *Re* appears to expedite lipid accumulation and subsequent assembly into smaller particles. Notably, an increase in buffer flow rate does not play a role in particle size dispersity, likely due to a fixed alcohol concentration (fixed FRR) at the mixing interface which is known to play a role in the stabilization of liposomal intermediates prior to ordering into spherical vesicular structures.[12]

4.5 Conclusion

Microfluidic systems enable the production of nearly monodisperse populations of liposomes whose sizes may be adjusted by controlling the flow rates within the device during synthesis. This chapter presents the first demonstration of three-dimensional microfluidic hydrodynamic focusing for the rapid manufacture of nanoscale liposomes. 3D-MHF was achieved through the use of a facile and cost-effective concentric capillary array. The device enabled the continuous flow synthesis of nanoscale, unilamellar liposomes with unprecedentedly low polydispersity, and relationships between flow conditions and device parameters on the resulting liposomes were investigated. Liposomal populations produced by this method are of tunable size at unprecedented rates (10^9 liposomes/min) without the need for any post-formation homogenization steps to achieve size characteristics necessary for biomedical application. Additionally, this technique is well suited for scale-up to support mass production of nanoscale liposomes which possess the beneficial qualities resulting from microfluidic synthesis with further improved throughput and size polydispersity over previous microfluidic techniques. The annular flow focusing method for liposome synthesis provides a rapid, simple avenue for the bulk scale generation of narrowly distributed liposomes of tunable size.

Chapter 5 : Microfluidic Preparation of Liposomes to Determine Particle Size Influence on Cellular Uptake Mechanisms

5.1 Summary

This chapter presents a series of experiments which were completed through combined efforts with Dr. Abhay U. Andar at the University of Maryland Baltimore School of Pharmacy. The chapter is adapted from a published journal article in which Dr. Andar and I share first authorship. Dr. Andar performed the work regarding cell culture, endocytosis studies, flow cytometry, and confocal imaging. Analysis and manuscript preparation were the result of a combined effort from both parties.

Cellular uptake and trafficking of liposomes in Caco-2 cells using vesicles with distinct average diameters ranging from 40.6 nm to 276.6 nm is investigated in this chapter. Liposomes were prepared by microfluidic hydrodynamic flow focusing, producing nearly monodisperse populations and enabling size-dependent uptake to be effectively evaluated. Populations of PEG-conjugated liposomes of various distinct sizes were prepared in a disposable microfluidic device using a simple continuous flow microfluidic technique. Liposome cellular uptake was investigated using flow cytometry and confocal microscopy. Liposome uptake by Caco-2 cells was observed to be strongly size-dependent for liposomes with mean diameters ranging from 40.6 nm to 276.6 nm. When testing these liposomes against endocytosis inhibitors, cellular uptake of the largest (97.8 nm and 162.1 nm in diameter) liposomes were predominantly subjected to clathrin-dependent uptake mechanisms, the medium-sized (72.3 nm in diameter) liposomes seemed to be influenced by all investigated pathways and the smallest liposomes (40.6 nm in diameter) primarily followed a dynamin-dependent pathway. In addition, the 40.6 nm, 72.3 nm, and 162.1 nm diameter liposomes showed slightly decreased accumulation within

endosomes after 1 h compared to liposomes which were 97.8 nm in diameter. Conversely, liposome colocalization with lysosomes was consistent for liposomes ranging from 40.6 nm to 97.8 nm in diameter. The continuous flow synthesis of nearly monodisperse populations of liposomes of distinct size via a microfluidic hydrodynamic flow focusing technique enabled unique *in vitro* studies in which specific effects of particle size on cellular uptake were elucidated. The results of this study highlight the significant influence of liposome size on cellular uptake mechanisms and may be further exploited for increasing specificity, improving efficacy, and reducing toxicity of liposomal drug delivery systems.

5.2 Introduction

Liposomes have received a great deal of attention as drug delivery vehicles owing to their ability to transport a range of therapeutic agents.[2,65,132,133] While the utility of liposomes as delivery vehicles for therapeutics and vaccines has been widely recognized, many hurdles remain for effective delivery to targeted tissues and cells.[134] Due to the inevitable size variability within a single population of liposomes prepared through conventional synthesis techniques, determination of an efficient size-based targeting mechanism remains a challenge. Liposome size and variability in size are important factors that can influence drug dosage, targeting and clearance,[35,37] initial cellular recognition,[135–137] and efficient cellular uptake and extended circulation time.[35,37] The microfluidic-based technique for liposome synthesis presents a new avenue for producing populations of liposomes with tunable size and exceptionally low polydispersity compared to traditional methods.[41–44]

This chapter investigates how endocytosis behavior in human epithelial colorectal adenocarcinoma (Caco-2) cells is affected by particle size by using liposome synthesized through the microfluidic technique, thus enabling inspection of each phenomenon with much finer resolution than studies involving liposomes produced by traditional preparation methods.

Cellular uptake mechanisms were investigated through the use of various endocytosis inhibitors. Additionally, intracellular trafficking of varied liposome vesicle size was investigated over time using confocal microscopy, distinguishing the internalization pathways and uptake mechanisms used by the Caco-2 cells upon exposure to liposomes of various sizes.

5.3 Materials and Methods

5.3.1 Microfluidic Preparation of Liposomes

5.3.1.1 Device Fabrication

Microfluidic devices were fabricated using soft lithography techniques.[138] Microchannel designs were created using AutoCAD software (Autodesk, San Rafael, CA) and printed onto a photomask (Fineline Imaging, Colorado Springs, CO). To create features for imprinting microchannels, SU-8 negative photoresist (MicroChem Corp., Newton, MA) was spin-coated onto a 4-inch silicon wafer (University Wafer, South Boston, MA), exposed to ultraviolet light through the photomask on an automated EVG 620 mask aligner (EV Group, Germany), and developed to establish a master mold with raised features which may be used repeatedly to create microchannels in poly(dimethylsiloxane) (PDMS) elastomer. The SU-8 mold was placed in a plastic petri dish and a 10:1 (w:w) mixture of pre-polymer PDMS elastomer and curing agent (Sylgard 184, Dow Corning Corp. Midland, MI) was poured over the mold. Vacuum was applied to the petri dish to remove air bubbles before being placed in a convection oven at 80 ºC for 4 h to ensure complete curing of the PDMS. The PDMS was carefully removed from the SU-8 mold and sectioned into devices by a scalpel. Inlet and outlet holes were made using a biopsy punch (Harris Uni-Core, Ted Pella, Inc., Redding, CA). The bonding surfaces of the PDMS and a glass slide were cleaned using isopropanol and DI water then exposed to oxygen plasma in a March Jupiter III Reactive Ion Etcher (Nordson Corp., Concord, CA). The PDMS and glass pieces were

mated and placed in a convection oven at 80 ºC for 2 h for bonding to occur. Microfluidic device channels were 15 μm wide and 150 μm high.

5.3.1.2 Lipid Mixture and Hydration Buffer Preparation

Lipid mixture preparation and hydration buffer were prepared as previously described (Chapter 2.3.2, p. 21). Briefly, DPPC, cholesterol, and PEG_{2000}-PE were mixed in chloroform at a molar ratio of 50:40:10, respectively. The lipid mixture was desiccated under vacuum then re-dissolved in anhydrous ethanol with 1 wt % DiI for a total lipid concentration of 15 mM. A 1x PBS solution at pH 7.4 was used as a hydration buffer. All fluids were passed through 0.22 μm filters before being introduced to the microfluidic device.

5.3.1.3 Microfluidic Liposome Synthesis

The PDMS-glass microfluidic devices were used to form PEGylated liposomes by including PEG-conjugated lipids during liposome synthesis with phosphate buffered saline (PBS) as a hydration buffer using the method demonstrated previous.[86] Briefly, PBS was injected into two side channels intersecting with a center channel containing the ethanol/lipid mixture. The flow rate ratio (FRR), defined as the ratio of volumetric flow rate of aqueous buffer to that of solvent, was varied from FRR 3 to FRR 15 to produce liposomes of various sizes. The linear flow velocity of the combined fluid streams for all FRRs was kept constant at 0.20 m/s. The hydrodynamic focusing region within the microfluidic device was monitored with a TE-2000 S epifluorescence inverted microscope (Nikon, Melville, NY) during liposome formation to ensure the presence of consistent and symmetric flow conditions.

5.3.1.4 Asymmetric Flow Field-Flow Fractionation (AF^4) with Multi-Angle Laser Light Scattering (MALLS) and Quasi-Elastic Light Scattering (QELS)

Liposomes manufactured using MHF techniques were analyzed using Asymmetric Flow Field-Flow Fractionation (AF^4) paired to dual Multi-Angle Laser Light Scatter (MALLS) and Quasi-Elastic Light Scattering (QELS) detection (Wyatt Technology, Santa Barbara, CA). The procedure described in Chapter 2.3.4 (p. 23) was followed for liposome characterization.

5.3.2 Cellular Uptake Studies[1]

5.3.2.1 Caco-2 Cell Culture

Caco-2 cells were cultured at 37 °C in an atmosphere of 95% relative humidity and 5% CO_2 (vol %). Cells were maintained in Dulbecco's Modified Eagle's Medium (DMEM) supplemented with 10% fetal bovine serum (FBS), 1% non-essential amino acids, 10,000 units/mL penicillin, 10,000 μg/mL streptomycin and 25 μg/mL amphotericin B. Media was changed every second day and cells were passaged at approximately 90% confluence using a 0.25% trypsin/ethylendiamine tetraacetic acid (EDTA) solution.

5.3.2.2 Cytotoxicity of Liposome Populations.

Cytotoxicity tests were performed to ensure that toxicity would have no influence on cellular uptake. The WST-1 reagent assay was used to examine the viability of Caco-2 cells in presence of the differently sized liposomes at varied concentrations. Caco-2 cells, seeded at 5×10^5 cells/well, were incubated for 2 days at 37 °C, 95% relative humidity and 5% CO_2. Cells were incubated with the test liposome solution and assessed by the WST-1 assay at different concentrations. 90% to 95% viability was chosen as the minimum allowable concentration for use in uptake studies.

[1] The experiments in Section 5.3.2 were performed by Dr. Abhay Andar at the University of Maryland School of Pharmacy (Baltimore, MD).

5.3.2.3 Cytotoxicity of Endocytosis Inhibitors

Cytotoxicity of endocytosis inhibitors was assessed in Caco-2 cells to ensure the cell viability over short-term exposure to these chemicals during uptake experiments. Endocytosis inhibitors were prepared at a range of concentrations known to reduce the different pathways. Inhibitors used for their respective pathways were as follows: monodansyl cadaverine (Mdc) (150 μM to 600 μM) for clathrin mediated endocytosis; filipin (Fil) (2 μM to 8 μM) for reduction of caveolin-mediated endocytosis; dynasore (Dyn) (25 μM to 100 μM) for dynamin-dependent endocytosis; and wortmannin (Wort) (50 nM to 200 nM) for macropinocytosis dependent endocytosis (The range of all the inhibitors was determined through literature[139–141]). Cytotoxicity of the inhibitors was assessed by the water-soluble tetrazolium salt (WST-1) assay (Roche Applied Science, Indianapolis, IN). Caco-2 cells were seeded at 50,000 cells per well in a 96-well plate (Corning, NY). Cells were incubated at 37 °C, 95% relative humidity and 5% CO_2 for 48 h. Cells were washed with warm Hank's balanced salt solution (HBSS) buffer and incubated for 2 h with 100 μL solutions containing a varied concentration of endocytosis inhibitors. The solutions were removed after 2 h and cells were washed twice with HBSS buffer. WST-1 assay reagent solution was added to each well (10 μL of WST-1 in 100 μL of HBSS for each well) and incubated for 4 h at 37 °C. Following the incubation time, the plate was mixed well and then measured for absorbance on a plate reader. Absorbance at 460 nm and background at 600 nm were measured using a SpectraMax plate reader (Molecular Devices, Sunnyvale, CA). Cells incubated in HBSS were used as the negative control for 100% viability and cells incubated in Triton-X were used as the positive control. Cell viability ≥85% was classified as concentrations acceptable for uptake studies. The inhibitor concentrations used for the cellular uptake studies are represented in **Table 5.2** (p. 84): Mdc at 300 μM, Wort at 100 nM, Fil 4 μM and Dyn at 50 μM were used for the cellular uptake studies.

5.3.2.4 Cellular Uptake Studies

Cellular uptake of the various sizes of liposomes was determined in the presence and absence of endocytosis inhibitors. Inhibitors used were at concentrations that showed a minimum of 85% of viability during the 2 h period of the assay incubation period. Cells were seeded at 150,000 cell/well in a 12-well plate (Corning, NY) and grown for 3-4 days at 37 °C, 95% relative humidity and 5% CO_2. Culture medium was then removed and cells were washed twice with warm HBSS. The required amount of HBSS and liposome solution was added to each well such that the total volume was 400 μL. Cells were incubated with the liposome solution for 15 min and 1 h at 37 °C. The liposome mixture was then removed and cells were washed twice with a 1 mL solution of ice-cold Dulbecco's phosphate buffered saline (DPBS). Cells were then incubated with trypsin for 5 min, then cell culture medium was added to halt this detachment process. Cells were removed from plates, transferred to microcentrifuge tubes, and centrifuged for 4 min at 1500 rpm. After removing the supernatant, cells were washed in DPBS and finally fixed in 1% paraformaldehyde (in DPBS) solution. Flow cytometry was used to measure the cellular fluorescence using the BD LSR flow cytometer (Becton Dickenson, Franklin Lakes, NJ) with filters, λ_{Ex} = 552 nm; λ_{Em} = 577/10 nm. A 200 μL solution of 0.4% (wt %) Trypan Blue was added to each sample and 10,000 to 20,000 events were taken per sample for 4 repeat experimental samples. Percentage uptake was determined for different cell populations by the shift in mean fluorescence (region of interest determined using FlowJo software) in the presence of endocytosis inhibitors compared to the controls in HBSS. Analysis to determine the influence of liposome size on cellular uptake was determined by comparing the shift in mean fluorescence between each liposome size sample. The data for fluorescence intensity events for all liposome sizes recorded by flow cytometry was normalized to the total uptake of liposomes at 37 °C in the absence of any inhibitor (representing the 100% value on the graph) and to the difference

between the uptake in presence of inhibitors by its uptake value at 4 °C (uptake at 4 °C represents the passive uptake and hence highlights the region of interest, which varied for each liposome size). Thus, the values presented in **Figure 5.4** (p. 88) represent the percentage of liposomes not affected by the inhibitor.

5.3.2.5 Intracellular Colocalization

Intracellular trafficking of liposomes of different sizes within Caco-2 cells was investigated in addition to uptake mechanisms. Caco-2 cells were seeded at 5000 cell/cm^2 on 8-chamber slides. Slides were used after 3-5 days of incubation at 37 °C, 95% relative humidity and 5% CO_2. Cells were washed with warm HBSS and then incubated with liposomes in HBSS for 15 min to 1 h. After which cells were washed with ice-cold DPBS, and fixed with 4% (wt %) paraformaldehyde, 4% (wt %) sucrose in DPBS for 15 min. Cells were washed with permeabilization buffer (PBS containing 300 mM sucrose, 50 mM NaCl, 3 mM $MgCl_2 \cdot 6H_2O$, 20 mM HEPES, 0.5% Triton X 100 (vol %), pH 7.2), which was added to the samples and kept at 4 °C for 5 minutes. The permeabilization buffer washed out twice with DPBS and later incubated at 37 °C with blocking buffer (3% bovine serum albumin (BSA) (wt/vol) in DPBS) for 5 minutes. Cells were washed with DPBS and primary antibodies for early endosomes (rabbit polyclonal early endosome antigen -1 (EEA-1; Molecular Probes) and lysosome-associated membrane protein 1 (rabbit polyclonal lysosome antigen – 1 (LAMP-1); Molecular Probes) (both solution prepared at 1:500 vol.ratio in 3% BSA solution) were added to separate cell sample chambers and left for 1 h in the incubator at 37 ºC. The primary antibody was then removed and the cells were washed 3 times with blocking buffer and then the secondary antibody Alexa Flour-488 goat anti-rabbit IgG (Molecular probes, Carlsbad, CA) was added at 1:1000 in the blocking agent solution for 1 h. The cells were then washed with 0.5 vol/vol % Tween 20 in DPBS and finally three times with DPBS. Cells were then incubated with 300 nM 4',6-diamidino-2-

phenylindole (DAPI) for 10 min to stain the nuclei. The cells were then washed twice with DPBS and the chambers were removed. The slides were mounted and covered with glass coverslips. They were allowed to dry for a few hours before they were sealed with nail varnish and stored at 4 °C. Images were acquired using a Nikon A1 Inverted confocal laser-scanning microscope (Nikon Instruments, Melville, NY). Colocalization between liposomes with early endosomes and lysosomes was quantified using the Elements software supplied with the Nikon microscope. The extent of colocalization between the overlapping channels was determined using the Mander's overlap coefficient ($M_{x(oc)}$), calculated directly through the Nikon Elements Software. The extent of colocalization between the red and green channels ($M_{x(oc)}$) was calculated by the software using **Equation 5.1**:[140]

$$M_{x(oc)} = \frac{\sum_i x_{i,coloc}}{\sum_i x_i} \qquad \textbf{(5.1)}$$

In this equation, $x_{i,\,coloc}$ is the value of voxels of the overlapped red with green components, and x_i is the value of the red component. $M_{x(oc)}$ is reported for each treatment as an average of the 6 images where the threshold was adjusted to 5% for all images in order to compensate for any background noise. The Nikon Elements software was used for acquisition and the Volocity 3D imaging software (Improvision, Lexington, MA) was used for automated determination of colocalization values.

5.4 Results

5.4.1 Microfluidic Liposome Synthesis

Liposome solutions prepared by microfluidic flow focusing were characterized using MALLS and QELS in-line with AF^4 to determine liposome diameter, size distribution, and final number concentration of liposomes in solution. The mean diameters of liposome populations

used for cellular uptake experiments ranged from 40.6 nm to 276.6 nm (**Figure 5.1**, **Table 5.1**). The relationship between FRR and average liposome diameter of populations made within the PDMS-glass device followed trends of previously demonstrated studies,[42,43] showing an decrease in liposome size corresponding to an increase in FRR. The populations of liposomes created for this study exhibited low levels of polydispersity with very distinct diameters.

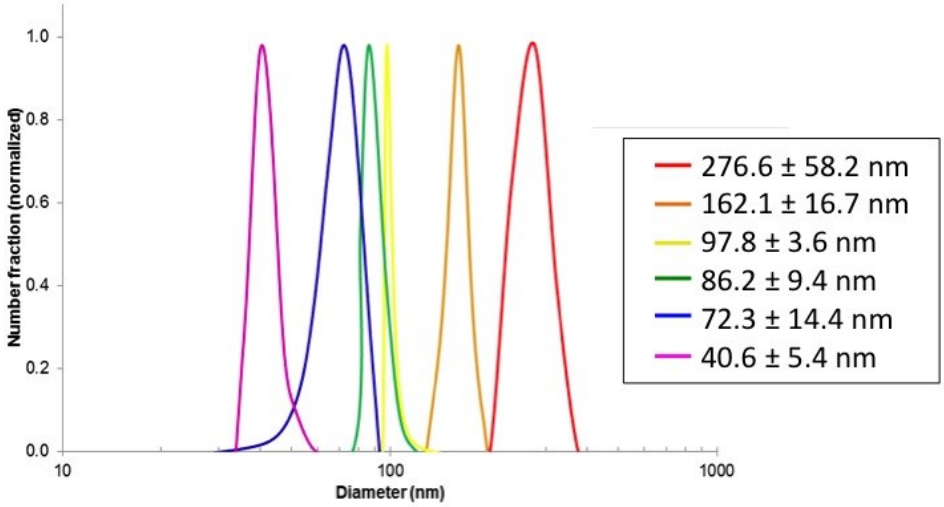

Figure 5.1: Diameter range determined by MALLS and QELS in line with AF^4. Data shows size and size distribution of the microfluidic-prepared liposomes. Mean diameter for liposomes is presented along with the size distribution (nm) for each sample. Liposome populations represented here are referenced by modal diameter throughout the text.

Table 5.1: Liposome particles represented as mean diameter, standard deviation (SD) and polydispersity index (PDI) after being prepared and collected through microfluidics channels at their respective flow rate ratios (FRR).

FRR	Mean Diameter ± SD	PDI
5	276.6 ± 58.2 nm	0.044
7	162.1 ± 16.7 nm	0.011
9	97.8 ± 3.6 nm	0.001
10	86.2 ± 9.4 nm	0.012
12	72.3 ± 14.4 nm	0.040
15	40.6 ± 5.4 nm	0.018

5.4.2 Size Dependent Uptake of Liposomes in Caco-2 Cells

Caco-2 cells were incubated with liposomes, with the number of liposomes introduced from each sample held constant. The values for total cellular uptake were determined by flow cytometry with the signal normalized to liposome surface area (DiI dye was encapsulated within the liposomal bilayer). The resulting fluorescence data from flow cytometry indicated that cellular uptake was dependent on liposome size (**Figure 5.2**). Liposome uptake was measured for two different incubation time points, 15 min and 1 h, both at 37 °C. The total cellular uptake for the smallest liposomes (40.6 nm) was significantly higher, almost a 12-fold increase, than the largest liposomes (162.1 nm and 276.6 nm). Cellular uptake of the medium-sized liposomes

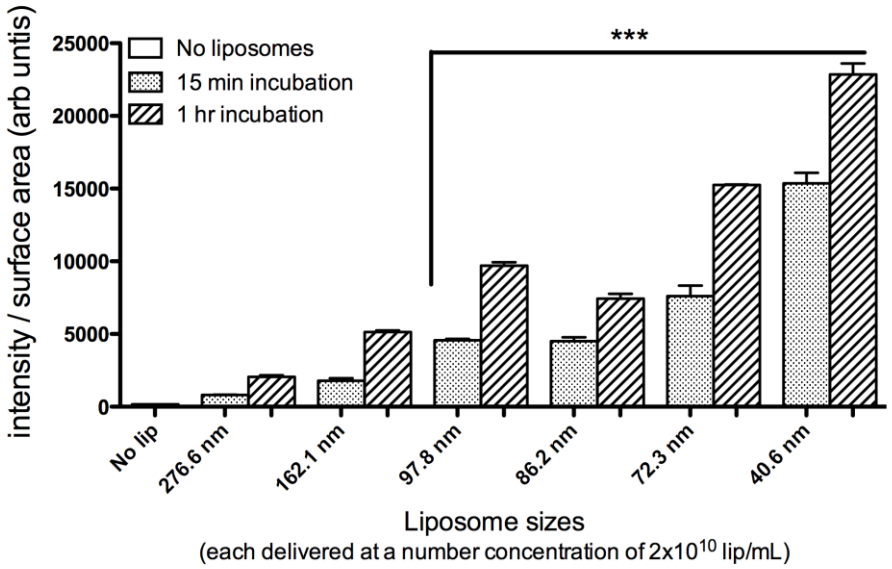

Figure 5.2: Size dependent uptake of liposomes. Flow cytometry results for Caco-2 cells were incubated for 15 min and 1 h at 37°C with liposomes ranging from 40.6 nm to 276.6 nm in mean diameter (liposomes contained DiI-C_{18} lipophilic dye). Fluorescence data was normalized to liposome diameter, revealing the highest liposome uptake for 40.6 nm. Each cell population was incubated with a consistent particle concentration (2 x 10^{10} liposomes/mL). *** indicates a significant difference ($p<0.001$) by One-way ANOVA test when compared with control sample without liposomes. *Figure generated by A.U. Andar.*

(86.2 nm and 97.8 nm) demonstrated an intermediate level of uptake compared to the liposomes on opposite ends of this size spectrum.

5.4.3 Endocytosis Inhibitors and Their Influence on Liposome Uptake

Four endocytosis inhibitors were used to examine the pathways of cellular uptake as a function of liposome size. Before initiating the uptake and transport studies, Caco-2 cell viability during 2 h assay time was confirmed in the presence of the endocytosis inhibitors and the concentrations were determined based on those found in literature.[139–141] Inhibitor concentrations that showed cell viability values ≥ 80% were selected for uptake experiments (results presented in **Figure 5.3** and **Table 5.2**). Monodansyl cadeverin (MDC), a clathrin-mediated endocytosis pathway inhibitor, was used at a concentration of 300 μM for cell studies. At this concentration,

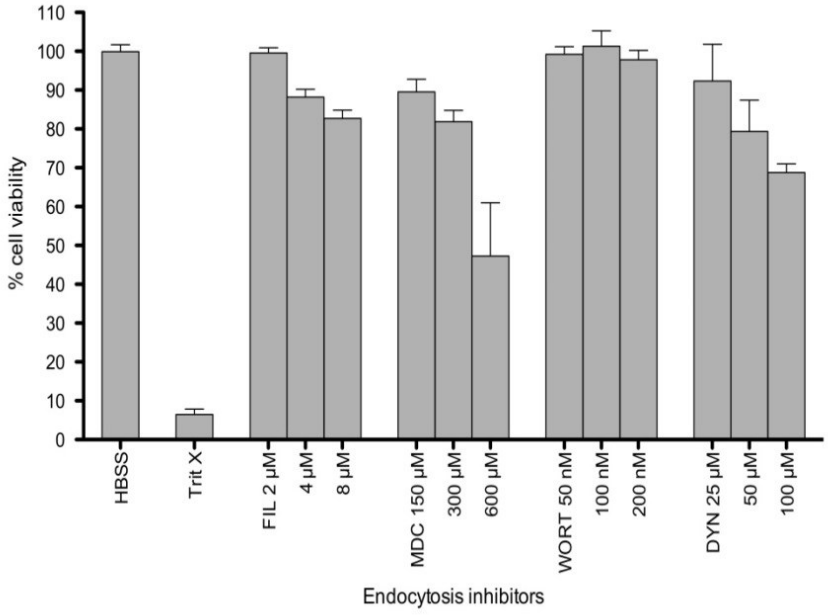

Figure 5.3: Cytotoxicity of endocytosis inhibitors. Cell populations were incubated for 2 h at 37°C with various endocytosis inhibitors. The graph indicates the percentage of cell viability for the different concentrations for each endocytosis inhibitor and results are reported mean ± standard deviation, n = 6. *Figure generated by A.U. Andar.*

Table 5.2: Cytotoxicity of endocytosis inhibitors. *Table generated by A.U.*

Endocytosis Inhibitor	Concentration (mM)	% Cell Viability (Mean± SD)
Monodansyl cadeverine (MDC)	300	81.84 ± 7.2
Wortmannin (WORT)	0.1	101.28 ± 9.8
Filipin (FIL)	4	88.17 ± 4.9
Dynasore (DYN)	50	79.36 ± 13.9

little toxicity was observed compared to the maximum tested concentration of 600 μM. Filipin (FIL), which inhibits the caveolae-mediated endocytosis pathway by binding to cholesterol inside caveolar pits and disrupting the pathway cycle, was used at a concentration of 4 μM for cell uptake experiments. Wortmannin (WORT), which inhibits the process of macropinocytosis, did not show a considerable level of toxicity at any of the tested concentrations (50 nM to 200 nM), thus 100 nM concentration was used for inhibition experiments as shown previously in literature.[141] Dynasore (DYN), an inhibitor which is responsible for vesicle scission during both clathrin- and caveolin- mediated pathways and selectively inhibits dynamin 1 and dynamin 2 GTPases during uptake,[140,142] showed increasing toxicity over the concentrations tested with an acceptable viability value at 50 μM, the value chosen for subsequent experiments.

It has been reported that liposomes are predominantly endocytosed through either the clathrin- or caveolin- mediated endocytosis.[143–145] Since liposomes prepared via microfluidics exhibit significantly decreased variability in size and polydispersity compared to those made through traditional processes, the present experiments are able to distinguish the uptake pathways experienced by each population of distinctly-sized liposomes and elucidate specific relationships between endocytic fate and vesicle size. The effect of vesicle size on cellular uptake was compared at different conditions of temperature (37 °C and 4 °C) and in the presence of each respective endocytosis pathway inhibitor at 37 °C.

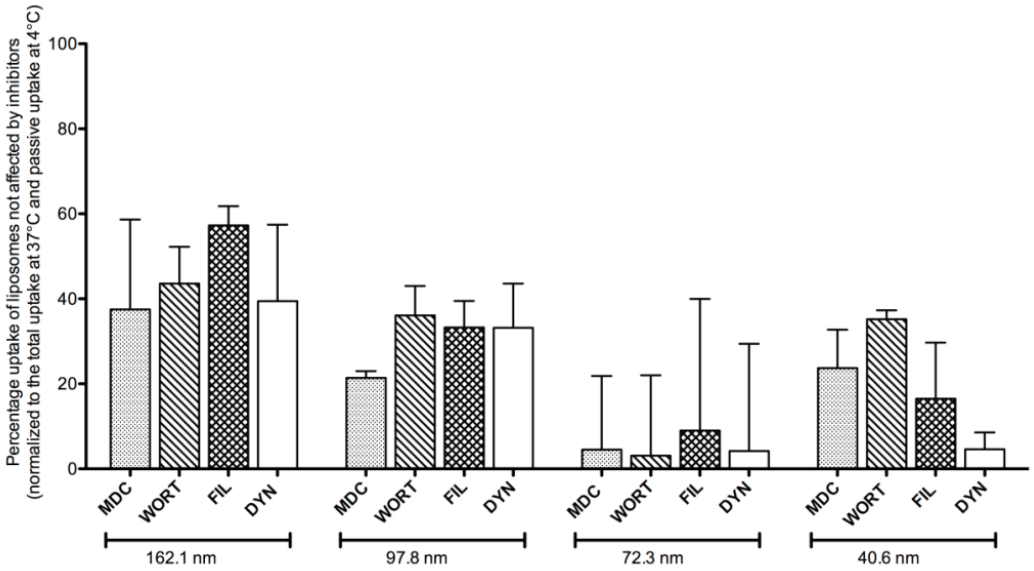

Figure 5.4: Liposome uptake in presence of endocytosis inhibitors. Liposomes of different sizes (162.1 nm, 97.8 nm , 72.3 nm and 40.6 nm) were used for uptake studies in presence of endocytosis inhibitors. Data is normalized to the total uptake at 37 °C (100%) and passive uptake at 4 °C (starting point, 0%). The graph represents the percentage of liposomes that are not affected by inhibitors, monodansyl cadeverin (MDC)(300 μM), wortmannin (WORT)(100 nM), filipin (FIL)(4 μM), and dynamin (DYN)(50 μM). All presented as the mean with error bars representing the standard deviation with n = 4 (10,000 to 20,000 events each sample repeat 'n'). *Figure generated by A.U. Andar.*

Uptake of liposomes at 4 °C represents passive cellular uptake: at this low temperature there is a global suppression of all active endocytotic pathways, thus any liposome uptake at 4 °C is completely dependent on the ability of the particle to be passively internalized through the cell membrane. Conversely, the uptake of liposomes at 37 °C in the absence of endocytosis inhibitors represents total cellular uptake when all available endocytosis mechanisms within Caco-2 cells may be fully utilized. In **Figure 5.4** and **Table 5.3**, the effects on uptake in presence of endocytosis inhibitors are represented (all normalized to the total uptake at 37 °C, which

Table 5.3: Total liposome uptake in presence of endocytosis inhibitors, represented by absolute values of number of liposomes endocytosed ($x10^9$), normalized to the total uptake at 37 °C (100%) and passive uptake at 4 °C (starting point, 0%) .

	Absolute Number of Liposomes Endocytosed ($x10^9$)			
Liposome Diameter	**MDC**	**WORT**	**FIL**	**DYN**
162.1 nm	3.00 ± 1.7	3.48 ± 0.6	4.56 ± 0.4	3.16 ± 1.4
97.8 nm	1.72 ± 0.1	2.88 ± 0.4	2.64 ± 0.6	2.64 ± 0.7
72.3 nm	0.32 ± 1.4	0.24 ± 1.5	0.76 ± 2.4	0.28 ± 2.1
40.6 nm	1.92 ± 0.7	2.80 ± 0.2	2.12 ± 0.2	0.36 ± 0.3

represents 100% total uptake in absence of endocytosis inhibitors, and passive uptake at 4 °C). Therefore, any difference between the uptake at 37 °C and the uptake under the influence of inhibitors represents the liposome uptake hampered by the inhibitor, while the difference between the uptake of liposomes in the presence of endocytosis inhibitors and the uptake at 4 °C represents the amount of liposomes not influenced by the pathway. Relative values of uptake are expressed in **Figure 5.4**, and absolute values of liposomal uptake presented in **Table 5.3**.

The presence of MDC (clathrin-mediated pathway inhibitor) caused a much greater inhibition of cellular uptake of 72.3 nm diameter liposomes compared to the other sizes, 162.1 nm, 97.8 nm, and 40.6 nm (**Figure 5.4**). An almost complete suppression of uptake was mainly observed for the medium sized liposomes (72.3 nm), suggesting that the 72.3 nm liposomes may rely on the clathrin-dependent uptake mechanism for entry into Caco-2 cells. In contrast, MDC caused minimal effect on the uptake of the smallest liposomes (40.6 nm). These observations suggest that 40.6 nm diameter liposomes might be exploiting a clathrin-independent pathway for entry into Caco-2 cells.

In the presence of WORT, (macropinocytosis uptake pathway inhibitor), the smaller liposomes (40.6 nm) experienced little change in their uptake as compared to the other sizes, suggesting that this pathway may not significantly influence their entry into Caco-2 cells. WORT

pathway inhibitor like the MDC inhibitor, caused almost complete inhibition in cellular uptake of 72.3 nm liposomes (**Figure 5.4**), suggesting that this size range may also be majorly influenced by the macropinocytosis uptake mechanism. The larger 162.1 nm and 97.8 nm liposomes were not very greatly influenced by this pathway in comparison to the other sizes.

Upon exposure to FIL (**Figure 5.4**), (caveolar-mediated endocytosis inhibitor), there was very little inhibition in cellular uptake of the larger liposomes (97.8 nm and 162.1 nm), but an increased inhibition of small- and medium-sized liposomes (40.6 nm and 72.3 nm). These results suggest the possibility of small- and medium-sized liposomes following caveolae-mediated (clathrin-independent) endocytosis pathways, as opposed to their larger counterparts.

Under the presence of DYN (dynamin inhibitor), nearly complete inhibition of cellular uptake of small- and medium-sized liposomes (40.6 nm and 72.3 nm) was observed, whereas larger 97.8 nm and 162.1 nm diameter liposomes were not affected much by the inhibitor in comparison.

In conclusion, exposure to the combination of inhibitors of specific endocytosis pathways and liposomes of various sizes has been studied here to elucidate size-based uptake mechanisms experienced by Caco-2 cells in culture. When deriving a comparison between the effect of inhibitor on cellular uptake of liposomes of different sizes, the size ranges of 162.1 nm and 97.8 nm appeared to not be heavily influenced for most of the tested pathway inhibitors. However, this comparison is more interesting when made between the different inhibitors within each size of liposome. For example, MDC and DYN have a slightly greater effect on the uptake than FIL and WORT for 162.1 nm liposomes, possibly suggesting that this size could possibly be influenced by a clathrin- and dynamin- dependent endocytosis pathways. Additionally, MDC seems to have the most effect compared to the other pathway inhibitors (FIL, DYN and WORT) for the 97.8 nm liposomes, suggesting that the clathrin-dependent pathway may influence this

size range. All pathway inhibitors tested here influenced the uptake of 72.3 nm diameter liposomes, indicating that liposomes of this size may have the ability to be taken up through several mechanisms within Caco-2 cells. Finally, the smallest tested liposomes (40.6 nm) were mainly inhibited by DYN, indicating that the fate of particle internalization may depend primarily on a dynamin-dependent endocytosis pathway. Dynamin-dependent pathways include caveolar- and clathrin-mediated pathways, but also include some alternative pathways. Therefore, a combination of the effect of the effect of DYN, FIL, and WORT provide interesting information of the Caco-2 cells and their liposomal uptake mechanisms.

5.4.4 Intracellular Trafficking Using Confocal Microscopy

Intracellular trafficking of liposomes was observed in addition to determining their uptake mechanisms (**Figure 5.5**). Liposomes were expected to colocalize with the endosomes and

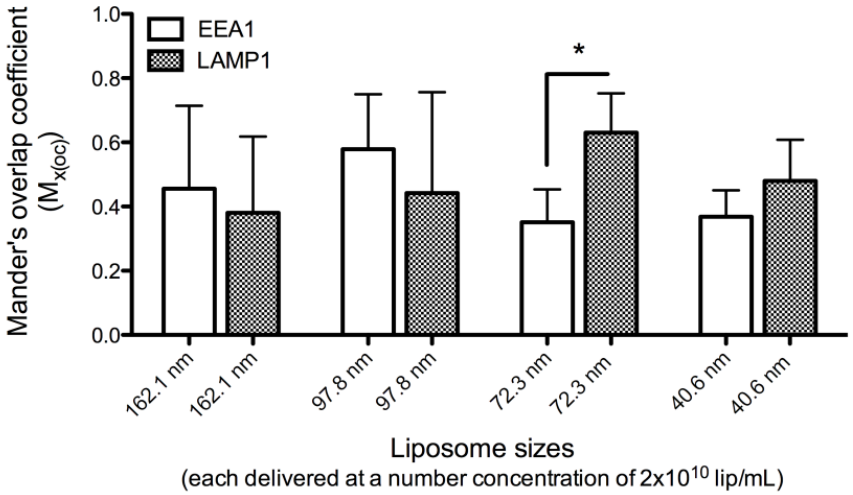

Figure 5.5: Colocalization of liposomes with EEA-1 and LAMP-1.Intracellular trafficking of liposomes was measured after 1 h incubation with Caco-2 cells. Colocalization between liposomes and endosomes (EEA1)/lysosomes (LAMP1) was measured using Mander's overlap coefficient ($M_{x(oc)}$). Results are reported as the mean with error bars representing standard deviation (n=8), where * represents a significant difference for ($p < 0.05$) by One-way ANOVA and by Tuckey's Multiple Comparison test. *Figure generated by A.U. Andar.*

lysosomes over time, thus the goal for this experiment was to see the differences in colocalization between the varied liposome sizes and endosome (EEA-1) or lysosome (LAMP-1) compartments after 1 h of incubation at 37 °C. From **Figure 5.5** and **Figure 5.6**, a trend was observed in the colocalization of liposomes, where the much smaller 40.6 nm and 72.3 nm liposomes colocalized with the endosomes slightly less than the 97.8 nm and 162.1 nm diameter liposomes. Although more than 40% of the 40.6 nm liposomes appear to have colocalized with endosomes, it may be possible that the remaining 60% may move further down the trafficking pathway, into late endosome or lysosome vesicles.

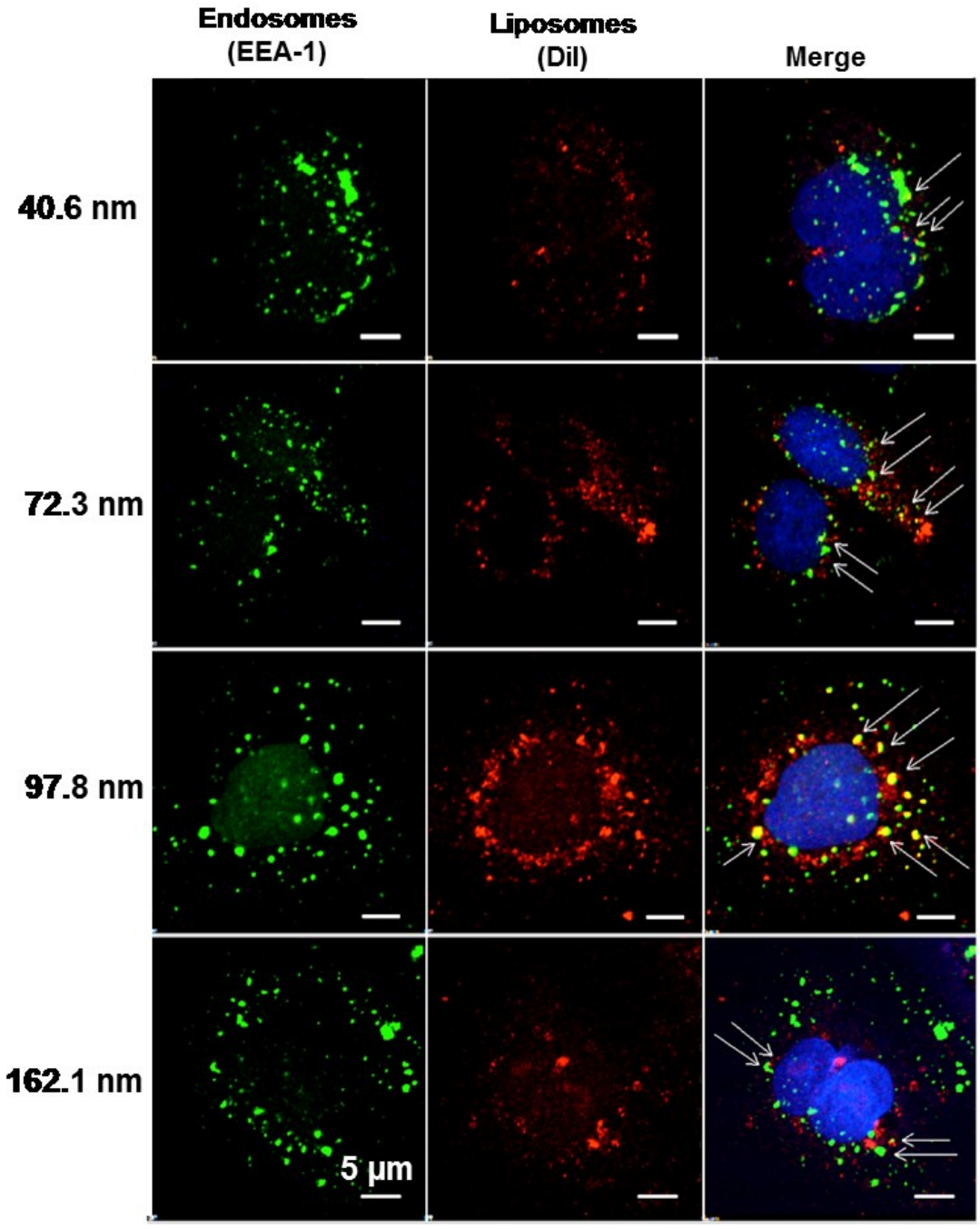

Figure 5.6: Confocal imaging of colocalization of liposomes with endosomal regions. Caco-2 cells incubated for 1 h with DiI-C_{18} (red) fluorescently labeled liposomes: A) 40.6 nm, B) 72.3 nm, C) 97.8 nm, and D) 162.1 nm liposomes. Endosomes were stained using AlexaFluor 488 (green) for anti EEA1 antibody. These samples were examined by confocal microscope (Nikon A1). The nucleus was stained with Dapi. The arrows in the merge image point to the colocalized regions. *Image generated by A.U. Andar.*

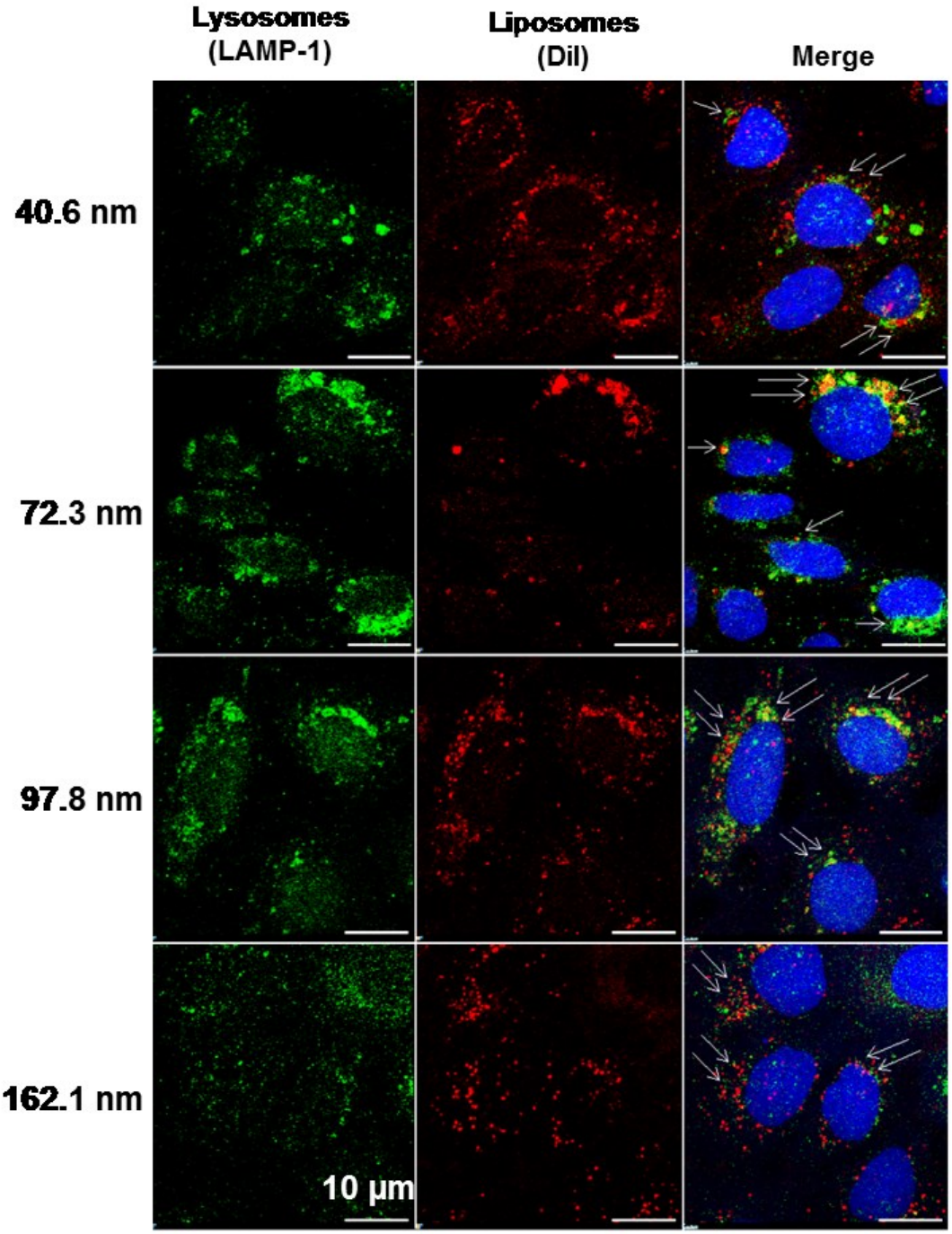

Figure 5.7: Confocal imaging of colocalization of liposomes with lysosomal regions. Caco-2 cells incubated for 1 h with DiI-C_{18} (red) fluorescently labeled liposomes: A) 40.6 nm, B) 72.3 nm, C) 97.8 nm, and D) 162.1 nm liposomes. Lysosomes were stained using AlexaFluor 488 (green) for anti Lamp-1 antibody. These samples were examined by confocal microscope (Nikon A1). The nucleus was stained with Dapi. Arrow in the merge images point to the colocalized regions. *Image generated by A.U. Andar.*

Figure 5.5 and **Figure 5.7** show that 72.3 nm and 40.6 nm liposomes are more highly colocalized with the LAMP-1 lysosomal region than with EEA-1 endosomal regions. The 72.3 nm diameter liposomes colocalizing with the LAMP-1 regions much more compared to any of the other tested sizes, suggesting that a higher percentage of these diameter range liposomes might accumulate in the lysosomes and drug release may be quicker and more effective.

5.5 Discussion

Microfluidic technology enabled the production of nearly monodisperse populations of liposomes with distinct diameters for size-specific cellular uptake studies. For this study, liposomes were prepared using an established microfluidic method where solutions of nearly monodisperse liposomes were achieved through hydrodynamic flow focusing.[41] Here, this method was adopted to prepare populations of liposomes for novel cellular uptake studies in which the relationships between endocytosis mechanisms and vesicle sizes were analyzed with high specificity. The ability to control liposome size and polydispersity, to an extent, has potential to have a large impact on numerous drug delivery applications and could improve upon currently available liposome-based drugs by rendering them more site-specific and efficient.[136] In order to design effective liposomal drug delivery systems, it is critical to also understand the detailed mechanisms of their cellular trafficking and transport.[135] In this chapter, liposomes prepared within microfluidic devices, via hydrodynamic flow focusing,[41,42] ranged in mean diameters of 40.6 nm to 276.6 nm.

The overall cellular uptake of liposomes over time (15 min and 60 min at 37 °C) was observed to be dependent on liposome size in Caco-2 cells. Total cellular accumulation was higher for the smallest liposomes (40.6 nm) and for the medium range liposomes (72.3 nm) in comparison to the largest liposomes (276.6 nm) (**Figure 5.2**). This illustrates the significant effect of size on cellular uptake, particularly that smaller liposomes are internalized more readily

over time. When considering liposome based drug targeting for *in vivo* conditions the circulation, accumulation, *in vivo* drug release and clearance have been extensively studied revealing that amongst other things, size is an important factor when considering a vehicle for drug delivery.[37,109] Previous studies have shown a positive correlation to the effect of liposome size on the rate of clearance from blood and also suggesting that a decrease in the liposome size may reduce recognition by components in blood, like the mononuclear phagocytic system (MPS).[37] Although in some cases liposome delivery and effectiveness is also dependent on the lipid composition [139,146,147] and surface charge or chemistry,[22,148,149] it has been shown that size is also a major factor determining effectiveness of drug delivery. When considering liposome delivery for antitumor drugs, size appears to be a major factor affecting drug permeation into the *in vivo* tumor environment and local tumor tissue, where the optimal size has been shown to in the range of ≤100 nm.[37,109] This size range has also been shown to accumulate more within tumor tissues compared to much larger sizes.[37] However, a liposome size of 100 nm may not always be optimal for all tumors, since tumor conditions such as the pore size of a given tumor's vessels varies depending on the type of tumor, site of the growth, size of the tumor and the regression of the tumor site.[150,151] This study reveals the higher *in vitro* effectiveness of smaller (40.6 nm) liposomes compared to much larger (97.8 nm to 276.6 nm) liposomes on uptake in Caco-2 cells, therefore suggesting that the former may be a more relevant size for specific targeting applications when translating this study to *in vivo* conditions.

Size-dependent liposome internalization was also evaluated by focusing on four major cellular uptake pathways: clathrin-mediated, caveolin-mediated, macropinocytosis and dynamin-dependent pathways, using liposomes with distinct diameters ranging from 40.6 nm to 162.1 nm. These endocytosis pathways represent unique internalization mechanisms by which cells respond to certain micro and nanoparticles. The clathrin-mediated pathway is dependent on the formation

of coated pits by the assembly of the protein clathrin, which forms a triskelion-like shape composed of three clathrin heavy chains and three light chains.[137] Upon endocytosis of particles, the coated pits form vesicles which are typically 120~150 nm in diameter.[136,137,152] The caveolae-mediated pathway is dependent on the protein caveolin, which binds cholesterol to sphingolipids in certain areas and forms flask-like invaginations of the cell plasma membrane. Caveolae vesicles range approximately 50~80 nm in diameter.[136,137] The macropinocytosis pathway is a clathrin- and caveolin- independent, actin-dependent process where the protrusions from the cell membrane collapse onto and fuse with the plasma membrane to generate large endocytic vesicles ranging from 500~1000 nm in diameter (depending on the cell type).[136,137] Macropinocytosis pathways are not size specific and can internalize small to large particles. The dynamin-dependent pathway is an important receptor-mediated pathway in which the enzyme dynamin pinches vesicles from the plasma membrane during endocytosis.[153,154] Some studies suggest that dynamin may also be involved in certain caveolae- and clathrin-independent pathways, including the Ras homolog gene family member A (RhoA)-dependent pathway, cell division control protein 42 (Cdc42)-dependent pathway, and flotillin-dependent pathways.[153] Studies have also suggested that dynamin may self-assemble into rings (typically 30~50 nm in diameter) which constrict invaginated coated pits around their necks to form budding coated vesicles.[155]

In these experiments, the dynamin-dependent pathway appeared to specifically influence the smaller 40.6 nm liposomes. Interestingly, 72.3 nm diameter liposomes were also seemingly affected by the dynamin-dependent pathway, while the 97.8 nm to 162.1 nm liposomes were nearly unaffected. The larger 97.8 nm to 162.1 nm liposomes were not influenced by any of the four pathways tested as much as the smaller 72.3 nm and 40.6 nm liposomes. The larger 162.3 nm liposomes seemed to be more affected by the MDC and DYN inhibitors than the FIL and WORT inhibitors, which may suggest that this size range may be influenced slightly by the

clathrin- and dynamin- dependent pathways. The 97.8 nm liposomes were more highly influenced by MDC in comparison to the other inhibitors (*i.e.* FIL, WORT and DYN), suggesting that this size range may be the most highly influenced by the clathrin-dependent endocytosis pathway. In contrast, the 72.3 nm liposomes appear to be affected by all tested pathway inhibitors, suggesting this may be a useful size range for drug delivery applications since it utilizes most of the major trafficking pathways within cells.

Chemical inhibitors have a varied effectiveness in different cell lines and have the ability to be somewhat non-specific,[140] therefore liposome particles may behave differently depending on cell type and these results may only be true specifically for cellular uptake in Caco-2 cells. Intracellular trafficking experiments, including confocal microscopy, shed further light intracellular fate of the liposomes after cellular uptake. Colocalization between the liposomes of varied size with endosomal and lysosomal markers was reported in Caco-2 cells. Early endosomal accumulation of 97.8 nm diameter liposomes was much greater than lysosomal accumulation after 1 h of incubation. The 72.3 nm liposomes appeared to be more highly accumulated within lysosomal regions compared to endosomal regions after 1 h incubation. A similar trend was observed for the 40.6 nm diameter liposomes, where a slightly higher lysosomal accumulation was observed in comparison to the endosomal regions. These observations suggest that greater amounts of the 40.6 nm and 72.3 nm diameter liposomes travel to lysosomes for degradation compared to their larger counterparts, which is a key step in the effective targeting and drug release.[137] Conclusively, these findings demonstrate a size dependence of liposomes on both overall cellular uptake in addition the various specific mechanisms which come into play during the endocytosis process.

Previous studies probing the cellular uptake and trafficking of liposomes have been based on populations of vesicles with high levels of polydispersity due to the limitations of contemporary

synthesis methods,[42,142] thus the ability to highlight the true fate of each individual vesicle size within the range of interest was limited. This study utilizes the ability of microfluidic mixing of chemical species to produce nearly monodisperse populations of liposomes with distinct, varying size for cellular uptake studies. The benefits of the microfluidic technique for liposome synthesis are highly advantageous for increasing specificity and efficacy while reducing toxicity of liposomes for drug delivery applications. Additionally, microfluidic liposome preparation is a continuous flow, one-step process; limits reagent consumption; and may be a more cost effective method for liposome production due to expenses for liposome production in both academia and industry.[156] The ability to synthesize homogenous populations of liposomes also permits a higher level of control over the intracellular fate of the drug carrier, thus aiding in more sophisticated design of liposomal drug delivery systems. Through these unique studies, the advantages of the microfluidic method for liposome synthesis have been highlighted by producing liposomes of very distinct sizes and showing highly specific interactions with Caco-2 cells *in vitro* which reveal a size dependence on both overall uptake as well as intracellular fate.

5.6 Conclusion

This chapter reports a detailed study of cellular uptake mechanisms and intracellular trafficking related to the uptake of liposome populations prepared by an established microfluidic flow focusing technique. The unique ability of microfluidic flow focusing to produce nearly monodisperse populations of liposomes with distinct sizes is highly advantageous for increasing the specificity for drug delivery applications. These findings reveal that intracellular uptake of liposomes in Caco-2 cells is size dependent and that overall uptake increases with a decrease in particle size. Specific endocytosis mechanisms involved in the uptake of liposomes also depend particle size. These studies show that the smallest 40.6 nm liposomes appear to depend on a

dynamin dominant uptake pathway. Additionally, the slightly larger liposomes (97.8 nm to 162.1 nm in diameter) did not show any significant dependency on any particular uptake pathways that were tested in comparison to their smaller counterparts, while in comparison to other larger liposomes a slight dependency on the clathrin-mediated pathway was observed. A unique observation from this study was the dependence of an intermediate size of liposomes (72.3 nm) on almost every endocytosis mechanism tested. In addition, the 72.3 nm liposomes showed the highest accumulation within lysosomal regions inside the Caco-2 cells in comparison to the other sizes of liposomes. In conclusion, microfluidic liposome preparation has enabled the demonstration of the important role of liposome size on facilitating the particle recognition by particular cellular mechanisms. In future work, the microfluidic technique for liposome synthesis may be utilized to further assist in designing more effective populations of liposomes for various drug delivery applications.

Chapter 6 : Size-Dependent Dermal Transport of Microfluidic-Enabled Liposomes

6.1 Summary

This chapter presents a series of experiments which were completed through combined efforts with Dr. Eric L. Kendall at the University of Maryland College Park. The chapter is adapted from a submitted journal article in which Dr. Kendall and I share first authorship. Experimental work, analysis, and manuscript preparation are a result of equal effort from both parties.

Microfluidic synthesis of small and nearly monodisperse liposomes is used to investigate the size-dependent passive transdermal transport of nanoscale lipid vesicles. While large liposomes with diameters above 105 nm are found to be excluded from deeper skin layers past the stratum corneum, the primary barrier to nanoparticle transport, liposomes with mean diameters between 31 nm to 41 nm exhibit significantly enhanced penetration. Furthermore, multicolor fluorescence imaging reveals that the smaller liposomes pass rapidly through the stratum corneum without vesicle rupture. These findings reveal that nanoscale liposomes with well-controlled size and minimal size variance are excellent vehicles for transdermal delivery of functional nanoparticle drugs.

6.2 Introduction

Transdermal drug delivery offers significant potential as an alternative to oral delivery and hypodermic injection due to the promise of pain-free local or systemic introduction of drugs with controllable delivery rates over extended time periods.[157] Effective delivery of drug through the skin is hampered by poor diffusive transport across the stratum corneum (SC) layer, a 10 μm to

20 μm thick tissue region comprised of a structured lipid/protein matrix.[158,159] Even when employing chemical penetration enhancers, a broad class of skin disrupting molecules including a variety of surfactants,[157,160] transdermal drug delivery has met only limited success. Techniques such as dermabrasion and thermal ablation can temporarily render the SC porous to enhance drug transport, but these methods require active disruption of the skin and do not allow controlled doses to be delivered over long time periods. Similarly, non-invasive active methods such as ionophoresis and ultrasound require specialized equipment and only enhance drug transport for short periods. Nanoparticles are an alternative strategy for passive transdermal delivery, offering increased drug loading, sustained release, and the potential for tissue-specific targeting. The structure of the SC includes lamellar lipid regions that present sub-nanometer intercellular spaces which can be widened in the presence of nanoparticle colloids to pores with dimensions on the order of several tens of nanometers.[159,161] Inorganic quantum dots ranging from approximately 4 nm to 12 nm in diameter exhibit efficient passive transport across the SC.[162,163] However, the utility of these nanoparticles for drug delivery is limited by high toxicity and low drug loading capacity.[164] In contrast, lipid nanoparticles present a highly attractive route for drug delivery due to their excellent biocompatibility.[65] In particular, nanoscale liposomes with lipid bilayers encapsulating aqueous internal volumes offer high loading of both hydrophilic and amphipathic drugs, low toxicity, and tunable stability. However, there is little evidence that lipid vesicles ranging from 60 nm to several micrometers in diameter can traverse the SC in significant numbers,[165–168] nor is there clear evidence of intact liposome passage through the SC. As a result, the application of lipid nanoparticles for transdermal drug delivery has largely focused on flexible liposomes such as transfersomes[74] and ethosomes,[169] which incorporate surfactants or alcohols to impart a high degree of flexibility to the vesicle membranes, putatively allowing relatively large vesicles to traverse the small intercellular pores within the SC. However, for

systemic delivery through the bloodstream, these nanoparticles are not ideal since large and flexible liposomes are subject to rapid opsonization and phagocytotic clearance. Furthermore, whereas both pharmacokinetics and biodistribution of traditional liposomes have been extensively studied and optimized, the behaviors of flexible liposomes remain largely unknown. More fundamentally, recent evidence indicates that ultraflexible transfersomes are highly compromised by passage through the skin, and may be no better than traditional liposomes for transdermal delivery of intact vesicles.[170]

This chapter leverages a microfluidic technique that employs hydrodynamic focusing of a stream of solvated lipid sheathed by a sheath flow of aqueous buffer within a continuous flow process.[41,42,44,86] This approach provides the ability to generate well-defined populations of small liposomes with narrow size distributions, enabling the effective study of the size-dependent transport of lipid vesicles across the SC. Conventional bulk methods of liposome production, including membrane extrusion[30] and sonication,[34] are limited in their ability to generate well defined populations of liposomes with diameters in the size range expected to support effective transport of nanoparticles through the SC. As a result, prior studies have not shown extensive penetration of traditional liposomes past the SC.[165–168] In the present study, the capacity of the microfluidic technique to produce small liposomes with low polydispersity was exploited to generate populations of dye-laden vesicles that are almost entirely within the 25 nm to 40 nm diameter range previously reported to result in high transdermal flux of other monodisperse nanoparticles.[171,172] Microfluidic-enabled liposome preparations with mean diameters ranging from 31 nm to 308 nm were prepared. Within this size range, two classes of liposomes were formed that differed by the incorporation of small amounts of either anionic lipids or PEGylated lipids, enabling the influence of surface chemistry on trans-SC flux to be investigated. For all liposome preparations in this study, the polydispersity index of the microfluidic-synthesized

liposomes ranged from 0.035 to 0.135; as a comparison, a previous study investigating vesicles as small as 120 nm reported the use of liposomes with polydispersity indices varying from 0.1 to 0.3.[173] Overall, the microfluidic-enabled liposomes produced here are both smaller and more narrowly distributed in diameter than bulk scale produced liposomes used in prior passive transdermal drug delivery studies. The use of smaller liposomes is significant due to the hypothesis that liposomes, like other nanoparticles [159,161,171,172] will exhibit size-dependent dermal transport, with vesicles smaller than approximately 40 nm in diameter traversing the SC more effectively than larger nanoparticles. Similarly, the low polydispersity is significant since the total fluorescence signal from a vesicle population with a wide size distribution will be biased by the presence of significant number of liposomes above the mean diameter, prohibiting accurate evaluation of transport as a function of vesicle size. While a French press technique for liposome preparation has been reported to enable the formation of small unilamellar vesicles with diameters below approximately 30 nm to 50 nm,[174,175] this method does not allow vesicle size to be readily tuned. The exceptionally low polydispersity of the microfluidic-enabled liposomes over a wide range of diameters allows a unique view into size-dependent dermal transport.

6.3 Materials and Methods

Ethics Statement. This research involved Yorkshire piglets sacrificed as part of a separate parallel study approved by the Institutional Animal Care and Use Committee (IACUC) at the Children's National Medical Center. All procedures were performed in accordance with the National Institutes of Health Guide for the Care and Use of Animals in Research.

6.3.1 Lipid Mixture and Hydration Buffer Preparation

Two variations of lipid mixtures were prepared to analyze the resulting penetration depth of both PEG-conjugated (PEGylated) and negatively-charged (anionic) into dermal tissue. In addition to enhancing liposome stability, PEG is commonly attached to the exterior of liposomes as a protective shield from the immune system during blood circulation,[3] potentially increasing the bioavailability of PEGylated liposomes that are able to reach and enter subcutaneous capillaries after transdermal transport. Lipid mixture preparation and hydration buffer were prepared as previously described (Chapter 2.3.2, p. 21). Briefly, for PEGylated liposomes, DMPC, cholesterol, and PEG_{2000}-PE were combined in chloroform at a molar ratio of 70:25:5 (respectively). For anionic liposomes, DMPC, cholesterol, and anionic surfactant DCP were mixed in chloroform at a molar ratio of 50:40:10 (respectively). All lipid mixtures were desiccated under vacuum then re-dissolved in anhydrous ethanol (Sigma Aldrich) for a total lipid concentration of 40 mM. To assist in fluorescent imaging, DiI was included into the lipid mixtures (1 wt%). A 1x PBS (10 mM) solution at pH 7.4 was used as a hydration buffer, with selected samples containing 1 mM hydrophilic sodium fluorescein salt (SF) (Sigma Aldrich) as a hydrophilic dye. All fluids were passed through 0.22 μm filters before being introduced to the microfluidic device.

6.3.2 Liposome Synthesis and Characterization

PEGylated and anionic liposomes were prepared using methods described previously.[41,42,44,86] Briefly, a flow focusing microchannel network for liposome synthesis was fabricated following previous work.[176] All microchannels in the final device were nominally 50 μm wide and 300 μm tall. The prepared lipid-ethanol solution was injected into the microfluidic device between two sheath flows of the aqueous buffer. The FRR was varied from 5 to 50 to produce liposomes with modal diameters ranging from 31 nm to 308 nm (**Figure 6.1**). Total average linear flow velocity

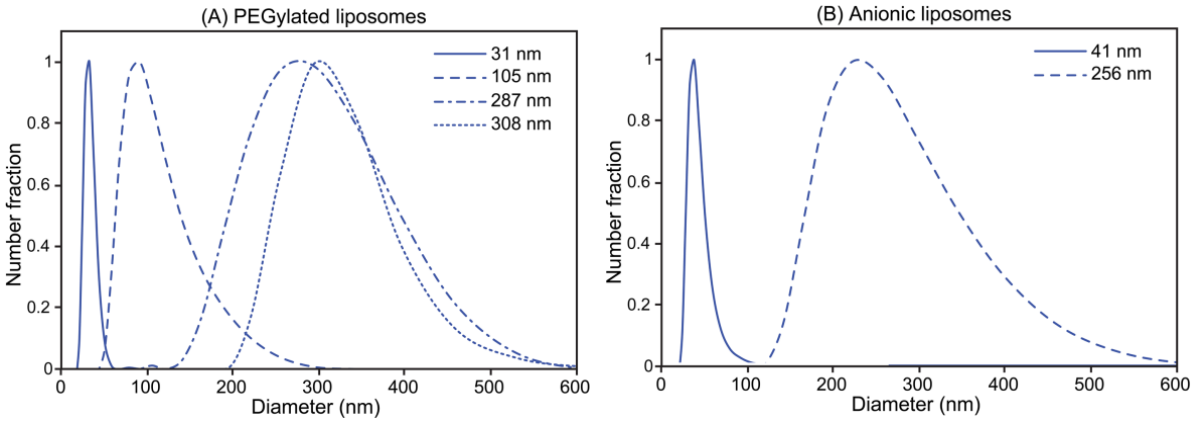

Figure 6.1: Volume-weighted size distributions of microfluidic-enabled (A) PEGylated and (B) anionic liposomes, revealing narrow size distributions over the full size range from 31 nm to 308 nm.

for all FRRs was kept constant (0.125 m/s) for a total volumetric flow rate of 112 μL/min. To enable the formation of smaller vesicles, the temperature of the microfluidic device was controlled by contacting the glass slide of the device with a hot plate at 50 °C throughout the entire synthesis process.[93] The resulting liposome populations were characterized for size via dynamic light scattering (Nano ZSP, Malvern Instruments Ltd., UK). Size distribution plots were generated by fitting spline curves to the binned distribution data imported from the dynamic light scattering instrument.

The microfluidic-generated liposomes contained lipophilic DiI in their bilayers and hydrophilic SF in their cores to enable fluorescence imaging of tissue penetration depth. To remove any remaining dye not incorporated into the liposomes during the synthesis process, all liposome samples were purified via size exclusion chromatography on Sephadex G-25 PD-10 columns (GE Healthcare, Piscataway, NJ) equilibrated with PBS immediately before application to the tissue. Gel filtration using the PD-10 columns provides efficient buffer exchange for removal of ethanol used in the liposome formation process, thereby preventing variations in

ethanol concentration (2–16%) used for different liposome populations from affecting skin permeation experiments. Final lipid concentrations following gel filtration ranged from 0.56 mM to 4.76 mM, depending on the FRR used for liposome synthesis.

6.3.3 Tissue Exposure and Cryosectioning[2]

Porcine ear tissue from Yorkshire piglets (4 weeks, 5 kg) was selected due to its morphological and functional resemblance to human skin. Porcine ear skin *in vitro* has shown remarkably similar biophysical properties to human skin *in vivo*, particularly in terms of the diffusivity and permeability coefficient of water across the SC.[177] Studies have also indicated that porcine skin is extremely similar both structurally and chemically to its human counterpart, exhibits chemical properties which are rather consistent across different samples and stable over time at room temperature, therefore porcine skin is a valuable tool for investigating diffusion dynamics of materials with human skin.[178] One ear from each animal was removed following general anesthesia. Liposome solutions were immediately applied in 50 μL aliquots for each size in different locations on the outside of the ear, resulting in spot areas ranging from 0.25–0.5 cm^2, and incubated for 15 min at room temperature. This exposure method was chosen over the use of a perfusion cell since the focus of this study is on short-term SC transport rather than long-term behavior of the nanoparticles within the dermis. For the characterization of size-dependent transport, all liposome solutions covering the full range of size distributions were deposited on ears from a single animal to minimize the influence of tissue morphology variations between animals. Different animals were used for each set of experiments characterizing PEGylated liposome transport, anionic liposome transport, and co-distribution of lipophilic and hydrophilic dyes. Following incubation, the ear tissue was placed in a plastic petri dish and frozen. The

[2] The experiments in Section 6.3.3 and Section 6.3.4 were performed through the combined efforts of Renee Hood and Dr. Eric Kendall at the University of Maryland (College Park, MD).

frozen tissue was bulk sectioned, embedded using Tissue-Tek Cryo-OCT compound (Fisher Scientific, Pittsburgh, PA), and frozen at −80 °C. The frozen tissues blocks were then sectioned into smaller slices, nominally 30 μm thick and revealing dermal tissues at least 300 μm from the surface, using a HM550 cryostat microtome (Richard Allan Scientific, Kalamazoo, MI) and placed onto gelatin-treated glass slides for imaging. Sections were procured from the tissue directly beneath each of the applied liposome volumes, with the plane of each section aligned through the center of its corresponding droplet. Sectioning was performed with the blade oriented perpendicular to the skin surface and the blade path in the direction of the SC to prevent artifacts that could result from mechanical displacement of liposomes, dye, or tissue normal to the SC layer.

6.3.4 Fluorescence Microscopy and Image Processing

The 30 μm thick tissue sections were imaged using a TE-2000 S inverted epifluorescence microscope (Nikon, Melville, NY). Brightfield images and fluorescence images at 528 nm – 553 nm (green filter; DiI) and 465 nm – 495 nm (blue filter; SF) excitation wavelengths were acquired and overlaid to confirm and evaluate the extent of liposome penetration into the dermal tissue and to assess colocalization of the lipophilic and hydrophilic dyes.

ImageJ software (National Institutes of Health, Bethesda, MD) was used to analyze the images. Fluorescence intensity profiles were extracted using 10 μm wide regions of interest (ROIs), with data from multiple ROIs combined to generate quantitative profiles of liposome penetration depth. The intensity data was averaged across 5 ROIs per sample, then normalized to peak intensity and aligned to reveal the average fluorescence signal seen within each tissue sample below the SC. Dye colocalization was analyzed using the JACoP plugin with ImageJ.[179] In all experiments, image analysis was performed independently for each dye.

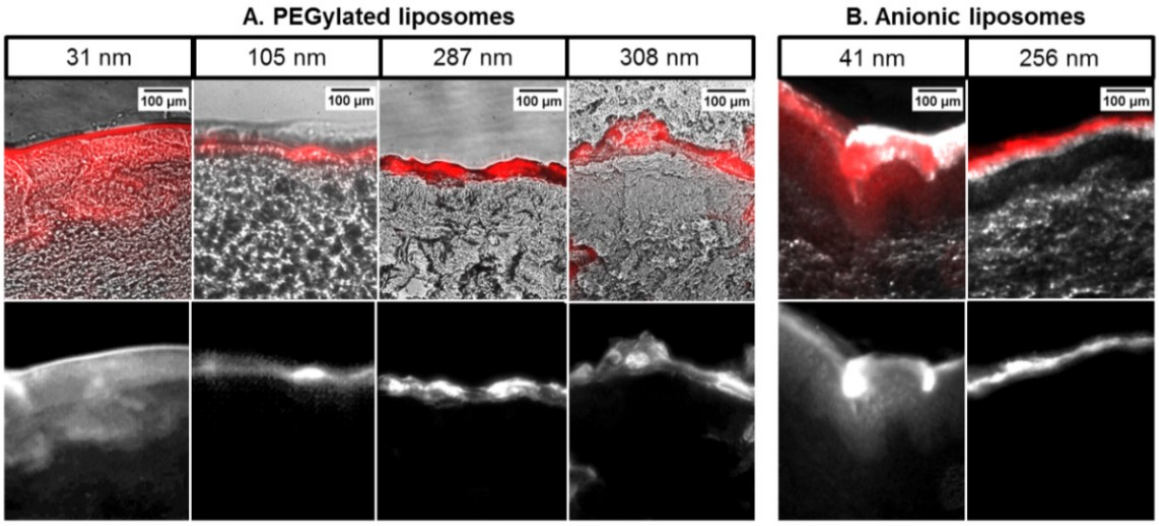

Figure 6.2: Brightfield/fluorescence image overlays (top) and single-channel fluorescence images (bottom) for microtomed tissue sections following 15 min application of PEGylated or anionic liposome samples of varying diameters containing DiI lipophilic dye. Significant dye penetration past the SC is observed with the smallest liposomes (31 nm diameter PEGylated and 41 nm anionic liposomes), while dye from the larger vesicles does not appear to cross the SC, indicating size-based passive transport independent of surface charge.

6.4 Results and Discussion

6.4.1 Transdermal Liposome Penetration

Fluorescence microscopy of microtomed porcine ear tissue after incubation with the various liposome preparations shows a marked difference in the dermal penetration of dyes between tissues exposed to either larger or smaller liposome preparations. **Figure 6.2** shows representative fluorescent images revealing the distribution of DiI dye within the tissue sections. Skin samples exposed to the larger 105 nm to 308 nm liposomes (PEGylated and anionic) consistently exhibit bright bands of fluorescence associated with the SC, with very little fluorescence within deeper skin layers, revealing that these larger liposomes are either physically

excluded by the narrow inter-corneocyte spaces, or are ruptured in the process of traversing the SC. In the latter case, the lipids and lipophilic dyes from the ruptured liposomes are likely to adhere to or associate with surrounding cells and extra-cellular material.[180] Conversely, the smaller 31 nm and 41 nm liposomes reveal a more evenly distributed dye profile throughout the skin, appearing to traverse the SC and enter the underlying layers of tissue in multiple instances with less significant accumulation in the SC (**Figure 6.2**). Several bright features that appear in deeper layers within some images are believed to be a result of imperfections caused by vessels or voids created during cryosectioning. Skin locations with capillaries were excluded due to the known autofluorescence of whole blood between wavelengths of 450-600 nm[181] and the relatively low concentration of fluorescent molecules in the liposome samples. Regions with significant voids created by tearing of the thin tissue sections during microtoming were excluded in order to maintain consistency throughout the samples. In control samples using free SF dye applied to the skin in liposome-free buffer, no penetration beyond the SC was observed. Dye penetration into deeper skin layers shows a strong dependence on liposome size, irrespective of charge state as determined by the presentation of PEG or anionic lipids on the vesicle surfaces. This is consistent with the hypothesis that dermal transport of lipid vesicles is a size-based phenomenon, and the ability of the smallest liposomes to traverse the SC and reach lower layers of skin is a direct result of the reduced liposome diameters. In some samples, bright and highly localized defects were visible in the dermis and epidermis. These features are routinely observed in dermal transport studies, and are the result of enhanced particle transport through hair-follicles, pores, and skin perforations.[182,183] This uneven, defect-based liposome penetration pathway is, by nature, not highly correlated to liposome size.[182,183] The more diffuse, evenly distributed fluorescence signal seen in the epidermis in the small (31 nm and 41 nm) liposome samples is evidence of liposome transport across the SC by a passive inter-corneocyte pathway, a

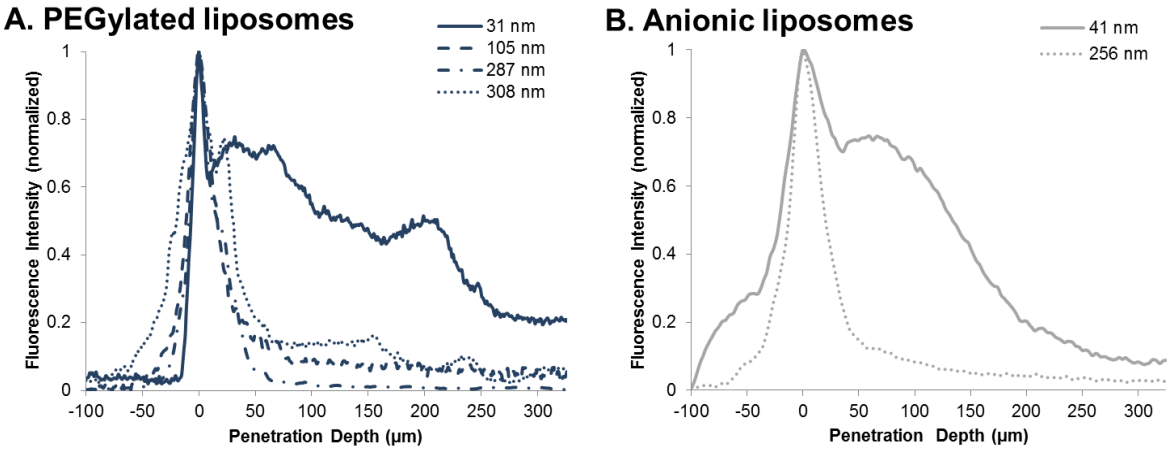

Figure 6.3: DiI fluorescence intensity plot profiles for (a) PEGylated liposomes and (b) anionic liposomes as a function of porcine skin tissue penetration depth. Measurements were performed 15 minute following liposome application. Each curve is representative of an average of 5 ROIs per image.

similar phenomenon seen with other nanoparticles below 40 nm in diameter.[159,161,171,172] For tissue samples where hair follicles were present, enhanced transport was observed for all liposomes populations. Results from these samples were omitted from analysis to prevent the confounding influence of follicular transport on analysis of SC penetration and to highlight the effect of transdermal diffusion of the liposomes through pathways which do not rely on follicular transport.

For quantitative comparison of liposome penetration, ImageJ software was used to obtain plot profiles of fluorescence intensity normal to the tissue surface. Profiles of each tissue section were averaged over 5 representative regions per sample (**Figure 6.3**). These profiles were normalized for maximum fluorescence intensity per profile and aligned to the midpoint of the SC, across all samples. The SC thickness was determined from averaged manual measurements using brightfield images of each tissue, ranging from 15 µm to 40 µm, which is in agreement with previously reported values for porcine skin.[184] The percentage of DiI fluorescence intensity observed beneath the SC compared to the total observed fluorescence signal was calculated from

the plot profiles for each sample and compared across different liposome sizes and surface chemistries (**Figure 6.4**). This technique assumes a linear relationship between fluorescence intensity and liposome concentration, an assumption that does not hold for samples where liposomes are highly concentrated in one area causing a local saturation of fluorescence intensity, as observed in some images from the larger (diameter greater than 105 nm) liposomes used in this study. This saturation effect leads to systematic underreporting of liposomes trapped

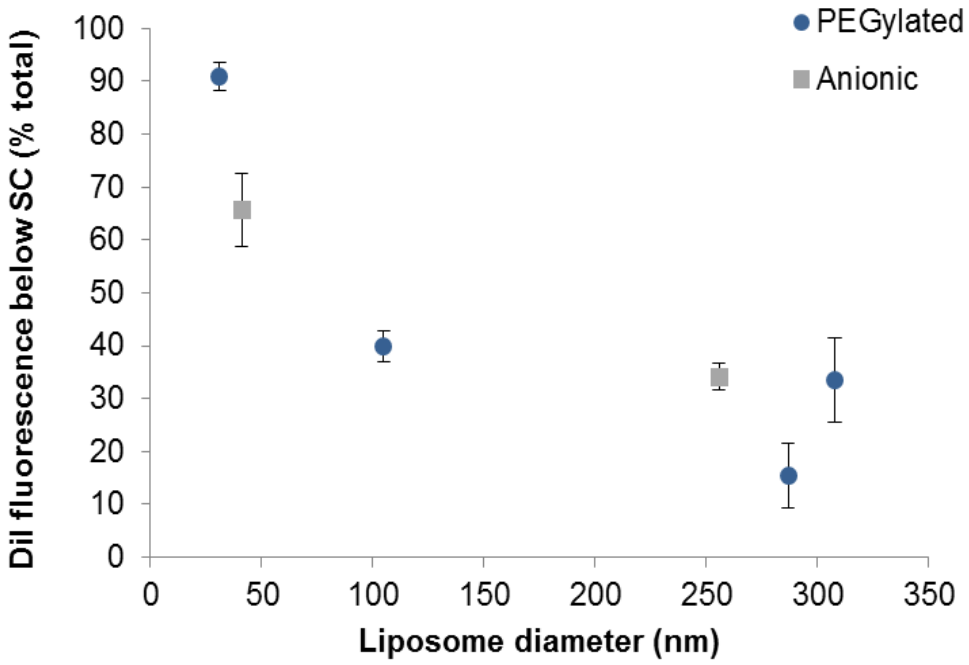

Figure 6.4: Percentage of total DiI fluorescence signal seen below the SC for the different sizes of PEGylated and anionic liposomes. Each plot reflects the average profile extracted from 5 ROIs per tissue section, with error bars reflecting standard deviation. SC thickness, estimated from averaged manual measurements using brightfield images of each tissue, ranged from 15 µm to 40 µm, in general agreement with previously reported values for porcine skin.[184] The small 31 nm PEGylated liposomes pass the SC in large numbers (91%), which is up to 590% greater than the larger 105 nm to 308 nm diameter liposomes. The small 41 nm anionic liposomes also reveal 65% of their total DiI signal under the SC, which is 200% greater than observed with 256 nm diameter liposomes of the same composition.

in the SC, and thus a bias toward higher measured penetration efficiencies for these larger liposomes can occur. Detector saturation was avoided as much as possible while maintaining identical imaging conditions across all samples used in this study. While efforts were made to omit from analysis tissue sections with large voids, blood vessels, or hair follicles, some regions with anomalous fluorescent patches do appear in several images, particularly for the larger 308 nm PEGylated liposomes as seen in **Figure 6.2**.

The small 31 nm PEGylated liposomes pass the SC in large numbers (91%), which is up to 590% greater than the larger 105 nm to 308 nm vesicles studied here. The small 41 nm diameter anionic liposomes show 65% of their total DiI signal under the SC, which is 200% greater than observed with 256 nm diameter liposomes. Both populations of smaller liposomes exhibit significantly enhanced penetration through dermal tissues compared to the larger vesicles, which is consistent with the behavior observed for other nanoparticles smaller than 40 nm in diameter,[171,172] and reveals that size-dependent transdermal transport of the microfluidic-enabled liposomes follows the same overall trend observed for other classes of nanoparticles.

6.4.2 Colocalization of Liposomal Dyes

Regardless of their transport efficiency, it has been unclear if liposomes can traverse the SC intact. Penetration of fluorescent reporter molecules may occur as a result of liposome rupture or leakage during passage through the SC, with enhanced permeation of free dye possibly resulting from interactions between liposomes and dermal lipid structures. To explore this issue for the case of the microfluidic-enabled liposomes, a combination of hydrophilic dye (SF) and lipophilic dye (DiI) were simultaneously incorporated during liposome formation into the vesicle cores and bilayers, respectively. Due to the lipid structure of the SC, diffusive transport of free hydrophilic and hydrophobic solutes is expected to vary significantly,[185,186] such that a lack of spatial correlation between the two dyes would imply that the liposomes had ruptured or leaked,

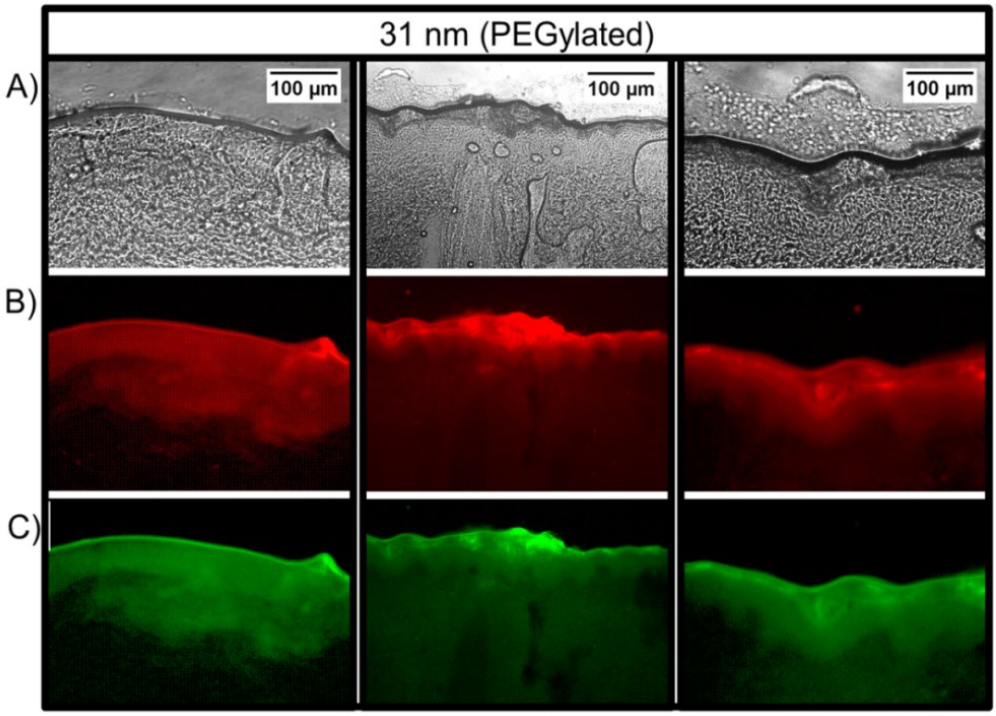

Figure 6.5: Brightfield images of 3 representative tissue regions following application of 31 nm PEGyated liposomes to porcine skin tissue (top), together with matched single channel fluorescence images for lipophilic DiI (middle) and hydrophilic SF (bottom). Similar fluorescence distributions for both dyes are seen across multiple tissue sections, indicating successful penetration of intact liposomes through the epithelium.

allowing the hydrophilic dye (SF) to permeate through the tissue at a different rate than the lipophilic dye (DiI). Conversely, a high degree of spatial correlation would suggest the presence of intact vesicles. For the case of 31 nm liposomes, two color imaging of the exposed tissue sections reveals strong agreement between the distributions of hydrophilic (green) and lipophilic (red) signals through the SC and into the epidermis for all samples, as revealed through both the images (**Figure 6.5**) and the dye penetration depth profiles taken along the depth of the tissue (**Figure 6.6**). Using Pearson's correlation coefficient (ρ) as a measure of the degree of linear dependence between the spatial distributions of each dye, an average value of $\rho = 0.92$ was determined for the 31 nm PEGylated liposomes, indicating a high degree of correlation between

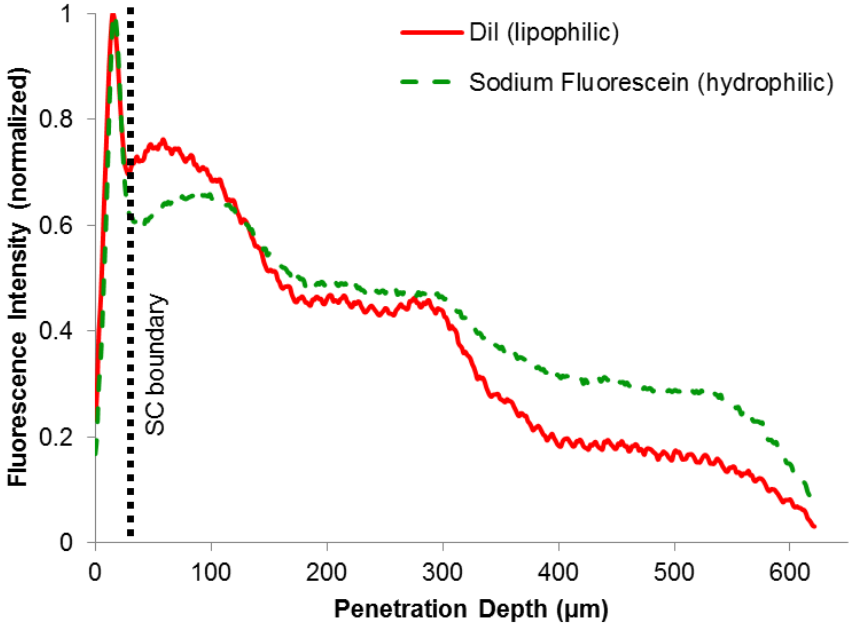

Figure 6.6: Penetration depth profiles of lipophilic and hydrophilic liposomal dyes within a tissue section following 15 min application of 31 nm PEGyated liposomes simultaneously loaded with both dyes. Each curve is representative of an average of 5 ROIs per image. A Pearson's correlation coefficient of $\rho = 0.92$ reveals a high degree of colocalization between the dyes.

the dye locations. While not conclusive, this evidence strongly suggests that the small liposomes successfully penetrate through the SC intact with minimal leakage of their cargo. Experiments performed using larger liposomes resulted in measured values of $\rho = 0.81$ and $\rho = 0.75$ for 308 nm and 105 nm liposomes (**Figure 6.6**), respectively. This relatively poor correlation, together with the overall lack of significant dye penetration (**Figure 6.3**), indicates that some degree of vesicle degradation and free dye diffusion occurs for these larger liposomes.

6.5 Conclusion

This chapter leverages a microfluidic liposome synthesis technique to evaluate size-dependent transdermal delivery of liposomes through *ex vivo* porcine tissues. Compared to larger

vesicles, where dye penetration across the SC is presumed to occur primarily through a combination of vesicle rupture and transport along follicular pathways, the smaller 31 nm diameter and 41 nm diameter liposomes traverse and transport their intra-liposomal contents across the full surface of the SC and into deep dermal tissues, with penetration depths of at least several hundred micrometers observed with a short 15 min incubation. Multicolor fluorescence imaging of hydrophilic and hydrophobic dyes incorporated into the liposomes during synthesis further reveals that the smallest 31 nm liposomes are able to traverse dermal layers intact, with implications for clinical applications requiring co-delivery of therapeutic reagents with dissimilar chemical properties, nanoparticle-mediated drug release, or transport of intact nanocarriers to the bloodstream for systemic delivery. The results presented here also represent the first demonstration of passive transdermal diffusion of nanoscale, microfluidic-generated liposomes, opening the door to the use of these nanoparticles for effective delivery of lipophilic, hydrophilic, and amphipathic compounds to underlying dermal layers. The transport of nanoparticles through the SC is a matter of much debate, and the findings of the present study will require additional validation using complementary methods to confirm the size-dependent behavior described here and assess the fate of both liposomes and cargo.

Chapter 7 : Conclusion

7.1 Dissertation Summary

In this dissertation, an established technique for microfluidic-directed liposome synthesis is advanced through the incorporation of additional on-line preparation methods and the demonstration of its usefulness through practical applications. Through the incorporation of large, functionalized lipids during liposome synthesis, the capability of the microfluidic technique to produce stealth, tumor-targeted liposomes which are relevant for a variety of drug delivery applications is demonstrated. By integrating additional functionalities to the microfluidic device including rapid buffer exchange via microdialysis and remote loading of amphipathic compounds in-line with liposome synthesis, the ability to further prepare samples of liposomes for use in drug delivery applications through an integrated, continuous flow microfluidic process has been proven. Investigating microfluidic-directed synthesis of liposomes through 3D flow focusing within a concentric capillary device requiring simple, inexpensive fabrication techniques enabled the examination of the impact of edge effects created during flow focusing in the typical 2D microfluidic device and the confirmation of the ability of the technique to produce liposomes in an apparatus with a different geometry, in addition to addressing the topic of scale up by producing liposomes at a rate which is a factor of 10^4 liposomes/min faster than the existing method. To demonstrate the usefulness of microfluidic-enabled liposomes for practical applications, the value of microfluidic-enabled liposomes in drug carrier design was revealed by preparing liposomes with distinct diameters to investigate size-based interactions with high resolution within a cancer cell line (Caco-2) *in vitro*. Additionally, transdermal delivery of liposomal carriers was investigated by utilizing the microfluidic method to prepare samples of liposomes below a proposed size cutoff (~40 nm) to demonstrate the

penetration of liposomes through *ex vivo* porcine skin. The collection of research presented here advances the established microfluidic method for liposome synthesis from a pilot technique to a more useful, practical system which is highly amendable for widespread use for a multiplicity of drug delivery applications.

7.2 Proposed Future Efforts

The research presented in this dissertation sets a solid foundation for a variety of subsequent efforts to further progress the microfluidic liposome synthesis platform. It should be noted that the technique described here has difficulty with reproducing similar size distributions with identical experimental conditions. Although this is a disadvantage, it is not extremely problematic as general the overall trends regarding the relationship between flow conditions, temperature, lipid compositions, etc. remain constant despite the variation in conditions for a given experiment. This is a feature which should be further explored to improve repeatability. For many applications, only a single size of liposome is necessary, thus the experimental parameters can be tweaked until the desired size is produced. Aside from this issue of repeatability, the following forthcoming research endeavors are proposed:

7.2.1 Microfluidic Synthesis of Immunoliposomes

As this dissertation improved the existing liposome synthesis technique through the incorporation of on-chip microfluidic buffer exchange and remote drug loading, additional functionalities may be incorporated for even further enhancement. One potentially valuable preparation technique for the device is in-line tethering of antibodies to liposome exteriors after synthesis. Studies in this dissertation focused on the use of folate to produce tumor-targeted liposomes; although folate is an effective targeting ligand for many diseases, there remain many drug delivery applications which benefit from the use of monoclonal antibodies or antibody

fragments for effective targeting.[187] Unlike folate, which has a low molecular weight (~440 Da) compared to the native lipid (600~800 Da) and the attached PEG (2000~5000 Da), both monocloncal antibodies and antibody fragments are quite large in molecular weight (150 kDa and 28~50 kDa, respectively). Consequently, lipids with pre-conjugated antibodies are too large to use for synthesizing liposomes through the microfluidic technique, with increasing difficulty as the resulting particle radius decreases. Thus, antibody-functionalized liposomes, or "immunoliposomes", must be formed through the attachment of antibodies to pre-formed vesicles.

Immunoliposomes are most commonly produced through the attachment of antibodies or antibody fragments to preformed liposomes using either coupling chemistry or post-insertion of antibody-functionalized lipids.[188] Through coupling chemistry, liposomes are formed with PEGylated lipid whose terminal ends contain a functional group (*e.g.,* biotin) and after formation are incubated with an antibody or antibody fragment which contains the appropriate functional group (in this case, streptavidin) to form a covalent or non-covalent bond with the vesicle membrane's outer leaflet, resulting an in immunoliposome.[189] The ability to form PEG-modified liposomes has been verified by the work presented in this dissertation, hence liposomes could be generated via microfluidic flow focusing using functionalized PEG lipid then introduced to functionalized antibodies or antibody fragments downstream of synthesis.

Alternatively, post-insertion involves the incubation of preformed liposomes with micelles of PEG-lipid derivatives (*e.g.,* PEG-PE), during which time the micelles spontaneously transfer their lipid molecules to the liposomes' membranes' outer leaflets to reduce the free energy of the hydrophobic lipid tail due to the higher radius of curvature within micelles.[190] Eventually, the micelles completely incorporate themselves into the lipid vesicles to form functionalized liposomes. Although this conjugation strategy typically occurs over a lengthy incubation (hours

to days), the decreased diffusion lengths within microfluidics could potentially facilitate a more rapid lipid transfer from the micelles into the liposomes in addition to a more uniform distribution of antibodies on the exterior monolayer.

Through either of these methods, liposomes could be generated using the established flow focusing method followed by downstream antibody conjugation for the *in situ* generation of immunoliposomes. These microfluidic immunoliposome formation strategies could be optimized to create customized lipid formulations which result in different antibody densities and types by simply changing the flow conditions within the device.

7.2.2 Passive Encapsulation Methods

This dissertation focused on the active encapsulation of drugs using a transmembrane ion gradient, a method which is extremely valuable the wide range of drugs which are amphipathic weak bases. However, the list of molecules which benefit from liposomal delivery is actively expanding and many of these molecules (*e.g.,* bioactive molecules, uncharged molecules, etc.) cannot traverse liposomal bilayers and therefore must still be encapsulated using traditional passive methods. Microfluidics also has an advantage for these techniques over bulk scale loading due to the decreased volumes used for production. Previous efforts have focused on passive liposome encapsulation during microfluidic liposome synthesis (see **Figure 1.6**, p. 13), in which the liposomes are formed directly adjacent to a thin stream of highly concentrated reagent, thereby encapsulating the highest possible concentration of solute during vesicle formation while eliminating waste.[43] In addition to optimizing this method (*i.e.* encapsulant concentration, flow rate ratios, etc.), downstream functionalities for collecting the leftover reagent which was not encapsulated could be incorporated and this extra reagent could be recycled back through the device.

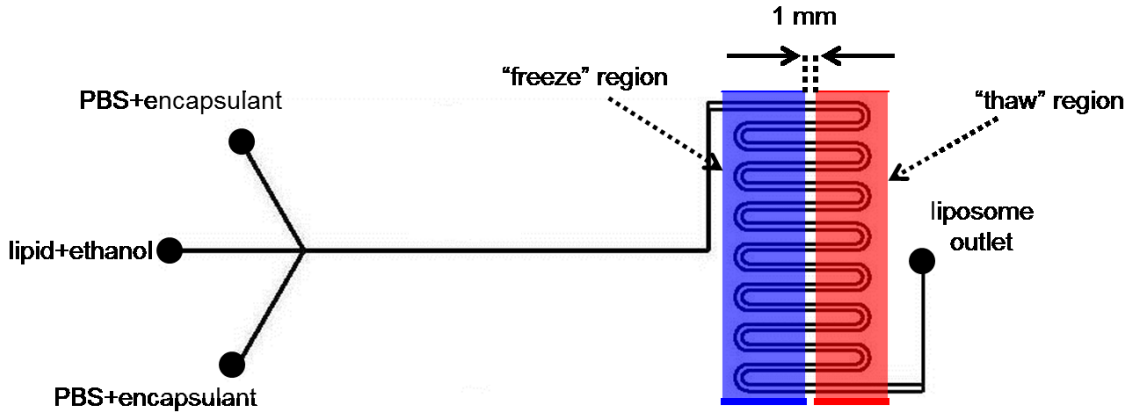

Figure 7.1: Schematic of a 3-inlet for microfluidic passive encapsulation via freeze-thaw cycling in-line with liposome synthesis. The device contains a serpentine channel downstream of the flow focusing region through a "freeze" region containing a liquid nitrogen supply line and a "thaw" region containing on-chip heating elements for passive solute encapsulation.

Another technique which is commonly used to enhance passive encapsulation of reagents into liposomes is freeze-thaw cycling,[191] in which dispersions of liposomes undergo multiple cycles of being frozen within a liquid nitrogen (-196 °C) bath and being thawed in a warm water (~50 °C) in order to bring the lipids above and below their melting point. This process assists in matching the interior liposome volume's solute concentration to that of the hydration buffer (equilibrium solute concentrations also cause an imbalance between interior and exterior environments[192]). Typically performed through a bulk scale process, this method could also be accomplished within a microfluidic system in which a device could be fabricated on a thin, heat resistant substrate such as microscope cover glass (<100 μm) and a segment of the channel downstream from liposome formation and reagent introduction could serpentine through two various chip segments: with on-chip heaters and one with an off-chip cooling block which delivers liquid nitrogen (**Figure 7.1**). This microfluidic passive encapsulation method could be

optimized for the encapsulation of materials such as DNA, siRNA, peptides, and other molecules which are not amendable to the active loading process.

7.2.3 High Throughput Microfluidic Liposome Preparation

Perhaps one of the most critical areas to address through forthcoming efforts to further develop the "pharmacy-on-a-chip" technique is scale up. Although this dissertation demonstrates a device which can produce liposomes on the order of milliliters per minute, a more rapid approach utilizing the 2D system would be ideal, particularly as this device geometry is more

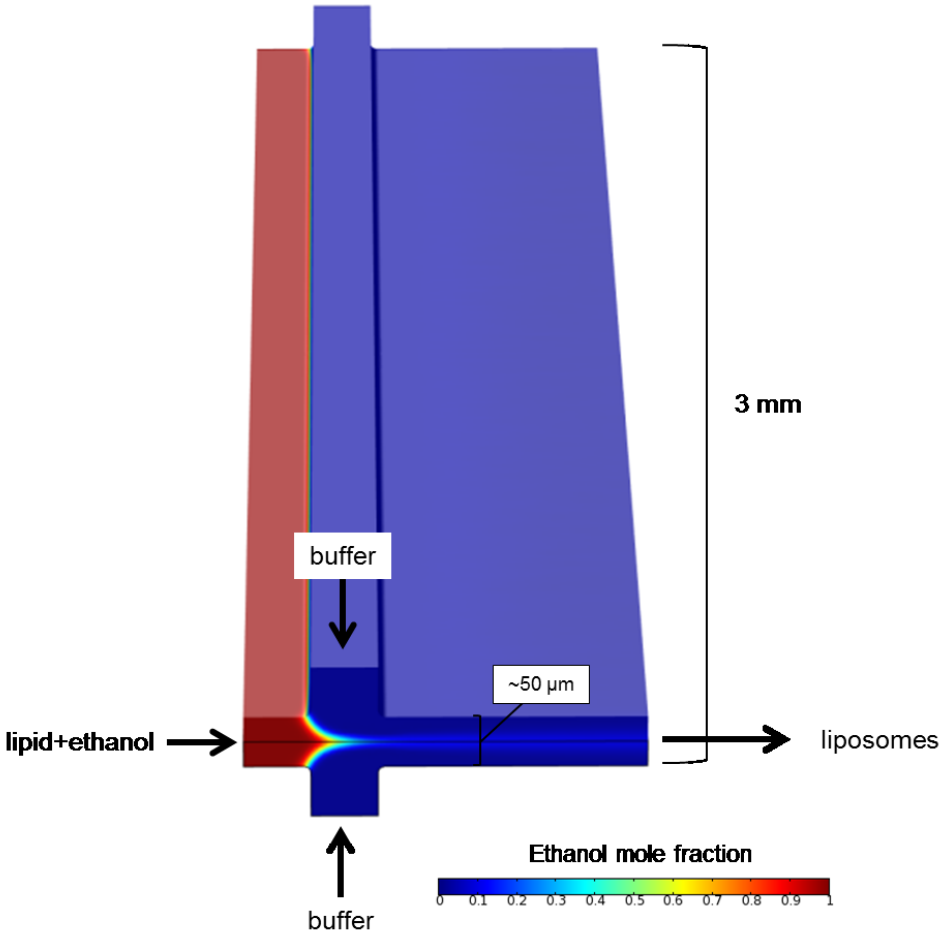

Figure 7.2: Simulation of the vertical focusing chip and diminishing mole fraction of ethanol along the length of the device. Height of microchannels is defined by cover glass or thin spin-coated PDMS, while the width of the channel exceeds 1 mm, enabling high throughput liposome production using similar flow velocities to previous experiments.

amendable to the further development of downstream functionalities. There are two basic strategies for achieving higher throughput of the 2D technique: scale up and size up.

To scale up, the microfluidic flow focusing technique can be implemented within a chip which has a very large width (millimeter scale) and narrow height (micron scale) and the flow focusing occurs perpendicular to the direction of tradition Y-channel flow focusing (**Figure 7.2***)*. This could be achieved through the fabrication of multilayer microfluidic devices made from materials such as thin cover glass, spin coated films of PDMS, adhesives, other thin film materials, or a combination of the above. Such a device would allow for much higher throughput as a result of the higher potential flow rates due to increased width dimension which results in a lower pressure system while delivering the same quality of liposomes due to the characteristic dimension of the device (height) remaining on the microscale. For example, a device with dimensions defined by 50 μm cover glass which are 3 mm wide, as depicted in **Figure 7.2**, would provide liposomes at a rate 10x faster than the devices used in the studies presented in this

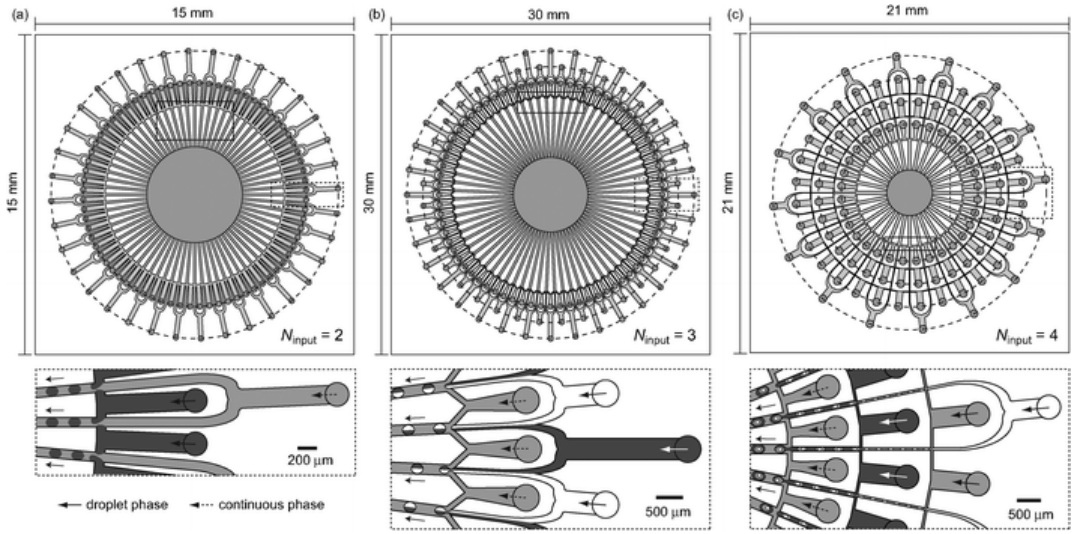

Figure 7.3: High-volume production of single and compound emulsions in a microfluidic parallelization arrangement coupled with coaxial annular device. This system could be adapted to the flow focusing method for microfluidic liposome preparation for high-throughput liposome production. Reproduced from Nisisako, *et al.*, 2012.[193]

dissertation (typically 50 μm wide by 300 μm tall) while operating under identical linear flow velocities. These vertical focusing devices could be optimized to provide a higher throughput system for generating extremely uniform populations of liposomes.

To size up, a network of microchannels containing multiple flow focusing elements contained within a single device could be fabricated (**Figure 7.3**). As previously demonstrated for high volume production of droplets,[193] the system would contain flow focusing elements in a parallelized arrangement coupled with a coaxial annular device fluidic circuit. Such a device would only require one inlet per fluid species and one outlet, resulting in one-step, high volume production of liposomes prepared via microfluidic hydrodynamic flow focusing.

7.2.4 Preclinical Research

Microfluidic liposome synthesis is poised to have a significant impact on numerous biomedical applications. The preliminary efforts demonstrated in the chapters of this dissertation have provided interesting and potentially very important information regarding the effect of a liposome's size on its fate for both cellular uptake mechanisms and passive delivery through the skin. To specifically advance the research presented here, further studies highlighting the effect of particle size on liposome interaction within an *in vitro* environment as well as *in vivo* studies to explore liposome fate versus size within the bloodstream could be performed. Using the microfluidic technique, populations of liposomes with a wide range of distinct diameters and surface chemistries could be readily prepared and used to elucidate the interactions with specific tissues and the bloodstream when administered systemically. Such studies could result in the ability to design drug carriers with an unprecedented level of sophistication which are specifically optimized for a wide variety of diseases.

To further investigate passive transdermal delivery of microfluidic-enabled liposomes, different time points after topical application of liposomes could be screened using a Franz

diffusion cell[194] to learn the effect of size on penetration depth over longer time periods. Additionally, *in vivo* studies could be utilized for the topical application of sub-40 nm liposomes which encapsulate various reagents. Topical liposome application would be followed by the measurement of neural activity or periodic collection and analysis of blood samples in order to investigate the effect of actual encapsulated therapeutics to passively traverse dermal layers and reach a viable target site. The ensuing information from these studies could be useful for developing transdermal drug delivery systems with prolonged release profiles, or to optimize delivery to different locations under the skin.

7.3 Closing Remarks

This dissertation presents a series of original research in which an established method for microfluidic-directed production of nearly monodisperse liposomes with tunable sizes was revolutionized through the incorporation of functionalized lipids during synthesis for production of tumor-targeted liposomes, the addition of new on-chip functionalities to enable microfluidic preparation of nanoscale drug carriers, and the implementation within a variety of substrate materials and microchannel geometries to render the technique more amendable for widespread use. Liposomes within size ranges enabled by the microfluidic synthesis technique were then exploited for innovative pharmaceutical and preclinical studies, highlighting genuine advantages of the technique through practical applications. Finally, various forthcoming research endeavors regarding the continuous evolution of the microfluidic technique have been suggested. With further evolution and optimization, microfluidic-directed synthesis and preparation of liposomal drug carriers has the potential to support instantaneous generation of populations of purified, tissue-targeted liposomal drug formulations containing high concentrations of drugs with minimal reagent waste for proficient, real-time liposomal drug preparation at the point of care.

Bibliography

1. Lasic, D. D. *Liposomes: from physics to applications*. (Elsevier, 1993).

2. Lasic, D. Novel applications of liposomes. *Trends Biotechnol.* **16,** 307–321 (1998).

3. Immordino, M. L., Dosio, F. & Cattel, L. Stealth liposomes: review of the basic science, rationale, and clinical applications, existing and potential. *Int. J. Nanomedicine* **1,** 297–315 (2006).

4. Park, J. W. Liposome-based drug delivery in breast cancer treatment. *Breast Cancer Res.* **4,** 95–9 (2002).

5. Maeda, H., Wu, J., Sawa, T., Matsumura, Y. & Hori, K. Tumor vascular permeability and the EPR effect in macromolecular therapeutics: a review. *J. Control. Release* **65,** 271–284 (2000).

6. O'Shaughnessy, J. Liposomal anthracyclines for breast cancer: overview. *Oncologist* **8 Suppl 2,** 1–2 (2003).

7. Campos, S. M. *et al.* The clinical utility of liposomal doxorubicin in recurrent ovarian cancer. *Gynecol. Oncol.* **81,** 206–12 (2001).

8. Gabizon, A. & Martin, F. Polyethylene Glycol-Coated (Pegylated) Liposomal Doxorubicin. *Drugs* **54,** 15–21 (1997).

9. Krishna, R. & Mayer, L. D. Liposomal doxorubicin circumvents PSC 833-free drug interactions, resulting in effective therapy of multidrug-resistant solid tumors. *Cancer Res.* **57,** 5246–53 (1997).

10. Glück, R. Liposomal presentation of antigens for human vaccines. *Pharm. Biotechnol.* **6,** 325–45 (1995).

11. Ebrahim, S., Peyman, G. A. & Lee, P. J. Applications of liposomes in ophthalmology. *Surv. Ophthalmol.* **50,** 167–82

12. Schreier, H., Gonzalez-Rothi, R. J. & Stecenko, A. A. Pulmonary delivery of liposomes. *J. Control. Release* **24,** 209–223 (1993).

13. Patri, A. K., Majoros, I. J. & Baker, J. R. Dendritic polymer macromolecular carriers for drug delivery. *Curr. Opin. Chem. Biol.* **6,** 466–471 (2002).

14. Moghimi, S. M. & Szebeni, J. Stealth liposomes and long circulating nanoparticles: critical issues in pharmacokinetics, opsonization and protein-binding properties. *Prog. Lipid Res.* **42,** 463–478 (2003).

15. Tazina, E. V, Kostin, K. V & Oborotova, N. A. DRUG SYNTHESIS METHODS AND MANUFACTURING TECHNOLOGY SPECIFIC FEATURES OF DRUG ENCAPSULATION IN LIPOSOMES (A REVIEW). **45,** (2011).

16. Immordino, M. L. *et al.* Preparation, characterization, cytotoxicity and pharmacokinetics of liposomes containing docetaxel. *J. Control. Release* **91,** 417–429 (2003).

17. Forssen, E. & Willis, M. Ligand-targeted liposomes. *Adv. Drug Deliv. Rev.* **29,** 249–271 (1998).

18. Zhao, X., Li, H. & Lee, R. J. Targeted drug delivery via folate receptors. *Expert Opin. Drug Deliv.* **5,** 309–319 (2008).

19. Torchilin, V. P. Passive and active drug targeting: drug delivery to tumors as an example. *Drug Deliv.* 3–53 (2009).

20. Weissleder, R., Kelly, K., Sun, E. Y., Shtatland, T. & Josephson, L. Cell-specific targeting of nanoparticles by multivalent attachment of small molecules. *Nat. Biotechnol.* **23,** 1418–23 (2005).

21. Lee, R. J. & Low, P. S. Delivery of liposomes into cultured KB cells via folate receptor-mediated endocytosis. — JBC. *J. Biol. Chem.* **269,** 3198–3204 (1994).

22. Lee, R. & Low, P. Folate-mediated tumor cell targetting of liposome-entrapped doxorubicin. *Biochim. Biophys. Acta (BBA)-Biomembranes* **1233,** 134–144 (1995).

23. Hansen, M. J. & Low, P. S. in (Jackman, A. L. & Leamon, C. P.) 181–193 (Springer New York, 2011). doi:10.1007/978-1-4419-8417-3_9

24. Lu, Y. & Low, P. S. Folate-mediated delivery of macromolecular anticancer therapeutic agents. *Adv. Drug Deliv. Rev.* **64,** 342–352 (2012).

25. Xia, W. & Low, P. S. Folate-targeted therapies for cancer. *J. Med. Chem.* **53,** 6811–24 (2010).

26. Meure, L. A., Foster, N. R. & Dehghani, F. Conventional and dense gas techniques for the production of liposomes: a review. *AAPS PharmSciTech* **9,** 798–809 (2008).

27. Szoka, F. & Papahadjopoulos, D. Procedure for preparation of liposomes with large internal aqueous space and high capture by reverse-phase evaporation. *Proc. Natl. Acad. Sci. U. S. A.* **75,** 4194–8 (1978).

28. Pidgeon, C., McNeely, S., Schmidt, T. & Johnson, J. E. Multilayered vesicles prepared by reverse-phase evaporation: liposome structure and optimum solute entrapment. *Biochemistry* **26,** 17–29 (1987).

29. Fischer, T. H. & Lasic, D. D. A Detergent Depletion Technique for the Preparation of Small Vesicles. *Mol. Cryst. Liq. Cryst.* **102,** 141–153 (1984).

30. Batzri, S. & Korn, E. D. Single bilayer liposomes prepared without sonication. *Biochim. Biophys. Acta* **298,** 1015–9 (1973).

31. Kremer, J. M. H., Van der Esker, M. W., Pathmamanoharan, C. & Wiersema, P. H. Vesicles of variable diameter prepared by a modified injection method. *Biochemistry* **16,** 3932–3935 (1977).

32. Szoka, F. & Papahadjopoulos, D. Comparative properties and methods of preparation of lipid vesicles (liposomes). *Annu. Rev. Biophys. Bioeng.* **9,** 467–508 (1980).

33. Wagner, A., Vorauer-Uhl, K., Kreismayr, G. & Katinger, H. The crossflow injection technique: an improvement of the ethanol injection method. *J. Liposome Res.* **12,** 259–70 (2002).

34. Maulucci, G. *et al.* Particle size distribution in DMPC vesicles solutions undergoing different sonication times. *Biophys. J.* **88,** 3545–50 (2005).

35. Litzinger, D. C., Buiting, A. M. J., van Rooijen, N. & Huang, L. Effect of liposome size on the circulation time and intraorgan distribution of amphipathic poly(ethylene glycol)-containing liposomes. *Biochim. Biophys. Acta* **1190,** 99–107 (1994).

36. Ishida, T., Harashima, H. & Kiwada, H. Liposome clearance. *Biosci. Rep.* **22,** 197–224 (2002).

37. Nagayasu, A. *et al.* The size of liposomes: a factor which affects their targeting efficiency to tumors and therapeutic activity of liposomal antitumor drugs. *Adv. Drug Deliv. Rev.* **40,** 75–87 (1999).

38. Ramachandran, S., Quist, A. P., Kumar, S. & Lal, R. Cisplatin Nanoliposomes for Cancer Therapy: AFM and Fluorescence Imaging of Cisplatin Encapsulation, Stability, Cellular Uptake, and Toxicity. *Langmuir* **22,** 8156–8162 (2006).

39. Uster, P. S. *et al.* Insertion of poly(ethylene glycol) derivatized phospholipid into pre-formed liposomes results in prolonged in vivo circulation time. *FEBS Lett.* **386,** 243–246 (1996).

40. Gu, F. X. X. *et al.* Targeted nanoparticles for cancer therapy. *Nano Today* **2,** 14–21 (2007).

41. Jahn, A., Vreeland, W. N. N. W. N., Gaitan, M. & Locascio, L. E. E. L. E. Controlled vesicle self-assembly in microfluidic channels with hydrodynamic focusing. *J. Am. Chem. Soc.* **126,** 2674–2675 (2004).

42. Jahn, A., Vreeland, W. N., DeVoe, D. L., Locascio, L. E. & Gaitan, M. Microfluidic Directed Formation of Liposomes of Controlled Size. *Langmuir* **23,** 6289–6293 (2007).

43. Jahn, A. *et al.* Preparation of nanoparticles by continuous-flow microfluidics. *J. Nanoparticle Res.* **10,** 925–934 (2008).

44. Jahn, A. *et al.* Microfluidic Mixing and the Formation of Nanoscale Lipid Vesicles. *ACS Nano* **4,** 2077–2087 (2010).

45. Song, Y., Hormes, J. & Kumar, C. S. S. R. Microfluidic synthesis of nanomaterials. *Small* **4,** 698–711 (2008).

46. Zhao, C.-X., He, L., Qiao, S. Z. & Middelberg, A. P. J. Nanoparticle synthesis in microreactors. *Chem. Eng. Sci.* **66,** 1463–1479 (2011).

47. Squires, T. M. Microfluidics : Fluid physics at the nanoliter scale. **77,** (2005).

48. Pamme, N. Continuous flow separations in microfluidic devices. *Lab Chip* **7,** 1644–59 (2007).

49. Metz, S., Trautmann, C., Bertsch, a. & Renaud, P. Flexible microchannels with integrated nanoporous membranes for filtration and separation of molecules and particles. *Tech. Dig. MEMS 2002 IEEE Int. Conf. Fifteenth IEEE Int. Conf. Micro Electro Mech. Syst. (Cat. No.02CH37266)* 81–84 (2002). doi:10.1109/MEMSYS.2002.984095

50. Metz, S., Trautmann, C., Bertsch, a & Renaud, P. Polyimide microfluidic devices with integrated nanoporous filtration areas manufactured by micromachining and ion track technology. *J. Micromechanics Microengineering* **14,** 324–331 (2004).

51. Cheang, P., Newman, G. & Murray, D. O. An Optimized Process for Ultrathick Photosensitive Polyimide Applications. *SEMICON Taiwan* (1996).

52. Bousse, L. *et al.* E c m a s. (2000).

53. Roberts, M. A., Locascio-Brown, L., MacCrehan, W. A. & Durst, R. A. Liposome Behavior in Capillary Electrophoresis. *Anal. Chem.* **68,** 3434–3440 (1996).

54. Zhang, C.-X. & Manz, A. High-speed free-flow electrophoresis on chip. *Anal. Chem.* **75,** 5759–66 (2003).

55. Wang, P. C., DeVoe, D. L. & Lee, C. S. Review Integration of polymeric membranes with microfluidic networks for bioanalytical applications. 3857–3867 (2001).

56. Xu, N. *et al.* A microfabricated dialysis device for sample cleanup in electrospray ionization mass spectrometry. *Anal. Chem.* **70,** 3553–6 (1998).

57. Xiang, F. *et al.* An Integrated Microfabricated Device for Dual Microdialysis and On-Line ESI-Ion Trap Mass Spectrometry for Analysis of Complex Biological Samples integrated microfabricated platform was constructed using. **71,** 1485–1490 (1999).

58. Lewrick, F. & Süss, R. Liposomes. **605,** 139–145 (2010).

59. Fritze, A., Hens, F., Kimpfler, A., Schubert, R. & Peschka-Süss, R. Remote loading of doxorubicin into liposomes driven by a transmembrane phosphate gradient. *Biochim. Biophys. Acta* **1758,** 1633–40 (2006).

60. Haran, G., Cohen, R., Bar, L. K. & Barenholz, Y. Transmembrane ammonium sulfate gradients in liposomes produce efficient and stable entrapment of amphipathic weak bases. *Biochim. Biophys. Acta* **1151,** 201–15 (1993).

61. Mayer, L. D. *et al.* Influence of Vesicle Size , Lipid Composition , and Drug-to-Lipid Ratio on the Biological Activity of Liposomal Doxorubicin in Mice Influence of Vesicle Size , Lipid Composition , and Drug-to-Lipid Ratio on the Biological Activity of Liposomal Doxorubicin. 5922–5930 (1989).

62. Rafiyath, S. M. *et al.* Comparison of safety and toxicity of liposomal doxorubicin vs. conventional anthracyclines: a meta-analysis. *Exp. Hematol. Oncol.* **1,** 10 (2012).

63. Kulkarni, S. B., Betageri, G. V & Singh, M. Factors affecting microencapsulation of drugs in liposomes. *J. Microencapsul.* **12,** 229–46

64. Lasic, D. D. *Liposomes in Gene Delivery*. (CRC Press, Inc., 1997).

65. Torchilin, V. P. Recent advances with liposomes as pharmaceutical carriers. *Nat. Rev. Drug Discov.* **4,** 145–60 (2005).

66. Maruyama, K. Intracellular targeting delivery of liposomal drugs to solid tumors based on EPR effects. *Adv. Drug Deliv. Rev.* **63,** 161–9 (2011).

67. Chang, H.-I. & Yeh, M.-K. Clinical development of liposome-based drugs: formulation, characterization, and therapeutic efficacy. *Int. J. Nanomedicine* **7,** 49–60 (2012).

68. Arakawa, E., Imai, Y., Kobayashi, H., Okumura, K. & Sezaki, H. Application of drug-containing liposomes to the duration of the intramuscular absorption of water-soluble drugs in rats. *Chem. Pharm. Bull. (Tokyo).* **23,** 2218–22 (1975).

69. Shaji, J. & Patole, V. Protein and Peptide drug delivery: oral approaches. *Indian J. Pharm. Sci.* **70,** 269–77

70. Jain, S., Patil, S. R., Swarnakar, N. K. & Agrawal, A. K. Oral delivery of doxorubicin using novel polyelectrolyte-stabilized liposomes (layersomes). *Mol. Pharm.* **9,** 2626–35 (2012).

71. Amani, A., Amini, M. A., Ali, H. S. M. & York, P. Alternatives to conventional suspensions for pulmonary drug delivery by nebulisers: a review. *J. Pharm. Sci.* **100,** 4563–70 (2011).

72. Willis, L., Hayes, D. & Mansour, H. M. Therapeutic liposomal dry powder inhalation aerosols for targeted lung delivery. *Lung* **190,** 251–62 (2012).

73. Chattopadhyay, S., Ehrman, S. H. & Venkataraman, C. Size distribution and dye release properties of submicron liposome aerosols. *Powder Technol.* **246,** 530–538 (2013).

74. Cevc, G., Gebauer, D., Stieber, J., Schätzlein, A. & Blume, G. Ultraflexible vesicles, Transfersomes, have an extremely low pore penetration resistance and transport therapeutic amounts of insulin across the intact mammalian skin. *Biochim. Biophys. Acta* **1368,** 201–15 (1998).

75. Samad, A., Sultana, Y. & Aqil, M. Liposomal drug delivery systems: an update review. *Curr. Drug Deliv.* **4,** 297–305 (2007).

76. Tan, M. L., Choong, P. F. M. & Dass, C. R. Recent developments in liposomes, microparticles and nanoparticles for protein and peptide drug delivery. *Peptides* **31,** 184–93 (2010).

77. Balazs, D. A. & Godbey, W. Liposomes for use in gene delivery. *J. Drug Deliv.* **2011,** 326497 (2011).

78. Schroeder, A., Levins, C. G., Cortez, C., Langer, R. & Anderson, D. G. Lipid-based nanotherapeutics for siRNA delivery. *J. Intern. Med.* **267,** 9–21 (2010).

79. Saupe, A., McBurney, W., Rades, T. & Hook, S. Immunostimulatory colloidal delivery systems for cancer vaccines. *Expert Opin. Drug Deliv.* **3,** 345–54 (2006).

80. Kaneda, Y. Virosomes: evolution of the liposome as a targeted drug delivery system. *Adv. Drug Deliv. Rev.* **43,** 197–205 (2000).

81. Torchilin, V. P. Liposomes as delivery agents for medical imaging. *Mol. Med. Today* **2,** 242–249 (1996).

82. Torchilin, V. P., Zhou, F. & Huang, L. pH-Sensitive Liposomes. *J. Liposome Res.* **3,** 201–255 (1993).

83. Chu, C.-J. & Szoka, F. C. pH-Sensitive Liposomes. *J. Liposome Res.* **4,** 361–395 (1994).

84. Needham, D., Anyarambhatla, G., Kong, G. & Dewhirst, M. W. A new temperature-sensitive liposome for use with mild hyperthermia: characterization and testing in a human tumor xenograft model. *Cancer Res.* **60,** 1197–201 (2000).

85. Babincová, M. *et al.* Site-specific in vivo targeting of magnetoliposomes using externally applied magnetic field. *Z. Naturforsch. C.* **55,** 278–81

86. Hood, R. R., Shao, C., Omiatek, D. M., Vreeland, W. N. & DeVoe, D. L. Microfluidic Synthesis of PEG- and Folate-Conjugated Liposomes for One-Step Formation of Targeted Stealth Nanocarriers. *Pharm. Res.* **30,** 1597–607 (2013).

87. Hood, R. R., Vreeland, W. N. & DeVoe, D. L. Remote Drug Loading In-Line with Microfluidic Liposome Synthesis. *Submitted. Lab Chip (2014).*

88. Hood, R. R., Atencia, J., DeVoe, D. L., Vreeland, W. N. & Omiatek, D. M. A Facile Route to the Synthesis of Monodisperse Nanoscale Liposomes Using Annular Flow Focusing in Concentric Capillaries. *Submitted. Lab Chip (2014).*

89. Andar, A. U., Hood, R. R., Vreeland, W. N., Devoe, D. L. & Swaan, P. W. Microfluidic Preparation of Liposomes to Determine Particle Size Influence on Cellular Uptake Mechanisms. *Pharm. Res.* **31,** 401–13 (2014).

90. Hood, R. R. *et al.* Microfluidic-enabled liposomes elucidate size-dependent transdermal transport. *PLoS One* **9,** e92978 (2014).

91. Jesorka, A. & Orwar, O. Liposomes: technologies and analytical applications. *Annu. Rev. Anal. Chem. (Palo Alto. Calif).* **1,** 801–32 (2008).

92. *Encyclopedia of Surface and Colloid Science, Second Edition*. (Taylor & Francis, 2006).

93. Zook, J. M. & Vreeland, W. N. Effects of temperature, acyl chain length, and flow-rate ratio on liposome formation and size in a microfluidic hydrodynamic focusing device. *Soft Matter* **6,** 1352 (2010).

94. Woodle, M. C. *et al.* Sterically stabilized liposomes. Reduction in electrophoretic mobility but not electrostatic surface potential. *Biophys. J.* **61,** 902–10 (1992).

95. O'Brien, R. W. & White, L. R. Electrophoretic mobility of a spherical colloidal particle. *J. Chem. Soc. Faraday Trans. 2* **74,** 1607 (1978).

96. Woodle, M. C., Newman, M. S. & Cohen, J. A. Sterically stabilized liposomes: physical and biological properties. *J. Drug Target.* **2,** 397–403 (1994).

97. Yilmaz, H. Excess Properties of Alcohol - Water Systems at 298.15 K. *Turk. J. Phys* **26,** 243–246 (2002).

98. Mitchell, H. K. Folic Acid. IV. Absorption Spectra. *J. Am. Chem. Soc.* **66,** 274–278 (1944).

99. Edwards, K. A. & Baeumner, A. J. Analysis of liposomes. *Talanta* **68,** 1432–41 (2006).

100. Couvreur, P. & Vauthier, C. *Nanotechnology: intelligent design to treat complex disease. Pharm. Res.* **23,** 1417–50 (2006).

101. Gaumet, M., Vargas, A., Gurny, R. & Delie, F. Nanoparticles for drug delivery: the need for precision in reporting particle size parameters. *Eur. J. Pharm. Biopharm.* **69,** 1–9 (2008).

102. Rosano, T. G. Methanol and Isopropanol Toxicology with Clinical Applications. *Am. Assoc. Clin. Chem.* (2011). at <http://www.aacc.org/events/online_progs/Documents/Methanol-Isopropanol_revised.pdf>

103. Montesano, G., Bartucci, R., Belsito, S., Marsh, D. & Sportelli, L. Lipid membrane expansion and micelle formation by polymer-grafted lipids: scaling with polymer length studied by spin-label electron spin resonance. *Biophys. J.* **80,** 1372–83 (2001).

104. De Gennes, P. G. Conformations of polymers attached to an interface. *Macromolecules* **13,** 1069–1075 (1980).

105. Almgren, M., Edwards, K. & Karlsson, G. Cryo transmission electron microscopy of liposomes and related structures. *Colloids Surfaces A Physicochem. Eng. Asp.* **174,** 3–21 (2000).

106. Nagle, J. F. & Tristram-Nagle, S. Structure of lipid bilayers. *Biochim. Biophys. Acta (BBA)-Reviews Biomembr.* **1469,** 159–195 (2000).

107. Cullis, P. R., Mayer, L. D., Bally, M. B., Madden, T. D. & Hope, M. J. Generating and loading of liposomal systems for drug-delivery applications. *Adv. Drug Deliv. Rev.* **3,** 267–282 (1989).

108. Abraham, S. A. *et al.* The liposomal formulation of doxorubicin. *Methods Enzym.* **391,** 71–97 (2005).

109. Drummond, D. C., Meyer, O., Hong, K., Kirpotin, D. B. & Papahadjopoulos, D. Optimizing liposomes for delivery of chemotherapeutic agents to solid tumors. *Pharmacol. Rev.* **51,** 691–743 (1999).

110. Stephan, K. *et al.* Fast prototyping using a dry film photoresist: microfabrication of soft-lithography masters for microfluidic structures. *J. Micromechanics Microengineering* **17,** N69–N74 (2007).

111. Pall Corporation. Selection Guide: Separation Products for Centrifugal and Tangential Flow Filtration. (2012). at <http://www.pall.com/main/Laboratory/Literature-Library-Details.page?id=7046#37147>

112. Kano, K. & Fendler, J. H. Pyranine as a sensitive pH probe for liposome interiors and surfaces. pH gradients across phospholipid vesicles. *Biochim. Biophys. Acta* **509,** 289–299 (1978).

113. Leaist, D. G. & Hao, L. Binary mutual diffusion coefficients of aqueous ammonium and potassium sulfates at 25°C. *J. Solution Chem.* **21,** 345–350 (1992).

114. Barenholz, Y. C. Doxil®--the first FDA-approved nano-drug: lessons learned. *J. Control. Release* **160,** 117–34 (2012).

115. Hortobágyi, G. N. Anthracyclines in the Treatment of Cancer. *Drugs* **54,** 1–7 (1997).

116. Minotti, G., Menna, P., Salvatorelli, E., Cairo, G. & Gianni, L. Anthracyclines: molecular advances and pharmacologic developments in antitumor activity and cardiotoxicity. *Pharmacol. Rev.* **56,** 185–229 (2004).

117. Allen, T. M. & Martin, F. J. Advantages of liposomal delivery systems for anthracyclines. *Semin. Oncol.* **31,** 5–15 (2004).

118. Clerc, S. & Barenholz, Y. A quantitative model for using acridine orange as a transmembrane pH gradient probe. *Anal. Biochem.* **259,** 104–11 (1998).

119. Clerc, S. & Barenholz, Y. Loading of amphipathic weak acids into liposomes in response to transmembrane calcium acetate gradients. *Biochim. Biophys. Acta - Biomembr.* **1240,** 257–265 (1995).

120. Zucker, D., Marcus, D., Barenholz, Y. & Goldblum, A. Liposome drugs' loading efficiency: a working model based on loading conditions and drug's physicochemical properties. *J. Control. Release* **139,** 73–80 (2009).

121. Lewrick, F. & Süss, R. Remote loading of anthracyclines into liposomes. *Methods Mol. Biol.* **605,** 139–45 (2010).

122. Mayer, L. D. *et al.* Characterization of liposomal systems containing doxorubicin entrapped in response to pH gradients. *Biochim. Biophys. Acta* **1025,** 143–51 (1990).

123. Sundararajan, N., Pio, M. S., Lee, L. P. & Berlin, A. A. Three-Dimensional Hydrodynamic Focusing in Polydimethylsiloxane (PDMS) Microchannels. *J. Microelectromechanical Syst.* **13,** 559–567 (2004).

124. Chang, C.-C., Huang, Z.-X. & Yang, R.-J. Three-dimensional hydrodynamic focusing in two-layer polydimethylsiloxane (PDMS) microchannels. *J. Micromechanics Microengineering* **17,** 1479–1486 (2007).

125. Mao, X., Waldeisen, J. R. & Huang, T. J. "Microfluidic drifting"--implementing three-dimensional hydrodynamic focusing with a single-layer planar microfluidic device. *Lab Chip* **7,** 1260–2 (2007).

126. Zhang, L., Wang, Q. & Liu, Y. On the mutual diffusion properties of ethanol-water mixtures. *J. Chem. Phys.* **125,** 104502 (2006).

127. Ismagilov, R. F., Stroock, A. D., Kenis, P. J. A., Whitesides, G. & Stone, H. A. Experimental and theoretical scaling laws for transverse diffusive broadening in two-phase laminar flows in microchannels. *Appl. Phys. Lett.* **76,** 2376 (2000).

128. Hertzog, D. E. *et al.* Femtomole mixer for microsecond kinetic studies of protein folding. *Anal. Chem.* **76,** 7169–78 (2004).

129. Carroll, M. R. J. *et al.* Experimental validation of proton transverse relaxivity models for superparamagnetic nanoparticle MRI contrast agents. *Nanotechnology* **21,** 035103 (2010).

130. Durst, F., Ray, S., Ünsal, B. & Bayoumi, O. A. The Development Lengths of Laminar Pipe and Channel Flows. *J. Fluids Eng.* **127,** 1154 (2005).

131. Batchelor, G. K. *An Introduction to Fluid Dynamics*. (Cambridge University Press, 1967).

132. Allen, T. M. Liposomes - Opportunities in Drug Delivery. *Drugs* **54,** 8–14 (1997).

133. Storm, G. & Crommelin, D. J. . Liposomes: quo vadis? *Pharm. Sci. Technolo. Today* **1,** 19–31 (1998).

134. Gregoriadis, G. Engineering liposomes for drug delivery: progress and problems. *Trends Biotechnol.* **13,** 527–37 (1995).

135. Petros, R. a & DeSimone, J. M. Strategies in the design of nanoparticles for therapeutic applications. *Nat. Rev. Drug Discov.* **9,** 615–27 (2010).

136. Wang, J., Byrne, J. J. D., Napier, M. E. M. & DeSimone, J. M. J. More Effective Nanomedicines through Particle Design. *Small* **7,** 1919–1931 (2011).

137. Hillaireau, H. & Couvreur, P. Nanocarriers' entry into the cell: relevance to drug delivery. *Cell. Mol. Life Sci. C.* **66,** 2873–2896 (2009).

138. Duffy, D. C., McDonald, J. C., Schueller, O. J. & Whitesides, G. M. Rapid Prototyping of Microfluidic Systems in Poly(dimethylsiloxane). *Anal. Chem.* **70,** 4974–84 (1998).

139. Allen, T. M., Austin, G. a, Chonn, a, Lin, L. & Lee, K. C. Uptake of liposomes by cultured mouse bone marrow macrophages: influence of liposome composition and size. *Biochim. Biophys. Acta* **1061,** 56–64 (1991).

140. Goldberg, D. S., Ghandehari, H., Swaan, P. W. & D.S. Goldberg, H. Ghandehari, and P. W. S. Cellular Entry of G3.5 Poly (amido amine) Dendrimers by Clathrin- and Dynamin-Dependent Endocytosis Promotes Tight Junctional Opening in Intestinal Epithelia. *Pharm. Res.* **27,** 1547–1557 (2010).

141. Pollock, S. *et al.* Uptake and trafficking of liposomes to the endoplasmic reticulum. *FASEB J.* **24,** 1866–78 (2010).

142. Edwards, K. a & Baeumner, A. J. Liposomes in analyses. *Talanta* **68,** 1421–31 (2006).

143. Straubinger, R. M., Hong, K., Friend, D. S. & Papahadjopoulos, D. Endocytosis of liposomes and intracellular fate of encapsulated molecules: Encounter with a low pH compartment after internalization in coated vesicles. *Cell* **32,** 1069–1079 (1983).

144. Kamps, J. & Scherphof, G. Receptor versus non-receptor mediated clearance of liposomes. *Adv. Drug Deliv. Rev.* **32,** 81–97 (1998).

145. Hong, K., Yoshimura, T. & Papahadjopoulos, D. Interaction of clathrin with liposomes: pH-dependent fusion of phospholipid membranes induced by clathrin. *FEBS Lett.* **191,** 17–23 (1985).

146. Barza, M., Stuart, M. & Szoka, F. Effect of size and lipid composition on the pharmacokinetics of intravitreal liposomes. *Invest. Ophthalmol. Vis. Sci.* **28,** 893–900 (1987).

147. Mayer, L. D. *et al.* Influence of vesicle size, lipid composition, and drug-to-lipid ratio on the biological activity of liposomal doxorubicin in mice. *Cancer Res.* **49,** 5922–30 (1989).

148. Souhami, R. L., Patel, H. M. & Ryman, B. E. The effect of reticuloendothelial blockade on the blood clearance and tissue distribution of liposomes. *Biochim. Biophys. Acta - Gen. Subj.* **674,** 354–371 (1981).

149. Koren, E., Apte, A., Jani, A. & Torchilin, V. P. Multifunctional PEGylated 2C5-immunoliposomes containing pH-sensitive bonds and TAT peptide for enhanced tumor cell internalization and cytotoxicity. *J. Control. Release* **160,** 264–73 (2012).

150. Hobbs, S. K. *et al.* Regulation of transport pathways in tumor vessels: role of tumor type and microenvironment. *Proc. Natl. Acad. Sci. U. S. A.* **95,** 4607–12 (1998).

151. Hirano, A. & Matsui, T. Vascular structures in brain tumors. *Hum. Pathol.* **6,** 611–621 (1975).

152. Bareford, L. & Swaan, P. Endocytic mechanisms for targeted drug delivery. *Adv. Drug Deliv. Rev.* **59,** 748–758 (2007).

153. Sever, S. Dynamin and endocytosis. *Curr. Opin. Cell Biol.* **14,** 463–467 (2002).

154. Gu, C. *et al.* Direct dynamin-actin interactions regulate the actin cytoskeleton. *EMBO J.* **29,** 3593–606 (2010).

155. Hinshaw, J. E. & Schmid, S. L. Dynamin self-assembles into rings suggesting a mechanism for coated vesicle budding. *Nature* **374,** 190–2 (1995).

156. Barenholz, Y. Liposome application: problems and prospects. *Curr. Opin. Colloid Interface Sci.* **6,** 66–77 (2001).

157. Prausnitz, M. R. & Langer, R. Transdermal drug delivery. *Nat. Biotechnol.* **26,** 1261–8 (2008).

158. Schreier, H. & Bouwstra, J. Liposomes and niosomes as topical drug carriers: dermal and transdermal drug delivery. *J. Control. Release* **30,** 1–15 (1994).

159. Cevc, G. Lipid vesicles and other colloids as drug carriers on the skin. *Adv. Drug Deliv. Rev.* **56,** 675–711 (2004).

160. Karande, P., Jain, A., Ergun, K., Kispersky, V. & Mitragotri, S. Design principles of chemical penetration enhancers for transdermal drug delivery. *PNAS* **102,** 4688–4693 (2005).

161. Bouwstra, J. A., Honeywell-Nguyen, P. L., Gooris, G. S. & Ponec, M. Structure of the skin barrier and its modulation by vesicular formulations. *Prog. Lipid Res.* **42,** 1–36 (2003).

162. Ryman-Rasmussen, J. P., Riviere, J. E. & Monteiro-Riviere, N. A. Penetration of intact skin by quantum dots with diverse physicochemical properties. *Toxicol. Sci.* **91,** 159–165 (2006).

163. Chu, M. *et al.* In vitro and in vivo transdermal delivery capacity of quantum dots through mouse skin. *Nanotechnology* **18,** 455103 (2007).

164. Schleich, N. & Préat, V. in *Nanostructured Biomater. Overcoming Biol. Barriers* (2012). doi:10.1039/9781849735292-00316

165. Du Plessis, J., Ramachandran, C., Weiner, N. & Muller, D. G. The influence of particle size of liposomes on the deposition of drug into skin. *Int. J. Pharm.* **103,** 277–282 (1994).

166. Prow, T. W. *et al.* Nanoparticles and microparticles for skin drug delivery. *Adv. Drug Deliv. Rev.* **63,** 470–91 (2011).

167. Sudhakar, C. K., Upadhyay, N., Jain, S. & Charyulu, R. N. in *Nanomedicine Drug Deliv.* (Sebastian, M., Ninan, N. & Haghi, A. K.) 1–15 (Apple Academic Press, 2012).

168. Sentjurc, M., Vrhovnik, K. & Kristl, J. Liposomes as a topical delivery system: the role of size on transport studied by the EPR imaging method. *J. Control. Release* **59,** 87–97 (1999).

169. Touitou, E., Dayan, N., Bergelson, L., Godin, B. & Eliaz, M. Ethosomes - novel vesicular carriers for enhanced delivery: characterization and skin penetration properties. *J. Control. Release* **65,** 403–18 (2000).

170. Brewer, J., Bloksgaard, M., Kubiak, J., Sørensen, J. A. & Bagatolli, L. a. Spatially resolved two-color diffusion measurements in human skin applied to transdermal liposome penetration. *J. Invest. Dermatol.* **133,** 1260–8 (2013).

171. Vogt, A. *et al.* 40 nm, but not 750 or 1,500 nm, nanoparticles enter epidermal CD1a+ cells after transcutaneous application on human skin. *J. Invest. Dermatol.* **126,** 1316–22 (2006).

172. Küchler, S. *et al.* Nanoparticles for skin penetration enhancement--a comparison of a dendritic core-multishell-nanotransporter and solid lipid nanoparticles. *Eur. J. Pharm. Biopharm. Off. J. Arbeitsgemeinschaft fur Pharm. Verfahrenstechnik eV* **71,** 243–250 (2009).

173. Verma, D. D., Verma, S., Blume, G. & Fahr, A. Particle size of liposomes influences dermal delivery of substances into skin. *Int. J. Pharm.* **258,** 141–151 (2003).

174. Barenholzt, Y., Amselem, S. & Lichtenberg, D. A new method for preparation of phospholipid vesicles (liposomes) - French press. *FEBS Lett.* **99,** 210–214 (1979).

175. Hamilton, R. L., Goerke, J., Guo, L. S., Williams, M. C. & Havel, R. J. Unilamellar liposomes made with the French pressure cell: a simple preparative and semiquantitative technique. *J. Lipid Res.* **21,** 981–992 (1980).

176. Hood, R. R., Andar, A. U., Vreeland, W. N. & DeVoe, D. L. Microfluidic synthesis of PEGylated and folate receptor-targeted liposomes. *Pharm. Res.* **in press,** (2013).

177. Sekkat, N., Kalia, Y. N. & Guy, R. H. Biophysical study of porcine ear skin in vitro and its comparison to human skin in vivo. *J. Pharm. Sci.* **91,** 2376–81 (2002).

178. Kong, R. & Bhargava, R. Characterization of porcine skin as a model for human skin studies using infrared spectroscopic imaging. *Analyst* **136,** 2359–66 (2011).

179. Bolte, S. & Cordelières, F. P. A guided tour into subcellular colocalization analysis in light microscopy. *J. Microsc.* **224,** 213–32 (2006).

180. Elsayed, M. M. a, Abdallah, O. Y., Naggar, V. F. & Khalafallah, N. M. Lipid vesicles for skin delivery of drugs: reviewing three decades of research. *Int. J. Pharm.* **332,** 1–16 (2007).

181. Gao, S. *et al.* Characteristics of blood fluorescence spectra using low-level, 457.9-nm excitation from Ar+ laser. *Chinese Opt. Lett.* **2,** 160–161 (2004).

182. Rolland, A., Wagner, N., Chatelus, A., Shroot, B. & Schaefer, H. Site-specific drug delivery to pilosebaceous structures using polymeric microspheres. *Pharm. Res.* **10,** 1738–44 (1993).

183. Mordon, S., Sumian, C. & Devoisselle, J. M. Site-specific methylene blue delivery to pilosebaceous structures using highly porous nylon microspheres: an experimental evaluation. *Lasers Surg. Med.* **33,** 119–25 (2003).

184. Jacobi, U. *et al.* Porcine ear skin: an in vitro model for human skin. *Skin Res. Technol.* **13,** 19–24 (2007).

185. Akomeah, F. K., Martin, G. P. & Brown, M. B. Variability in human skin permeability in vitro: comparing penetrants with different physicochemical properties. *J. Pharm. Sci.* **96,** 824–834 (2007).

186. Mitragotri, S. Modeling skin permeability to hydrophilic and hydrophobic solutes based on four permeation pathways. *J. Control. Release* **86,** 69–92 (2003).

187. Sapra, P. & Allen, T. M. Ligand-targeted liposomal anticancer drugs. *Prog. Lipid Res.* **42,** 439–462 (2003).

188. Allen, T. M. Ligand-targeted therapeutics in anticancer therapy. *Nat. Rev. Cancer* **2,** 750–63 (2002).

189. Loughrey, H., Bally, M. B. & Cullis, P. R. A non-covalent method of attaching antibodies to liposomes. *Biochim. Biophys. Acta - Biomembr.* **901,** 157–160 (1987).

190. Ishida, T., Iden, D. L. & Allen, T. M. A combinatorial approach to producing sterically stabilized (Stealth) immunoliposomal drugs. *FEBS Lett.* **460,** 129–133 (1999).

191. Mayer, L. D., Hope, M. J., Cullis, P. R. & Janoff, A. S. Solute distributions and trapping efficiencies observed in freeze-thawed multilamellar vesicles. *Biochim. Biophys. Acta - Biomembr.* **817,** 193–196 (1985).

192. Gruner, S. M., Lenk, R. P., Janoff, A. S. & Ostro, N. J. Novel multilayered lipid vesicles: comparison of physical characteristics of multilamellar liposomes and stable plurilamellar vesicles. *Biochemistry* **24,** 2833–2842 (1985).

193. Nisisako, T., Ando, T. & Hatsuzawa, T. High-volume production of single and compound emulsions in a microfluidic parallelization arrangement coupled with coaxial annular world-to-chip interfaces. *Lab Chip* **12,** 3426–35 (2012).

194. Karande, P. & Mitragotri, S. High throughput screening of transdermal formulations. *Pharm. Res.* **19,** 655–60 (2002).